REVIEW

Advanced Materials for Energy Storage

By *Chang Liu, Feng Li, Lai-Peng Ma,* and *Hui-Ming Cheng**

Popularization of portable electronics and electric vehicles worldwide stimulates the development of energy storage devices, such as batteries and supercapacitors, toward higher power density and energy density, which significantly depends upon the advancement of new materials used in these devices. Moreover, energy storage materials play a key role in efficient, clean, and versatile use of energy, and are crucial for the exploitation of renewable energy. Therefore, energy storage materials cover a wide range of materials and have been receiving intensive attention from research and development to industrialization. In this Review, firstly a general introduction is given to several typical energy storage systems, including thermal, mechanical, electromagnetic, hydrogen, and electrochemical energy storage. Then the current status of high-performance hydrogen storage materials for on-board applications and electrochemical energy storage materials for lithium-ion batteries and supercapacitors is introduced in detail. The strategies for developing these advanced energy storage materials, including nanostructuring, nano-/microcombination, hybridization, pore-structure control, configuration design, surface modification, and composition optimization, are discussed. Finally, the future trends and prospects in the development of advanced energy storage materials are highlighted.

1. Introduction

Energy is one of the most important topics in the 21st century. With the rapid depletion of fossil fuels and increasingly worsened environmental pollution caused by vast fossil-fuel consumption, there is high demand to make efficient use of energy and to seek renewable and clean energy sources that can substitute fossil fuels to enable the sustainable development of our economy and society. Energy storage, an intermediate step to the versatile, clean, and efficient use of energy, has received worldwide concern and increasing research interest.

Energy storage can be dated back to ancient times and it is quite simple and natural. Mankind initially made fire using wood and charcoal, which are biomass energy storage carriers of solar energy. Fire brings warmth, brightness, cooked food, and later bronze wares and iron wares, and thus charcoal energy acted as one of the most important driving powers for ancient civilization. About 900 years ago, coal, which evolves from buried plants grown millions and even billions of years ago and stores solar energy in a much higher density than wood or charcoal, was discovered and used as fuel. Later on, coal was used to power steam engines in the 18th century, the symbol of the first industrial revolution, and later to produce electricity. Petroleum, which is derived from the remains of biodegraded organic materials, is another high-density energy storage medium for solar energy and has been mined and used massively since the beginning of the 20th century. Petroleum is obviously more than a fuel, and is used not only to power vehicles via internal combustion engines but also to make synthetic fibers, resins, plastics, and almost everything in our lives today. Coal, oil, and natural gas are primary energy sources, and they are energy carriers that have naturally collected and stored solar energy for billions of years.

Since electric motors and generators were invented in the 1870s, electrical energy has become the most important secondary energy source and the primary form of consumed energy. Electricity can be generated from fuel-burning power, solar power, hydropower, wind power, nuclear power, tide power, and biopower systems, and is indispensable in almost every part of our lives from lighting, warming and cooling, from cooking to entertainment, transportation, and communication. With the rapid development of modern industries and the durative increase of global population, the rate of electrical energy consumption has dramatically increased and its consumption manner is diversified. Energy storage becomes even more complex and important, and desirable and high-performance energy storage techniques are needed to enable efficient, versatile, and environmentally friendly uses of energy including electricity. In a typical energy storage process, one type of energy is converted into another form of energy that can be stored and converted for use when needed. Therefore, various energy storage systems are being developed aimed at proper utilization of different energy sources.

1.1. Energy Storage Systems for the Efficient Use of Energy

The consumption of electricity is usually not even and there are on-peak and off-peak loading vibrations. By storing the off-peak electricity and releasing the stored energy during the on-peak

[*] Prof. H.-M. Cheng, Prof. C. Liu, Prof. F. Li, Dr. L.-P. Ma
Shenyang National Laboratory for Materials Science
Institute of Metal Research
Chinese Academy of Sciences
72 Wenhua Road, Shenyang 110016 (China)
E-mail: cheng@imr.ac.cn

DOI: 10.1002/adma.200903328

period, the efficiency, stability, and reliability of an electricity supply system can be significantly improved. Mechanical energy storage and thermal energy storage are mainly used for such peak load shifting.

1.1.1. Mechanical Energy Storage

Mechanical energy storage is carried out by conversion between electrical energy and mechanical energy at demand. When inexpensive off-peak electricity power is available, electrical energy is stored by converting into mechanical energy; the stored energy is released when the electricity power supply is insufficient. Mechanical energy storage can be typically divided into flywheel energy storage (FES), pumped hydropower storage (PHS), and compressed-air energy storage (CAES).

A FES system is basically composed of a column-shaped rotation part and a magnetic suspension axletree as supporting component. Its working principle is that a flywheel is driven by an electromotor to rotate with a high speed where electrical energy is converted into kinetic energy; when the flywheel slows down, its kinetic energy is converted into electrical energy and thus the storage and release of electrical energy is realized. FES shows advantages of high energy density, rapid charge/discharge rate, long working life, high reliability, wide working temperature range, high energy storage efficiency (≈90%), and environmental friendliness, and therefore it finds applications in electric power, telecommunications, and aeronautic and astronautic areas. The energy density of an FES system is linearly related to the mass and the square of the angular velocity of the flywheel; therefore, it is largely determined by the material used for making the flywheel. The higher the strength of the material, the higher the rotating speed of the flywheel, and the higher the energy density of a FES system. Carbon-fiber-reinforced carbon composites with high strength are now a promising candidate for FES. Nanomaterials such as carbon nanotubes (CNTs), which show much higher tensile strength and Young's modulus than carbon fibers, may have potential applications in FES.

For a PHS system, when off-peak power is available, water is pumped from a low-altitude reservoir to a high-altitude reservoir, where the PHS system works as an electromotor. During the load peak of electric power supply, the stored water at the high-altitude reservoir is used for generating electricity, where the PHS system works as an electric generator. The efficiency of a PHS system is typically 71%–85%.[1]

A CAES system usually uses cheap off-peak electric power to compress air, and at peak load the compressed air is released and used for electric power generation. Compared with normal gas turbines, CAES may save around 40% gas for the equal amount of electric power output. The compressed air is stored in underground caves or abandoned mines. The major constraint to CAES is that it relies on favorable geography, that is, it is only economically feasible for power plants that have nearby rock mines, salt caverns, and aquifers or depleted gas fields.[1]

1.1.2. Thermal Energy Storage

Thermal energy storage is another method for adjusting the time discrepancy between power supply and demand. Excess thermal energy is stored in a material as sensible or latent heat by warming up or melting the material. The stored thermal energy is utilized later by cooling the material back down.[2] In addition, thermal energy storage also has potential applications for waste heat recovery, solar energy utilization, energy saving in buildings, and electronic device management.[3] Thermal energy storage can be classified as sensible heat storage (SHS), latent heat storage (LHS), and thermal chemical energy storage (TCES).

The principle of SHS is that when the temperature of a storage medium increase, thermal energy is stored; when the temperature of the storage material decreases, the stored energy is released. The thermal energy storage density is mainly determined by the specific heat capacity of the storage material and the working temperature range of the system. Water shows advantages of low cost and high specific heat as a SHS medium. For systems working at temperatures higher than 100 °C, materials with higher evaporation points, such as heat-transfer oils, molten nitrates, liquid sodium, and concrete, are used.[4] Recently, ionic liquid was reported to be promising for working under ≈400 °C with desirable nonflammable properties. However, it is too expensive to be used practically.

LHS is based on phase-change materials (PCMs). PCMs adsorb/release heat during their phase-change process, and thus thermal energy storage/release is realized. LHS shows advantages of high energy storage density and small temperature alteration range during thermal energy charge/discharge. A LHS system is typically composed of a PCM, a heat exchanger, and a

Hui-Ming Cheng received his Ph.D. in Materials Science from the Institute of Metal Research, Chinese Academy of Sciences (IMR, CAS). He worked at AIST, Nagasaki University of Japan, and MIT, USA. He is Professor and Director of the Advanced Carbons Research Division at Shenyang National Laboratory for Materials Science, IMR, CAS. His research interests focus mainly on carbon nanotubes, graphene, and high-performance bulk carbons, as well as on new energy materials for batteries, supercapacitors, and hydrogen production from water photosplitting.

Chang Liu is a professor of the Institute of Metal Research, Chinese Academy of Sciences (IMR, CAS). He received his Ph.D. in materials science at IMR, CAS in 2000 supervised by Prof. Hui-Ming Cheng. He worked at the International Center for Young Scientists, National Institute for Materials Science, Japan during 2004–2005. He mainly works on the synthesis and application of carbon nanotubes and the preparation and properties of electrode materials for lithium-ion batteries.

suitable container. When choosing a PCM for a particular LHS system, the following points should be considered: the phase-transition temperature should match the working temperature range of the system, the phase-change specific heat should be large enough, the PCM should be chemically stable, a high thermal conductivity is desirable, the volume change should be small so that a higher volumetric energy storage density of the system can be achieved, the cost of the PCM should be low, and so on.

PCMs can be basically classified into solid–solid and solid–liquid types according to their phase-change forms (the phase transitions involving the gas state are usually impractical due to the large volume change accompanied). Solid–solid PCMs adsorb/release heat during their crystal transition. Typical solid–solid PCMs include polyalcohols, macromolecules, laminated perovskite, and inorganic salts. These materials show advantages of small volume changes, long cycling lives, environmental friendliness, limited undercooling effects, no phase disengagement, and simple accessories. For polyalcohol (such as pentaerythritol and neopentyl glycol), the hydrogen bonds connecting interlayer molecules are broken during the phase change and the latent energy is released. The phase-change entropy is closely related to the number of hydrogen bonds contained in a polyalcohol molecule. By changing the composition of a mixture of different polyalcohols, their phase-change temperature can be tuned to some extent. High-density polyethylene is a commonly used macromolecular PCM and shows advantages of low costs, good machinability, and high thermal conductivity. Laminated perovskite is a type of organometallic compound—a bis(n-decylammonium) tetrachlorometallate(II)—whose composition can be expressed as $(n\text{-}C_xH_{2x+1}NH_3)MY_4$, where M is a divalent metal (e.g., Cu, Fe, Co, Zn, or Mn), Y is a halogen, and x is usually in the range of 8–18. The phase transition of this type of material originated from the ordering change of their alkyl chain. The laminated perovskite is stable at temperatures lower than 200 °C and shows good cycling performance. Some inorganic salts like KH_2F and NH_4SCN were also proposed and studied as PCMs.[3]

Solid–liquid PCMs are the most frequently used latent-heat-storage material and can be subgrouped into organic and inorganic materials. Organic solid–liquid PCMs mainly include paraffin and fatty acids. Paraffin is a mixture of straight chain alkenes and can be expressed as C_nH_{2n+2}. The melting point and fusion heat of the alkene chains increase with their chain length. By changing the composition of paraffin, that is, the ratio of alkenes with short carbon chains to those with long carbon chains, the phase-change temperature can be tuned in a wide range of 5–80 °C. Paraffin is chemically stable and noncorrosive, has a low vapor pressure, does not undercool and separate out, and is less expensive. However, low thermal conductivity, flammability, and limited volumetric energy storage density are disadvantages of paraffin. Some specific techniques aiming at reducing the undesirable features of paraffin are developed by modifying the wax and the storage unit, such as by micro-encapsulation and shape-stabilization.[4] Fatty acid is another category of important solid–liquid PCMs and can be expressed as $CH_3(CH_2)_{2n}COOH$. The phase-change heat of fatty acid is comparable to that of paraffin. Fatty acids also show desirable features of good cyclability, no supercooling, and tunable phase-change temperature.[5] A drawback of fatty acids is the comparatively high cost. Inorganic solid–liquid PCMs include salt hydrates, metals, and molten salts. Salt hydrates are inorganic salts containing water, which can be expressed as $A_xB_y \cdot n(H_2O)$, where A_xB_y is a sulfite, nitrite, acetate, phosphate, carbonate, or chloride. At the phase-change temperature, salt hydrates lose some or all of the crystal water molecules and dissolve, and thus the latent heat (heat of dissolution) is adsorbed. In the reverse process, the latent heat is released. Salt hydrates have advantages of high energy density, good thermal conductivity, low cost, and are nontoxic and noncorrosive. The main drawbacks of salt hydrates are undercooling and precipitation. The problem of undercooling can be tackled by adding nucleation seeds and using the so-called ''cold finger'' method, where a cold area is retained and the undissolved crystallites can serve as nucleation seeds. Precipitation can be relieved by adding thickening agents, stirring or rotating, modifying the chemical composition, and designing the shape of the containers.[4] Another kind of inorganic solid–liquid PCM is metals and eutectics. Pure, binary, or ternary low-melting-point metals can be used as PCMs and their melting point is usually in the range of tens of degrees to more than one hundred degrees. These materials possess a high volumetric energy density and high thermal conductivity, but also a highly corrosive feature, which may hinder their practical use. Some inorganic compounds like K_2CO_3, Na_2CO_3, Li_2CO_3, MgO, LiOH, and NaOH are also used as PCMs. These materials show very high specific heats of fusion and high phase-change temperatures (several hundred degrees). Therefore, they may find applications in industrial waste heat recovery and solar heat storage.[6]

TCES is based on endothermic/exothermic chemical-reaction heat for energy storage and release. The chemical reactions employed are usually reversible, such as $Ca(OH)_2 \leftrightarrows CaO + H_2O$. TCES shows advantages of a high energy density and a long and stable storage period. Moreover, this technique is considered to be suitable for solar-thermal-power generation and a demo-equipment was established in Australia based on the ammonia decomposition reaction.[7]

1.2. Energy Storage Systems for the Environmentally Friendly Use of Energy

The vast consumption of fossil fuels has brought serious environmental problems, such as the greenhouse effect, acid rain, and air pollution. Therefore, people are seeking renewable and clean energy sources that can support the sustainable development of the global economy and society. Hydrogen is a clean and reproducible energy carrier, which only emits water, for both transportation and stationary applications. Its high energy density makes it one of the most promising alternatives to replace petroleum. Therefore, interest in the research and development of hydrogen energy has grown dramatically since the 1990s. Basically, the development of hydrogen energy involves the following three processes: production, storage, and utilization. Big scientific and technological barriers need to be overcome before any large-scale utilization of hydrogen energy can occur. The key to addressing these problems depends highly on

advancement in the development of high-performance materials for hydrogen storage systems. Since urban air pollution is heavily caused by automotive exhaust emission, applicable on-board hydrogen storage techniques are crucial for improving the air quality in urban areas. However, the requirements that hydrogen storage materials be of high capacity, reversible, and safe is a bottle-neck for fueling automobiles with hydrogen. The recent developments in advanced hydrogen storage materials will be reviewed in detail in Section 2.

1.3. Energy Storage Systems for the Versatile Use of Energy

The demand for powering systems of portable electronic devices and zero-emission vehicles has been increasing. In these cases, electrochemical energy storage devices, including batteries and supercapacitors, play an important role. On the other hand, the production of renewable energy, such as solar and wind energy, significantly relies on natural conditions (day time, night time, wind, etc.) and is not even and continuous. Therefore, matching high-performance energy storage systems are needed to store the energy generated and to stabilize the electricity grid connected. Electrochemical energy storage and electromagnetic energy storage systems are promising for serving as such supporting facilities.

1.3.1. Electrochemical Energy Storage

Electrochemical energy storage/release is realized by electron and ion charge/discharge. Batteries and supercapacitors are two kinds of typical electrochemical energy storage devices, both of which store electricity in electrochemical processes. An electrochemical energy storage device is usually composed of an anode, a cathode, a separator, and an electrolyte. During discharge, electrochemical reactions occur at the electrodes, generating electrons that flow through an external circuit; during charge, an external voltage across the electrodes is applied, driving the movements of electrons and reactions at the electrodes. According to the component of their electrodes, rechargeable batteries can be classified as lead-acid, zinc-air, nickel-cadmium, nickel-hydrogen, sodium-sulfur, sodium-nickel-chloride, and Li-ion batteries (LIBs). The principles of supercapacitors include an electric double layer and pseudo-capacitive charge-storage modes. The former, similar to a physical dielectric capacitor, is based on the separation of charges at the interface between a solid electrode and an electrolyte and the latter is a fast Faradaic process involving electrochemical redox reactions. The electrode materials for supercapacitors mainly include carbon, transition metal oxides, and conducting polymers.

Among the various alternative energy storage technologies, electrochemical energy storage shows advantages of high efficiency, versatility, and flexibility. LIBs are the most important and widely used rechargeable battery with advantages of high voltage, low self-discharge, long cycling life, low toxicity, and high reliability. Supercapacitors have attracted increasing interest because of their high power storage capability, which is highly desirable for applications in electric vehicles (EVs) and hybrid electric vehicles (HEVs). The performance of LIBs and supercapacitors is intimately related to the electrode materials used. With the development of materials design strategies, synthesis techniques, and characterization methodologies, electrode materials and consequently the performance of batteries and supercapacitors have been progressing rapidly. We will give a detailed overview of the advanced materials for LIBs and supercapacitors in Sections 3 and 4, respectively. The "advanced materials" we refer to herein differentiate from the conventional electrode materials by showing a superior electrochemical energy storage performance that originates from the smart design strategy, unique structural characteristics, and specific synthesis techniques.

1.3.2. Electromagnetic Energy Storage

Superconductive magnetic energy storage (SMES) was first proposed in the 1970s. A SMES unit is mainly made up of a superconducting coil and a liquid nitrogen cooling system. Energy storage/release is achieved by charging/discharging the coil. The SMES shows advantages of a prompt electromagnetic response and a very high energy storage efficiency (>97%). SMES is suitable for applications that require constant, full cycling and a continuous mode of operation. For example, SMES can be used for stabilizing the power generated by solar and wind systems and to improve the quality of electrical power supply, and it can also be used for solving voltage stability and power quality problems for large industrial customers.[1] Compared with other energy storage systems, the cost of a SMES is very high due to expensive superconductors as well as the cost for maintaining the cryogenic temperature. With the development of high-temperature superconducting (high-T_c) materials, it is expected that the cost for operating a SMES system can be lowered in future.

As discussed above, various energy storage systems, including mechanical energy storage, thermal energy storage, electrochemical energy storage, electromagnetic energy storage, and hydrogen storage, have been developed and applied for peak load shifting, recovery of waste heat, power supply of portable electronic products and EVs, matching facilities of renewable energy generators, and so on. Energy storage is crucial for the efficient production, consumption, and distribution of fossil and renewable energy sources. The conversion and storage of energy is closely related to energy storage materials. Therefore, the development of energy storage techniques can be largely attributed to the innovation and advancement of energy storage materials. Studies on hydrogen storage and electrochemical energy storage materials are most active in recent years and notable progresses have been made. Thus, we will focus on advanced hydrogen storage materials and electrochemical energy storage materials in this Review. The state-of-the-art progresses on hydrogen storage materials, electrode materials of LIBs, and electrode materials of supercapacitors are presented in Sections 2, 3, and 4, respectively. Section 5 is the summary and outlook for future research and development of advanced energy storage materials. For more detailed advances in other energy storage systems, there are a few recent review articles.[1,3,5]

2. Advanced Hydrogen Storage Materials

Efficient hydrogen storage is regarded as the key challenge in large-scale applications of hydrogen energy. Given that

transportation consumes almost one quarter of the world total energy,[8] on-board hydrogen storage receives the most intensive research efforts, aimed at realizing the commercialization of hydrogen-powered fuel-cell vehicles with hydrogen as a clean energy carrier. Material-based storage is expected to provide an ultimate solution to safe and efficient on-board hydrogen storage, because the well-developed pressurized tank and cryogenic liquid hydrogen techniques fail to satisfy the primary requirements of vehicular applications as a result of low volumetric hydrogen density, problematic energy efficiency, safety concerns, and/or high cost.[9] In general, a desirable on-board hydrogen storage material (HSM) should possess the following characteristics: high storage capacity, moderate operating temperature, fast kinetics, low cost and/or excellent reversibility (reversibility may not be necessary if the cost is low enough), and low toxicity. Specifically, the benchmark targets set by the US Department of Energy (DOE) are widely cited as necessary technical criteria.[10] Up to now, however, extensive investigations on various candidates including metal hydrides, complex hydrides, chemical hydrides, and novel adsorbents have not led to any viable system that meets simultaneously all the DOE benchmark requirements.

Among these requirements, a high hydrogen capacity (e.g., the system target of 6 wt% for 2010) is the prerequisite for vehicular application. Yet, high-capacity materials are typically plagued by the dilemma between dehydrogenation temperature (T_{de}) and reversibility. Many recent efforts have focused on improving the overall dehydrogenation performance of high-capacity materials in an attempt to satisfy all the stringent requirements. We discuss in this part some efficient strategies, such as hybridization, cation/anion substitution and exchange, catalytic activation, and nanoscaling, as well as morphology tailoring and surface modification, used to develop state-of-the-art materials for reversible or irreversible hydrogen storage, which may provide valuable indications for the exploration of novel high-performance HSMs. Several excellent reviews are also available for discussions on specific HSMs.[11–19]

2.1. Hybridization

One prominent aspect of the T_{de}/reversibility dilemma is the high T_{de} of reversible high-capacity materials. For instance, equilibrium dehydrogenation (under 1 atm pressure) of MgH_2 (7.6 wt% hydrogen) and $LiBH_4$ (18.4 wt% hydrogen) occurs at ≈280 and ≈410 °C, respectively.[11,13] Such high T_{de}(1 atm) values are intrinsic characteristics of the high thermodynamic stability imposed by the high bond strength.[11,13] Therefore, modification of dehydrogenation thermodynamics is required to lower the T_{de} of these hydrogen-rich but strongly bound hydrides. Hybridization is widely implemented as one of the most effective and applicable strategies for tuning thermodynamics, and two representative approaches are summarized.

2.1.1. Destabilization

Thermodynamic modifications of MgH_2 were accomplished by using additives that form alloys with Mg in the dehydrogenated and/or hydrogenated state as early as 1960s.[20] On the basis of similar principles, a destabilization strategy was recently developed to lower the equilibrium T_{de} of thermodynamically stabilized hydrides. This strategy involves the use of destabilizing agents to generate new reaction pathways that can stabilize the dehydrogenated products and thereby destabilize the hydride reactants (Fig. 1).[13,21] For example, Si is used to react with MgH_2 to form a stable $MgSi_2$ alloy rather than elemental Mg. The resultant decrease in the formation enthalpy of $MgSi_2$ relative to that of the reactants lowers the overall enthalpy of reaction from 75.3 kJ mol^{-1} H_2 to 36.4 kJ mol^{-1} H_2.[21] An even more significant improvement is observed in the Si-destabilized LiH material, in which enthalpy is reduced by 70 kJ mol^{-1} H_2 due to the generation of Li_4Si.[21] Despite the unacceptable capacity loss resulting from the incorporation of inert Si in both systems, destabilization is unambiguously demonstrated to be an effective strategy to lowering the T_{de} of strongly bound hydrides.

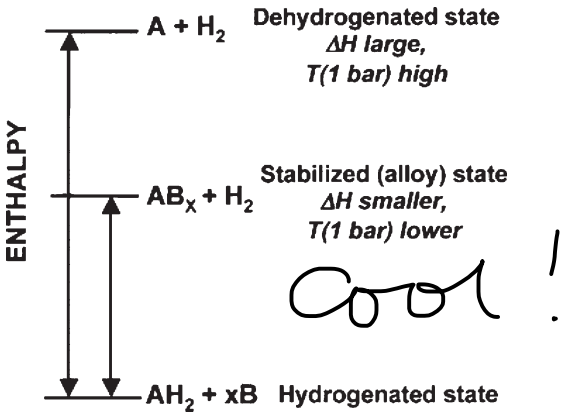

Figure 1. Generalized enthalpy diagram illustrating destabilization through alloy formation upon dehydrogenation. Reproduced with permission from Reference [13]. Copyright 2007, Elsevier Ltd.

An extended application of this strategy to complex hydrides results in the identification of several destabilized $LiBH_4$ materials, commonly known as Li−M−B−H systems (M = Mg, Al, Ca, or Ce).[22–24] In particular, MgH_2 is found to be an effective destabilizing agent for producing thermodynamically favorable $LiBH_4/MgH_2$. The reaction enthalpy is reduced from ≈67 to 41 kJ mol^{-1} H_2 by the formation of more stable MgB_2 relative to B:[22]

$$2LiBH_4 + MgH_2 \leftrightarrow 2LiH + MgB_2 + 4H_2 \quad (11.4\ wt\%\ H_2) \qquad (1)$$

In contrast to the former case, the use of hydrogen-rich hydride as destabilizing agent largely mitigates the capacity loss. Even within the capacity constraint, a number of light-element compounds may be used and the elaborate selection can be further facilitated by thermodynamic estimations.[13] However, few candidates are practically available and limited reversibility can be observed, both of which are virtually determined by the large kinetic barriers resulted from the insufficient reactivity for the interphase reactions involved.[15,22–24]

Interestingly, destabilization is also an important strategy in identifying feasible regeneration routes by generating new

pathways for hydrogenation reactions. For instance, $LiAlH_4$ cannot be directly recovered from LiH and Al due to the endothermic conversion of Li_3AlH_6 to $LiAlH_4$, suggesting that Li_3AlH_6 is too stable to be hydrogenated into $LiAlH_4$. Successful regeneration attempts essentially involve a two-step route: the facile formation of a $LiAlH_4 \cdot$solvent adduct from LiH and activated Al in the presence of organic solvent (typically THF) followed by a desolvation step to recover $LiAlH_4$.[25–27] Thermodynamic analysis suggests that the key is to form a more stable hydrogenation product (e.g., a $LiAlH_4 \cdot$THF adduct) relative to $LiAlH_4$ and Li_3AlH_6, thus leading to an exothermic hydrogenation reaction.[25–27] This mechanism can be well-understood from the destabilization strategy: Li_3AlH_6 is destabilized to enable the rehydrogenation reaction by forming a stabilized hydrogenation product. Despite the exothermic nature of AlH_3 formation (e.g., approximately $-10\,kJ\,mol^{-1}$ AlH_3 for α-AlH_3[28]), its low thermodynamic stability leads to impractical operating conditions (e.g., 3×10^4 bar at 573 K[29]) for the direct rehydrogenation from spent Al. Similarly, Al is destabilized by generating a more stable $AlH_3 \cdot$triethylenediamine adduct in the presence of triethylenediamine and THF, but the recovery of AlH_3 is almost impossible due to the high stability of this adduct.[30] Alternatively, electrochemical regeneration is a promising route, which involves the catalytic rehydrogenation of NaH and spent Al to the more stable $NaAlH_4$, and the subsequent electrolysis of $NaAlH_4$ into NaH and AlH_3.[31]

Further insight into the destabilization strategy suggests a generalized approach for modifying reaction thermodynamics: designing a new reaction with desirable enthalpy by combining the host material with appropriate reactants to generate specific reaction products. Following this principle, stabilization may be applicable to hydrogen-rich but thermodynamically unstable hydrides (e.g., ammonia borane) with the addition of stabilizing agent. However, it should be pointed out that kinetic limitation still remains and in some cases dominates the de-/rehydrogenation reactions, which primarily originates from the intrinsic high directionality of covalent/ionic bonds in host hydrides.[13] Adding to the challenge is the fact that kinetic barriers associated with mass transport and interface reaction are involved as a result of the multiphase reactions incorporated.

2.1.2. H^+/H^- Coupling

In terms of the oxidation state of hydrogen, the majority of current HSMs are characterized by H^- and the dehydrogenation reaction involved may be described by[11]

$$2H^- \rightarrow H_2 + 2e^- \qquad (\Delta H^0 = -3.02eV) \tag{2}$$

where ΔH^0 is the standard enthalpy change. To a large extent, the identification of previous HSMs was based upon Equation (2) until Chen et al. reported that Li nitride (Li_3N) reversibly stored over 10 wt% hydrogen via a two-step reaction:[32]

$$Li_3N + H_2 \leftrightarrow Li_2NH + LiH \tag{3}$$

$$Li_2NH + H_2 \leftrightarrow LiNH_2 + LiH \tag{4}$$

In contrast to Equation (2), the above two reactions involve the H^+/H^- coupling as a novel strategy for hydrogen storage, which generally follows

$$H^+ + H^- \rightarrow H_2 \qquad (\Delta H^0 = -17.37eV) \tag{5}$$

Two competitive models have been proposed to describe the reaction pathways. One suggests that the dehydrogenation reaction proceeds via the direct combination of H^+ and H^- from $LiNH_2$ and LiH, respectively.[33] Another involves the ammonia-mediation process: the amide phase first decomposes to yield ammonia, which is then captured by the hydride phase to release H_2.[34,35]

Equation (5) exhibits a much larger driving force of dehydrogenation compared to Equation (2). In principle, any combination of H^- source (e.g., hydrides or complex hydrides) and H^+ source (typically amides or imides) will contribute to hydrogen release. This approach opens up great possibilities for the rational design of novel HSMs (e.g., M–N–H systems) by combining conventional ones with amides/imides. Meanwhile, Equation (5) provides an alternative route for the modification of dehydrogenation thermodynamics and hydrogen capacity with regard to hydride reactants. Even for strongly bound H^- sources, the majority of hydrogen is available at moderate temperatures upon coupling with a suitable H^+ source. For instance, the $2LiNH_2/MgH_2$ [or $Mg(NH_2)_2/2LiH$] system exhibits a favorable combination of thermodynamics and reversibility:[36,37]

$$\begin{aligned} &2LiNH_2 + MgH_2 \rightarrow Li_2Mg(NH)_2 + 2H_2 \\ &\leftrightarrow Mg(NH_2)_2 + 2LiH \qquad (5.6\ wt\%\ H_2) \end{aligned} \tag{6}$$

By comparison with MgH_2, the dehydrogenation enthalpy of the $2LiNH_2/MgH_2$ system decreases from 75.3 to $\approx$40 kJ mol^{-1} H_2.[11,38] More significant reduction in the thermodynamic stability is attained in $2LiNH_2+LiBH_4$ material when comparing the highly endothermic dehydrogenation reaction of host $LiBH_4$ with the resultant exothermic process, which leads to an irreversible hydrogen release of $\approx$10 wt%.[39]

Unfortunately, combination of favorable thermodynamics (which means moderate operating temperature and excellent reversibility) with other main characteristics has not been attained via H^+/H^- coupling so far. In general, the potential vehicular application of H^+/H^- coupling materials is hampered by two primary obstacles: a high kinetic barrier and the release of poisonous gases. Similar to the destabilized system, multiphase reactions introduced by combining H^- and H^+ sources add to the kinetic barrier associated with mass transport and interface reactions. An effective solution to this issue is to develop novel molecular complexes comprising both H^+ and H^-. The favorable dehydrogenation kinetics of ammonia borane (AB)[40,41] and $Mg(BH_4)_2 \cdot 2NH_3$[42] may be regarded as demonstrations of this approach, although complicated reaction pathways are involved in the dehydrogenation reaction. However, the key issue related to the vehicular application of most H^+/H^- coupling systems (typically M–N–H systems) is the concomitant release of poisonous NH_3 upon dehydrogenation, which reduces the proton conductivity of proton-exchange membrane in fuel cells.

Currently, elimination of NH_3 byproduct remains a grand challenge in developing M–N–H systems, which is almost inevitable while using amides/imides as the H^+ source. However, when $C^{nano}H_x$ was used as alternative H^+ source, another byproduct hydrocarbon was released.[43]

2.2. Cation/Anion Substitution and Exchange

The undesirable thermodynamic stabilities of all hydrides are essentially related to their intrinsic binding characteristics. Appropriate substitution of cation and/or anion in host structures is able to influence the binding state and thereby alter the dehydrogenation thermodynamics and kinetics to some extent. In this regard, considerable efforts have been directed toward complex hydrides and chemical hydrides. It is noteworthy that theoretical calculations play a crucial role in the identification of thermodynamically favorable materials and many promising materials are proposed. However, substitution of reversible materials is plagued by the cycling stability of the substituted cation/anion, which is prominent as the complete decomposition/restoration of the lattice is required (typically for complex hydrides).[14] Therefore, only a portion of candidates were experimentally prepared and evaluated.

Cation substitution attracts much interest due to the relatively large availability of metal cations. In an attempt to destabilize $LiBH_4$, Miwa et al. focused on the charge compensation effect of Li^+ and proposed the partial substitution of more electronegative elements for Li to lower the thermodynamic stability.[44] Although preliminary studies suggest the favorable effects of Cu substitution,[44] it appears to be questionable whether the proposed $Li_{1-x}Cu_xBH_4$ composition would remain upon cycling. In the kinetic modification study of a Li–Mg–N–H material, several potassium salts were found to be highly effective in lowering the peak dehydrogenation temperature (up to 54 °C).[45] Structural analysis suggests that potassium substitution is responsible for the kinetic enhancement by forming the K–N bond.[45] On the other hand, intensive efforts in modifying the irreversible thermal-decomposition performance of AB lead to promising metal amidoborane materials by stabilizing parent AB, which is accomplished through the substitution of the protonic amine-hydrogen by a stronger electron-donating metal. For instance, the substitution of one H in the NH_3 group by the more electron-donating Li and Na affects the intramolecular B–N, B–H, and N–H chemical bonds and may facilitate intermolecular B–H···H–N interactions (Fig. 2).[46] As a consequence, encouraging thermodynamic modification is attained in both substituted AB materials: their dehydrogenation enthalpies are tuned to be −3 to −8 kJ mol^{-1} H_2 compared with approximately −20 kJ mol^{-1} H_2 of AB.[46,47] Notably, the Li substitution also leads to combined effects in lowering peak dehydrogenation temperature (by ≈30 °C) and improving hydrogen purity, coupled with high hydrogen capacity (≈10 wt%).[46,47]

Anion substitution acts as an alternative route to tune the thermodynamic stability of complex hydrides. Kang et al. demonstrated a substantial increase in the plateau pressure of TiF_3-doped Na_3AlH_6[48] and attributed the thermodynamic destabilization to the substitution of F^- in the hydrogen sublattice.[49] Similar effects have also been predicted by forming a F^--substituted $LiBH_4$ material.[50] These results highlight the positive role of F^- substitution for destabilizing alanates and borohydrides.

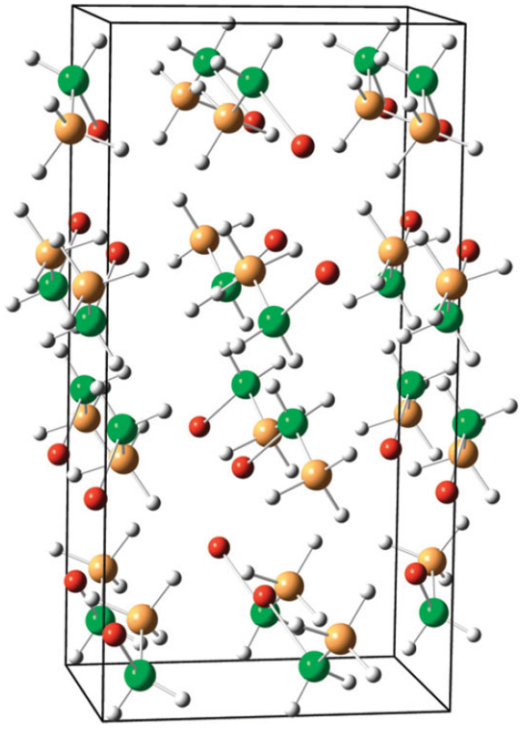

Figure 2. Schematic diagram of the crystal structure of $LiNH_2BH_3$ and $NaNH_2BH_3$ determined from high-resolution X-ray powder diffraction data at room temperature. Boron is represented by orange spheres, nitrogen by green spheres, hydrogen by white spheres, and lithium (or sodium) by red spheres. Reproduced with permission from Reference [46]. Copyright 2008, Nature Publishing Group.

Rather than engendering property enhancement of host materials, cation/anion exchange (or metathesis reaction) has been extensively employed to synthesize novel HSMs, which encompasses a wide range of materials including alanates, borohydrides, AB-related compounds, and even CNTs.[51–56] This approach significantly promotes the development of metal borohydrides. A generalized reaction route may be described as

$$MR_x + xM'BH_4 \rightarrow M(BH_4)_x + xM'R \quad (7)$$

where M represents an alkaline-earth metal or transition metal, for example, Mg, Zn, Ti; M′ is Li or Na; R is Cl or F.[52–54] Further, varying the ratio between reactants allows the formation of mixed metal borohydrides (e.g., $LiSc(BH_4)_4$) in the case of M = Sc, Zr, and Mn, M′ = Li or Na, and R = Cl or F.[57] The application of this approach largely depends on the use of ball-milling technique (mechanochemical route) or organic solvent (wet-chemical route). Ball-milling is a facile process, but limited by the presence of byproducts (e.g., M′R in Eq. (7)), which lowers the overall hydrogen capacity as an inert component. While being relatively complex, solution reaction

is a general approach for producing well-crystallized products. Thus, the combination of both approaches may lead to a more efficient route for synthesizing high-quality HSMs.

2.3. Catalytic Activation

Compositional modification (e.g., hybridization and cation/anion substitution) allows a substantial reduction in operating temperature via tuning the thermodynamic stability of host materials. However, favorable reaction thermodynamics do not necessarily ensure an appreciable de-/rehydrogenation rate at moderate temperatures while significant kinetic barriers remain untouched. In terms of reaction kinetics, a series of elemental steps are involved in de-/rehydrogenation reactions, which primarily include chemisorption (i.e., dissociation or recombination of H_2), interface reaction (e.g., nucleation), and diffusion (or mass transport). To overcome kinetic limitations, it is crucial to identify and reduce the energy barrier associated with the rate-limiting step for a specific reaction.

Catalysts are widely used to increase the hydrogen sorption rate by lowering the activation energy of de-/rehydrogenation reactions. An obvious advantage of catalytic addition is that a small amount of an efficient catalyst results in a significant kinetic enhancement coupled with negligible capacity loss. Currently, the majority of catalytic reactions involved in HSMs can be described as heterogeneous catalysis in solid–gas and solid–solid reactions. The efficiency of such catalysts is influenced by a series of factors including the intrinsic activity, particle size, and morphology, as well as their dispersion and contact state within host materials. Previous catalyst studies have mainly focused on noble/transition metals and their compounds that are highly active in promoting dissociation or recombination of H_2, which demonstrated their efficiency in metal hydrides by facilitating chemisorption and nucleation steps. Recently, significant advances have been achieved in understanding the catalytic mechanism involved and the identification of novel catalysts such as nanostructured carbons, complex hydrides, and ionic liquids, some of which are effective in lowering the kinetic barrier associated with diffusion (or mass transport).

In addition to a high T_{de} (i.e., thermodynamic limitation), the potential practical application of MgH_2 is hampered by the slow hydrogen sorption rate (i.e., kinetic limitation) as well. Extensive catalyst studies indicate that most noble metals and transition metals are capable of improving the hydrogen sorption rate of MgH_2 at $\approx$300 °C, yet exhibit a limited activity at moderate temperatures. The use of metal compounds allows further improvement by varying the valence and anion. In particular, the discovery of Nb_2O_5 as a superior catalyst promotes not only the identification of efficient catalysts among transition-metal compounds but also the understanding of the catalytic mechanism involved.[58] It has been proposed that the multivalency of transition-metal cations and the tailoring role of specific anions in compounds are responsible for the higher catalytic activity towards hydrogen dissociation/recombination relative to transition metals, the latter of which is realized through the appropriate chemical interaction between compound catalyst and host material.[59,60] Furthermore, substantial kinetic enhancement can be attained by the use of nanostructured Nb_2O_5 at moderate temperatures, which is presumably due to the improved efficiency of catalytic activation by reducing particle size and promoting dispersion.[61]

Complex hydrides with favorable thermodynamics may also confront a high kinetic barrier. For instance, $NaAlH_4$ was not considered suitable for reversible hydrogen storage until the discovery of Ti-based catalysts that are capable of substantially accelerating its de-/rehydrogenation reactions at moderate temperatures.[62] Particular attention then focused on the clarification of the underlying catalytic mechanisms, and diverse assumptions have been proposed. Up to now, the mechanistic investigation remains a subject of great controversy. However, the interaction between the Ti-based catalyst and the host material is generally emphasized in understanding the nature of catalytically active species.[63] As a prototype system of catalyzed complex hydrides, the Ti-doped $NaAlH_4$ system not only has fundamental significance for mechanistic investigation, but also facilitates the rational design of novel catalysts for related materials. Another kinetically stabilized system is the Li−Mg−N−H material. While its favorable reaction enthalpy ($\approx$40 kJ mol^{-1} H_2) thermodynamically predicts a T_{de}(1 atm) of 90 °C, dehydrogenation with a reasonable rate is typically obtained at $\approx$200 °C, in which significant kinetic limitations from the interface reaction and mass transport are identified.[64] Only a few metal-based catalysts were reported to be active toward this material,[65] yet were far from being efficient. Unexpectedly, $LiBH_4$ has been identified to be a promising catalyst for the Li−Mg−N−H system.[66,67] Even the addition of 0.05 mol of $LiBH_4$ enables a substantial de-/rehydrogenation of Li−Mg−N−H at 140 °C.[67] In contrast to the stable metal-based catalysts, $LiBH_4$ interacts with host $LiNH_2$ to form a low melting-point solid solution $Li_4BH_4(NH_2)_3$.[66] Based on the downward shift of N−H stretching and the elongated N−H bond, it has been proposed that the weakening of the strong N−H bond may be responsible for the enhanced dehydrogenation kinetics.[67] This understanding highlights the significance of an appropriate interaction between catalysts and the host material in efficient dehydrogenation by activating strongly bound hydrogen in complex hydrides. In addition, in situ seeding was also developed as an effective strategy to lower the kinetic barriers associated with intermediate/product nucleation upon dehydrogenation of Li−Mg−N−H.[66,68] This approach may be generalized to multiphase systems kinetically limited by an interface reaction.

A peculiar heterogeneous catalyst worth mentioning is CNTs, which finds general use in the kinetic enhancement of both metal hydrides and complex hydrides. The effect of CNTs was first examined in the catalyzed MgH_2 material, in which multiwalled CNTs (MWCNTs) were used as coadditives with Zr and Ni to improve the capacity and hydrogen sorption rates.[69] A systematic investigation by Wu et al.[70] found that single-walled CNTs (SWCNTs) are superior to MWCNTs and some other commonly used carbon/non-carbon additives. They used a comparative study to preclude the primary role of SWCNTs as a milling agent and proposed that the favorable effect originates from the combination of its composition and unique structure, that is, the metal ''impurities'' contained promote the dissociation/recombination of hydrogen while the hollow tubular nanostructure facilitates the hydrogen diffusion by acting as rapid diffusion

channel and increasing the grain boundary of the host hydride.[70] Similar results were also observed in the SWCNT-catalyzed $NaAlH_4$, Li−Mg−N−H, $LiBH_4$, and Li−Mg−B−H materials.[71–74] On the basis of the characteristics of dehydrogenation from $LiBH_4$, SWCNTs were also proposed to function as a structure-directing agent by forming a network structure upon milling with host material, which shortens the diffusion distance and mitigates particle agglomeration/sintering.[73,74] In addition, theoretical calculations also suggest that the catalytic effect of SWCNTs arises from the high electron affinity determined by the curvature of the graphitic sheet.[75] Clearly, these results emphasize the importance of morphology and nanoscale effect in tailoring the catalytic efficiency.

The capability of SWCNTs in facilitating hydrogen diffusion also suggests that comprehensive effects may be expected while combining SWCNTs with metal catalysts. A prototype catalyst of such type is the so-called as-prepared SWCNTs, which contain a large amount of transition-metal particles (typically Fe/Co/Ni) and exhibit a higher activity relative to purified ones.[72,73] Notably, the recently developed VTi/CNT catalyst was found to be one of the most active catalysts for MgH_2.[76] Accordingly, a strategy for designing composite catalysts is proposed: active alloys can be used to enhance the kinetics while incorporating CNTs to increase the reversible capacity.[76,77] However, systematic analyses of reaction kinetics and microstructure characterizations are required to gain further insight into the mechanism of CNTs in accelerating hydrogen diffusion.

Another significant aspect in the catalytic activation of HSMs involves hydrogen generation from the solid–liquid interaction. One representative example is the catalytic hydrolysis of $NaBH_4$. $NaBH_4$ is stabilized in its aqueous solution by adding alkali (e.g., NaOH) under ambient conditions and catalysts are used to accelerate the hydrolysis reaction while hydrogen is required. A catalyst is the key to achieving controlled hydrogen release from the hydrolysis reaction of $NaBH_4$. Noble metals/alloys (e.g., Ru, Pt, and PtRu alloys) exhibit favorable combination of catalytic activity and cyclic stability,[78,79] but their high cost has stimulated extensive efforts in identifying more affordable alternatives. Several transition metals and their alloys (e.g., Co and its alloys) are found to be competitive in terms of cost and catalytic activity.[80,81] However, the problematic deactivation during cycling remains a challenge and only few works have dealt with this issue. From the viewpoint of practical application, this is of great significance under any occasions and thus deserves intensive investigation in future work. Here, it should be pointed out that the combined constraints of low capacity, high cost, low regeneration efficiency, and problematic hydrolysis product currently preclude the solution-based $NaBH_4$ system from any vehicular application.[82] Provided that the production cost could be decreased to an acceptable level, catalytic hydrolysis of $NaBH_4$ may be a solution for a portable hydrogen source.

In contrast to most catalyzed HSMs, which are based on heterogeneous catalysis, dissolving AB into solvents enables more efficient homogeneous catalysis, which is characterized by molecule-level dispersion/contact of catalyst within the host material. Catalytic dehydrocoupling of AB in organic solutions (e.g., THF and polyether) in the presence of transition-metal complexes is a typical route to release hydrogen at moderate temperatures (typically ≈45–60 °C).[83] Alternatively, ionic liquids are identified as both a novel solvent and an effective catalyst to replace volatile organic solvents.[84] However, the above two systems suffer from moderate hydrogen capacity as a result of the limited solubility of the host material in solvents.

In most cases, catalyst identification still relies on time-consuming screening, which is primarily due to the lack of mechanistic guidance and the complexity of catalytic reactions. Therefore, an in-depth understanding of the catalytic mechanism involved in kinetic enhancement is required in future work and will promote the rational design of novel catalysts.

2.4. Nanoscaling

Despite the demonstrated efficiency of catalytic activation, identification of efficient catalysts currently remains a challenge for several HSMs due to the complicated reaction pathways involved. Alternatively, significant kinetic enhancement can be achieved by simply tailoring grain/particle size to the nanoscale for the vast majority of HSMs. In general, nanoscaling is effective for overcoming the kinetic barriers associated with diffusion by increasing the diffusion rate and/or decreasing the diffusion distance.

2.4.1. Nanocrystalline Materials

Nanocrystalline materials are characterized by micrometer-sized particles comprising nanometer-sized grains. Notably, a large portion of grain boundaries were involved, which may serve as a fast diffusion path for active species and lead to an increased diffusion rate. High-energy ball-milling is widely used as an efficient technique to produce nanocrystalline materials. Zaluska et al. investigated the hydrogen-absorption kinetics of nanocrystalline Mg prepared by ball-milling and found that the absorption rate improved with the reduction of grain size upon increasing the milling time.[85] A positive correlation can be observed between kinetic enhancement and milling time for most kinetically limited solid HSMs. A noteworthy exception is the hydrogen release from $LiBH_4$, in which melting prior to dehydrogenation eliminates the desired effects from increased grain boundary. Two other contributing factors are also involved in the nanocrystalline materials prepared by ball-milling: the abundance of defects and lattice strain introduced, which need to be considered in understanding the resultant improvement of sorption kinetics.

2.4.2. Low-Dimensional Materials

Low-dimensional materials combine both nanoscale morphology and grains, which leads to a more significant kinetic enhancement compared with nanocrystalline materials. Similarly, a size–performance relationship is established for the dehydrogenation of $NaAlH_4$ nanoparticles supported on carbon nanofibers (CNFs), that is, a successive reduction in activation energy (from 116 to 58 kJ mol^{-1} H_2) with the decrease of particle size (from 1–10 μm to 2–10 nm).[86] Yet, such an enhancement is accomplished with unacceptable capacity penalty resulting from the use of carbon support. In the kinetic modification of the Li−N−H material, a more significant reduction in activation energy (by 119 kJ mol^{-1} H_2) was observed while comparing the

hydrogenation property of Li_2NH hollow nanospheres with that of micrometer-sized particles.[87] In addition to kinetic enhancement arising from shortening the diffusion distance, density functional theory (DFT) calculation results suggest that substantial thermodynamic modification may also be achieved by reducing the particle size of MgH_2 to the nanoscale (e.g., <1.3 nm).[88] Motivated by this, Li et al. prepared Mg nanowires with diameters of ≈30–50 nm and investigated their kinetic and thermodynamic properties. Compared to the ball-milled Mg powders, the activation energies of hydrogen absorption/desorption reactions are reduced dramatically from 120–140 to 33.5 and 38.8 kJ mol^{-1} H_2, respectively.[89] Unfortunately, a relatively slight reduction in reaction enthalpy was attained,[89] presumably due to the larger particle size than the desired value. However, the mechanism of kinetic enhancement in low-dimensional materials is still unclear. Although the nanoscale morphology shortens the diffusion distance and thus improves the de-/rehydrogenation rates, it fails to explain the substantially reduced activation energies in the absence of generating lower energy-barrier pathways. Such low activation energies may be related to the change of surface structure upon tailoring particle size to the nanoscale.[86]

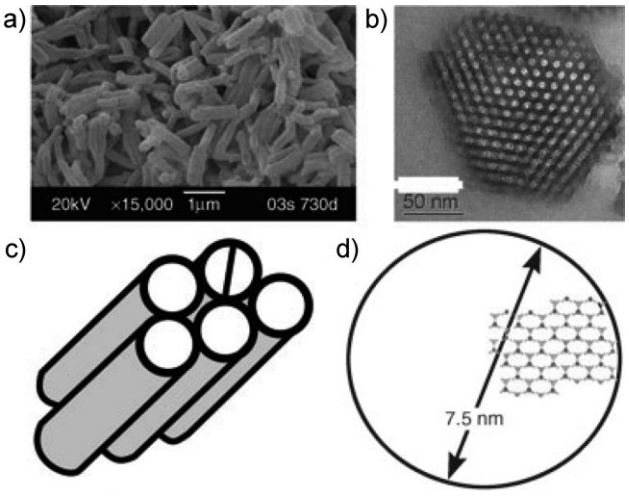

Figure 3. Schematic representation of AB in SBA-15: a) scanning electron microscopy (SEM) image of SBA-15; b) transmission electron microscopy (TEM) cross-sectional image of SBA-15; c) schematic representation of parallel channels in SBA-15; d) schematic representation of AB network in the cross section of a single pore. Reproduced from Reference [91].

2.4.3. Nanoconfined Materials

A major issue related to low-dimensional HSMs is the inevitable particle agglomeration and growth (even sintering occurs at elevated temperatures) driven by the high surface energy during hydrogen cycling, thus leading to significant property degradation. In addition, it is rather difficult to synthesize freestanding nanoparticles (e.g., several nanometers in diameter) for the vast majority of hydrides. Toward overcoming these two barriers, nanoconfined materials were developed, in which the use of nanoscaffolds ensures the combination of nanostructure and morphology stability. For multiphase reactions, nanoconfinement also limits the phase segregation. Thus, the overall effect is to improve the interfacial contact and interaction between reacting phases.[13]

Nanoconfinement was first used to improve the dehydrogenation kinetics of $NaAlH_4$ by loading the hydride into carbon aerogels.[90] Recently, synergetic enhancement in dehydrogenation properties was attained in nanoconfined AB composites by incorporating an AB solution into mesoporous silica (SBA-15) using the impregnation technique (Fig. 3).[91] A combination of reduced dehydrogenation temperature, enhanced dehydrogenation rate, and suppressed gas impurity release are realized compared to the bulk material. More importantly, the first hydrogen release step is modified to be nearly thermoneutral ($\Delta H = -1 \pm 1$ kJ mol^{-1}), which favors off-board material regeneration from an energetic viewpoint.[91] Further analysis of structural evolution suggests that nanoconfinement modifies the dehydrogenation properties by altering the intermolecular interaction of AB.[92] Similarly, $LiBH_4$ localized within a mesoporous carbon aerogel exhibits a decreased dehydrogenation temperature (up to 70 °C) and an increased cycling capacity.[93] Mechanistic investigation suggests that such favorable properties mainly originate from kinetic enhancement, which is closely related to a series of contributing factors such as enhanced diffusion rate, decreased diffusion distance, and facilitated nucleation. Favorable modification in thermodynamics is further achieved upon using microporous activated carbon as a nanoscaffold, in which an enhanced nanoconfinement effect can be expected.[94] However, the incorporation of "inert" structure-directing agents leads to an unacceptable capacity loss in all the above materials. Therefore, a lightweight nanoscaffold material with an optimized pore structure is required to achieve a high loading ratio while maintaining the nanoconfinement effect. In addition, the currently adopted loading technique is limited by the melting point, solubility, or wetting property of the hydride material as well as the difficulty of incorporating a multiple-phase system. A possible solution to the above issues is the development of an appropriate technique for in situ synthesizing nanoscaffold materials with a tunable structure, which may combine in situ loading with optimized pore structure. However, inadequate hydride/substrate bonding must be avoided, which otherwise would alter the reaction pathway and lead to the generation of undesirable byproducts.[95]

2.5. Morphology Tailoring and Surface Modification

Hydrogen storage by physisorption is a promising solution to the reversible high hydrogen uptake at ambient temperature. In contrast to chemisorption where hydrogen is chemically bonded within host hydrides, hydrogen molecules are adsorbed on the surface of adsorbents through a 4–10 kJ mol^{-1} interaction. Recently, such HSMs are of increasing interest as they obviate the daunting dilemma between T_{de} and reversibility as well as the heat exchange issue encountered in the hydrogen-rich but strongly bound hydrides. However, the low hydrogen binding energy essentially limits hydrogen uptake to no more than ≈1–2 wt% at ambient temperature. To meet the system requirements of an on-board hydrogen storage, the interaction

between hydrogen and the adsorbents must be enhanced and a binding energy of 15–20 kJ mol^{-1} H_2 is estimated to be desirable. Thus, an ideal adsorbent should possess sufficient accessible sorption sites of such binding energy to achieve high-capacity storage at ambient temperature.

Essentially, physisorption-based hydrogen storage is determined by two fundamental properties of adsorbents: accessible surface area and hydrogen binding energy. Morphology tailoring and surface modification are effective strategies for enhancing hydrogen capacity by increasing the accessible surface area and/or hydrogen binding energy. Morphology of materials determines their accessible surface area, and to some extent influences the hydrogen binding energy. A variety of nanostructured materials have been proposed as potential adsorbents on the basis of their unique or rationally designed morphology, such as microporous scaffolds,[96–99] nanotubes,[100–102] nanofibers,[103] nanohorns,[104] and hybrid nanostructures.[105] However, promising results are merely experimentally demonstrated in microporous adsorbents, which enable the highest specific surface area ever known and allow simultaneous control over hydrogen binding energy by optimizing pore size (which increases the hydrogen affinity of the porous material by overlapping the potential from the pore walls). Typically, a desirable pore structure (large proportion of uniform pores with appropriate size) can be attained by varying reactant precursors and synthesis conditions. Carbon material with a tunable pore structure was synthesized by using different starting carbides and chlorination temperature, in which an optimized pore structure leads to both a high specific surface area (≈2000 m^2 g^{-1}) and an increased hydrogen binding energy (up to 11 kJ mol^{-1}).[96] A micropore (1 nm or below) was found to be responsible for efficient hydrogen storage at ambient pressure and liquid-nitrogen temperature.[96] Alternatively, using zeolite as the template allows the development of carbon materials with narrow pore-size distribution (predominantly below 1 nm), which combines a high surface area (up to 3200 m^2 g^{-1}) with a high hydrogen binging energy (8.2 kJ mol^{-1}).[97] The leading candidate of microporous materials is metal–organic frameworks (MOFs), in which metal building units are connected by organic bridging ligands to form 3D networks with a uniform pore-size distribution. The characteristic structural and compositional flexibility offer great potential for developing an extensive class of promising microporous materials with extremely high specific surface areas (≈1000–6000 m^2 g^{-1}).[17] Interestingly, the structural flexibility of organic bridging ligands can also be used to dynamically sequester hydrogen molecules inside MOFs.[106] Similarly, polymers of intrinsic microporosity with narrow size distribution of micropores (0.6–0.7 nm) have also been synthesized, which exhibit moderately high hydrogen uptakes (1.43 wt% at 1 bar and 77 K).[98] However, in view of the structural limit, it seems unlikely that sufficient enhancements in the hydrogen binding energy would be achieved to realize a room temperature high capacity by merely tailoring the morphology.

Surface modification can be used to further enhance the hydrogen binding energy of adsorbents with tailored morphology, which involves novel types of interaction with hydrogen. Rather than strengthening the interaction with hydrogen molecules, hydrogen spillover by supported metal catalyst was proposed as a versatile approach to enhance the hydrogen uptake at ambient temperatures by enabling a stronger atomic hydrogen adsorption in a wide range of adsorbents including nanostructured carbons, MOFs, zeolites, and mesoporous silica.[18,107,108] Hydrogen molecules dissociate on the metal surface into hydrogen atoms, which then migrate via surface diffusion to adsorb on the host materials.[18] Upon adding 10 wt% Pt/ activated carbon (which contains 5 wt% Pt), the hydrogen uptake of IRMOF-8 was increased from 0.5 to 1.8 wt.% at 298 K and 10 MPa.[108] Notably, a hydrogen binding energy as high as 21 kJ mol^{-1} was reported.[18] However, the mechanistic understanding of the hydrogen spillover process is quite limited and a correlation between hydrogen adsorption and structural characteristics needs to be established in future work.[109] Further, the essential dependence of capacity enhancement by spillover on the availability of high binding energy sites suggests that even in the presence of spillover effects, incorporation of more high binding energy sites are necessary. Extensive research efforts have focused on decorating the surface of adsorbents with metal species to achieve this goal, which suggests that it is pivotal to develop a Kubas interaction between hydrogen and active metal sites.[19] Theoretical calculations on fullerenes,[110] CNTs,[111] ethylene,[112] and polymers[113] modified by transition metal atoms invariably predicted high hydrogen binding energy and hydrogen uptake on the low-coordinate metal species. Although no experimental data is available from the above materials as a result of the technical difficulty in materials synthesis, it has been demonstrated that incorporating the coordinatively unsaturated metal sites into MOFs significantly improves the hydrogen adsorption.[114–118] The strongest MOF–H_2 interactions (13.5 kJ mol^{-1}) are obtained through directly binding hydrogen molecules to the exposed metals.[119] Given that MOFs can be tailored to incorporate a large number of selected metal cations, further improvement can be anticipated and this presents a promising strategy for achieving the desirable hydrogen binding energy. In addition, a more surprising result was obtained in a Ti-decorated mesoporous silica, in which grafting Ti(III) benzyl species on the silica surface increases the hydrogen binding energy from 3.5 to ≈22 kJ mol^{-1}.[120] However, a significant improvement in hydrogen capacity has not been achieved at ambient temperature for all the above materials, which is primarily due to the limited number and accessibility of active metal sites. Therefore, combining large numbers of accessible active metal sites with high surface area and optimized pore size is critical in the development of novel adsorbents.

2.6. Summary

HSMs are important to provide safe and efficient vehicular hydrogen sources. Decades of efforts have been devoted to identifying potential HSMs that can meet the stringent requirements for on-board application. Hybridization leads to the development of several novel systems with favorable thermodynamic stability by creating new reaction pathways. Alternatively, cation/anion substitution in host structures tailors the intrinsic binding states and thus modifies the dehydrogenation thermodynamics and kinetics. Catalytic activation is a versatile and efficient manner to enhance the hydrogen sorption rate of kinetically stabilized materials by lowering the activation energy, which is applicable to both solid–gas and solid–liquid

interactions. Nanoscaling has been demonstrated to be particularly effective for overcoming the kinetic barrier associated with diffusion (mass transport), and the enhanced nanoscale effect may also result in thermodynamic modification. Utilization of nanoscale confining techniques offers new possibilities to address the dilemma between T_{de} and reversibility encountered in high-capacity hydrides. In contrary to the above-mentioned chemisorption mechanism, physisorption allows facile reversible storage at ambient temperature, in which morphology tailoring and surface modification currently play an important role toward achieving high hydrogen capacity.

None of the existing HSMs can currently meet the US DOE 2010 benchmark target. Therefore, continuous efforts are required to develop novel materials, and efficient synthetic techniques and strategies are necessary. In this regard, the role of organic chemistry is of increasing significance, which is widely used in hybridization, cation/anion substitution and exchange, catalytic activation, and nanoscaling. In particular, the combination of organic chemistry with cation/anion substitution and exchange significantly facilitates the synthesis of novel metal borohydrides and AB-based compounds.

3. Advanced Materials for LIBs

3.1. Introduction to LIBs

A LIB is mainly composed of an anode (negative), a cathode (positive), an electrolyte, and a separator. The positive electrode materials are typically Li-containing metal oxides with a layered structure (such as lithium cobalt oxide) or tunnel-structured materials (such as lithium manganese oxide). The negative electrode materials include insertion-type materials (such as carbon, $Li_4Ti_5O_{12}$, TiO_2, etc.), conversion-type materials (such as iron oxides, nickel oxides, cobalt oxides, etc.), and alloying-type materials (such as Si, Sn, etc.). The electrolyte should be a good ionic conductor and electronic insulator. Most of the electrolytes are based on the solution of inorganic lithium salts dissolved in a mixture of two or more organic solvents. The function of the separator is to prevent short circuiting between the negative and positive electrodes and to provide abundant channels for transportation of Li ion during charging/discharging.[121] When a battery is cycled, Li ions exchange between the positive and negative electrodes. LIB is also referred to a rocking-chair battery as Li ions "rock" back and forth between the positive and negative electrodes. LIB was commercialized in the early 1990s and has become the most important and widely used secondary battery. LIB shows advantages of high voltage, high energy density, long cycling life, good environment compatibility, and light weight over traditional lead-acid batteries and Ni-based batteries. LIBs are widely used as a convenient power source for various portable electronic devices. However, there are continuous demands for batteries with higher power and energy density and longer cycling life to power newly emerging electronic devices, advanced communication facilities, and in particular, EVs or HEVs. The energy density of a battery is mainly determined by its output voltage and specific capacity, which are dependent on the electrochemical properties of electrode materials. For different application fields, there are different requirements for batteries. For example, the rechargeable batteries for EVs or HEVs should have the ability to be charged sufficiently fast and the current available from the batteries should be high enough to produce a desirable power.

3.2. Electrode Materials for LIBs

3.2.1. Anode Materials

Commercial LIBs are usually based on carbonaceous anode materials, in which Li is inserted during charging. The resulting Li-interacted carbons show a low potential close to that of a metallic Li electrode. By using a carbonaceous anode, the knotty problem of dendrite formation in the initially employed Li metal anode can be avoided, and the safety and reliability of LIBs are improved. Carbon materials can be typically specified into three groups, namely, graphite and graphitized materials, ungraphitized soft carbon, and hard carbon.[122] Graphite is most widely used due to its stable specific capacity, small irreversible capacity, and good cycling performance. Mesocarbon microbeads (MCMBs) derived from petroleum or coal products exhibit desirable overall performance with moderate high capacity and excellent cyclability. The electrochemical properties of soft carbons heat-treated below 1000 °C and hard carbons are largely determined by their surface characteristics and pore structures. Hard carbon displays a high lithium storage capacity and good power capability, but poor electrical conductivity and a large irreversible capacity.[122,123] Although carbonous anode materials receive wide-range applications in commercialized LIBs, it is recognized that graphitic carbons suffer from solvent co-intercalation in propylene-carbonate-based electrolytes, which results in large interlayer expansion and subsequent degradation of the graphitic structure. More importantly, the gravimetric and volumetric capacity of carbon materials is limited. The rapid development of electronic devices and EVs demands a much higher energy density as well as a higher power density and a smaller irreversible capacity for anodes. Therefore, other elements, including Al, Si, Ge, Sn, Pb, Sb, and Bi, and their alloys or oxides, have been examined as anodes for LIBs. Among them, Si shows the highest gravimetric capacity of up to 4200 mAh g^{-1}. However, during charging and discharging, unavoidable large volume expansion of these electrode materials results in pulverization of the electrode materials and loss of electrical contact upon prolonged cycling, which cause rapid capacity fading that hinders their practical use as electrodes.

3.2.2. Cathode Materials

Basically, there are two kinds of cathode materials for LIBs.[124] The first contains layered compounds with an anionic closely packed lattice in which alternate layers between the anion sheets are occupied by a redox-active transition metal, and Li ions can insert into the essentially empty remaining layers. This group is exemplified by $LiTiS_2$, $LiCoO_2$, $LiNi_{1-y}Co_yO_2$, and $LiNi_yMn_yCo_{1-2y}O_2$. The materials in the second group have more open structures, including many vanadium oxides, the tunnel compounds of manganese dioxides, and transition-metal

phosphates. The first group, because of their more compact lattices, has an inherent advantage in specific volumetric energy density, but some in the second group, such as $LiFePO_4$, show advantages of much lower cost and higher rate capability.[124] Specifically, $LiCoO_2$, $LiMn_2O_4$, and $LiFePO_4$ are the most widely used cathode materials.

$LiCoO_2$ has desirable electrochemical properties, such as good structural stability and moderately high capacity, and the fabrication of high-quality $LiCoO_2$ is facile. The major drawbacks of $LiCoO_2$ are high cost and toxicity.[125,126] The use of manganese oxides in LIBs is stimulated due to their low cost and environmental impact. The discharge curve for $Li_xMn_2O_4$ has two concentration portions, occurring near 4 V and 3 V versus Li^+/Li, which correspond to the addition of one more Li, resulting in $Li_2Mn_2O_4$.[127] The pristine $LiMn_2O_4$ shows severe capacity fading upon cycling. This problem can be tackled by the substitution of different cations (Li, B, Mg, Al, Fe, Co, Ni, or Zn) or by the introduction of nanodomain structures.[128,129] $LiFePO_4$ possesses advantages of potentially low cost, rich resources, and environmental friendliness.[130] The discharge potential of $LiFePO_4$ is about 3.4 V versus Li^+/Li and no obvious capacity fading is observed even after several hundred cycles. Its capacity approaches 170 Ah kg^{-1}, higher than that of $LiCoO_2$ and comparable to stabilized $LiNiO_2$. However, this material has a very low electrical conductivity at room temperature. Therefore, to achieve its theoretical capacity, the current density has to be controlled at a very low level.[131] Efforts have been made to improve the conductivity of $LiFePO_4$ by carbon-coating, metal-rich phosphide nanonetworking, super-valence ion-doping, and aliovalent substitution.[132,133]

3.3. Advanced Materials for LIBs

The ever-enlarging markets of portable electronic products, advanced communication facilities, and EVs/HEVs stimulate and require the development of LIBs with superior performances, such as higher energy density, larger power density, and longer cycling life. To obtain LIBs with superior performances, the morphology, composition, ionic diffusion kinetics, conductivity, and surface characteristics of electrode materials need to be optimized. The studies on the development of electrode materials for high-performance LIBs are quite active, and considerable advancement has been made based on smart material-design strategies.

3.3.1. Nanostructuring

Traditional electrode materials for LIBs are on the milli- or microscales in size. Recently, more and more nanostructured materials, including 0D nanoparticles, 1D nanowires and nanotubes, 2D nanosheets and nanoflakes, and core–shell structured nanomaterials have been explored for the electrodes of LIBs. Due to their small size and large surface area, the contact area between the electrode material and the electrolyte is increased and the distance that Li ions have to diffuse across the electrode is shortened. Therefore, a faster charge/discharge ability, that is, higher rate capability, can be expected for the nanomaterial-based LIBs. For some materials with high Li storage capacity made by forming Li-containing alloys (such as Si, Sn, etc.), a large volume change is accompanied with the charging/discharging process, which results in a large inner stress and exfoliation of the electrode material and a rapid capacity fading upon prolonged cycles. By using nanomaterials, the lattice stress can be largely alleviated due to their small grain size and large portion of surface atoms, and thus their cycling performance can be improved.

Low-Dimensional (LD) Electrode Materials: Powders or particles of metal oxides, metal phosphides, and oxysalts with diameters ranging from several to tens of nanometers have been investigated as the electrode materials of LIBs. Due to their nanoscale particle size, the Li-ion diffusion path can be shortened and the inner stress caused by Li insertion/desertion can be lowered. Consequently, improved rate performance and cyclability can be anticipated. Anode materials of metal oxides, phosphides, and oxysalts like MoO_3,[134] TiO_2,[135] SnO_2,[136] MoP_2,[137] $ZnCo_2O_4$,[138] and $FePO_4$[139] in the nanoscale were recently reported, and nanoparticles of $Li(Ni_{1/3}Co_{1/3}Mn_{1/3})O_2$[140] and $LiCoO_2$[141] were prepared as the cathode of LIBs. As an example, Hu et al. prepared a nanometer-sized rutile TiO_2 that shows a high specific charge capacity of 160 and 70 mAh g^{-1} after 50 cycles at rates of C/20 and 30C (*n*C being the charge/discharge cycles in $1/n$ hour) respectively, which are much higher than those of micrometer-scale rutile TiO_2. The improved electrochemical properties of the nanosized TiO_2 are attributed to their shorter transport length for both electrons and Li ions, as well as a larger electrode–electrolyte contact area.[135]

One problem for these nanoparticles is their relatively low conductivity. To solve this problem, Paek et al. prepared a SnO_2 nanoparticle/graphene composite, where graphene nanosheets confine the volume change of SnO_2 and serve as an electronic conductive medium in the electrode.[142] Thus, the composite anode displays a desirable rate capability and high capacity. Another problem is that when the particle size of lithium transition metal oxides is reduced to the nanometer scale, their stability becomes worse. To suppress the dissolution of metals in electrolytes, coatings of phosphates[143] and oxides[144] on these nanoparticles were reported. As a result, the cycling performance of these nanosized cathode materials were improved significantly.[145]

Compared to nanoparticles, 1D materials including nanowires,[146–149] nanorods,[150] nanofibers,[151] and nanotubes,[152,153] are propitious to both improving electrical conductivity of the electrode and allowing enhancement of Li diffusion into the nanostructure. Especially for nanotubes with a hollow inner core, the inner stress caused by the volume change can be better alleviated. Park et al. reported that SnO_2 nanowires synthesized by a thermal evaporation and self-catalyzed growth procedure showed a high initial Coulombic efficiency and an improved cyclic retention compared with those of SnO_2 powders and SnO_2 nanowires containing Au catalyst particles.[146] They found that the electrochemical performance of SnO_2 nanomaterials is closely related to their morphological features.[147] Lou et al. reported a needle-like Co_3O_4 nanotube that has a non-constant diameter in the range of 150–400 nm and a length up to 10 μm. A very high charge capacity of 950 mAh g^{-1} is attained in the first cycle, and about 97% of this high capacity is retained after 30 cycles. At a relatively high current density of 100 mA g^{-1}, the

performance of the Co_3O_4 nanotubes is basically unaltered.[153] Single-crystalline spinel $LiMn_2O_4$ nanowires and nanorods were reported by Hosono et al.[148] and Kim et al.[150] These materials show an improved rate capability and cycling performance compared to the commercially available samples. The enhanced performances of the nanotubes and nanowires are attributed to their 1D morphology and the high quality of the single crystal. Nam et al. reported self-assembled Co_3O_4 nanowires and hybrid Au–Co_3O_4 nanowires using a M13 virus as template, and prepared a 2D organized assembles of these nanowires on a polymer film. The assembly produced lightweight, flexible, and transparent active material/substrate multilayers as free-standing films. It was found that a cell constructed by the assembled Co_3O_4 nanowires/polymer layer/Li can deliver 94% of its theoretical capacity at 1.12C and 65% at 5.19C. These self-assembled materials are anticipated to find applications in thin, flexible LIBs.[154]

Zhang et al. synthesized nickel silicide nanosheets and nanobelts (Fig. 4a and b) by a thermal chemical reaction method using nickel and $SiHCl_3$ as starting materials. The nanosheets were 20–80 nm in thickness and several to tens of micrometers in length and width. Two phases of Ni_3Si and $Ni_{31}Si_{12}$ were found to coexist in the nanosheets. The Ni silicide nanosheets stably delivered a high capacity of 540 mAh g^{-1} after 20 cycles (Fig. 4c). The excellent electrochemical performance of the nanosheets was attributed to its large surface area, small thickness, and proper phase composition, which bring more reaction sites for charge transfer on the surface, a shorter diffusion length for Li ions, and an enhanced ability to accommodate large volume expansion and contraction during the insertion and extraction of Li ions.[155]

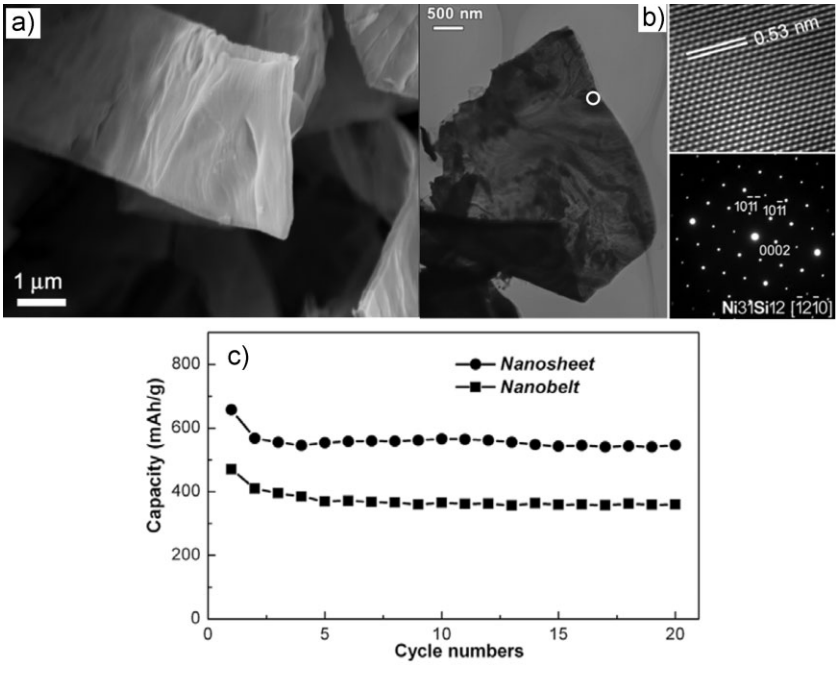

Figure 4. a) SEM image of the nickel silicide nanobelts. b) TEM image of a nickel silicide nanosheeet. c) Electrochemical cycling performance of the nickel silicide nanobelts and nanosheets. Reproduced with permission from Reference [155]. Copyright 2008, IOP Publishing.

Similarly, layered SnS_2 nanoplates[156] and α-Fe_2O_3 nanoflakes[157] were reported. These 2D materials present a finite lateral size and enhanced open-edges, which facilitate Li-ion diffusion through active materials and decrease the overvoltage caused by Li alloying.[156]

Core/Shell-Structured Nanomaterials: Electrode materials exhibiting a high capacity, long cycling life, and good rate capability are highly desirable. However, it is difficult to achieve all these objectives simultaneously for a single-phase material even with reduced dimensions. Thus, the design and synthesis of hybrid nanoscale electrode materials containing two or more components have been widely investigated, such as core/shell nanostructures with synergistic functionality of the composing components. There are two main categories of core/shell nanostructures, namely, core/shell nanoparticles and coaxial nanocables. The core part is usually an electrochemically active material with high Li storage capacity, and a thin carbon layer is most frequently used as the shell, which functions in enhancing electrical conductivity, preventing aggregation, improving chemical stability, and buffering stress of the inner nanoscale active material.[158–160]

Wang et al. prepared a core/shell-structured $LiFePO_4$/C composite by an in situ polymerization restriction. The composite was composed of a highly crystalline $LiFePO_4$ core with a size of 20–40 nm and a semigraphitic carbon shell with a thickness of 1–2 nm. The discharge capacity of the prepared composite was 168 mAh g^{-1} at 0.6C, and it delivered a capacity of 90 mAh g^{-1} at a high rate of ≈60C. The prepared composite also exhibited an excellent cycling performance, with less than 5% discharge capacity loss over 1100 cycles at 0.6C.[160]

Distinct from the above carbon-coated hybrid materials, Sun et al. prepared a concentration-gradient cathode material by coprecipitation. Each of the spherical particles had a central core rich in Ni and a Mn-rich outer layer with decreasing Ni concentration and increasing Mn and Co concentrations to the surface (Fig. 5). The composition of the core was a nickel-rich layered $Li[Ni_{0.8}Co_{0.1}Mn_{0.1}]O_2$, which can satisfy high energy and power requirements. In the outer layer, the reactive nickel ions were gradually replaced with manganese ions to provide outstanding cycling life and safety. The resulting surface composition was $Li[Ni_{0.46}Co_{0.23}Mn_{0.31}]O_2$, which was much more stable in contact with the electrolyte than the core material. A high capacity of 209 mAh g^{-1} was achieved. This concentration-gradient material also showed good cyclability, thermal stability, and safety. The enhanced electrochemical performance was attributed to the superior stability of the concentration-gradient outer layer and the surface composition of $Li[Ni_{0.46}Co_{0.23}Mn_{0.31}]O_2$.[161]

Kang et al. reported a coated $LiFePO_4$ nanomaterial with high rate capability. Their synthesis strategy was to create an appropriate off-stoichiometry in the starting materials of

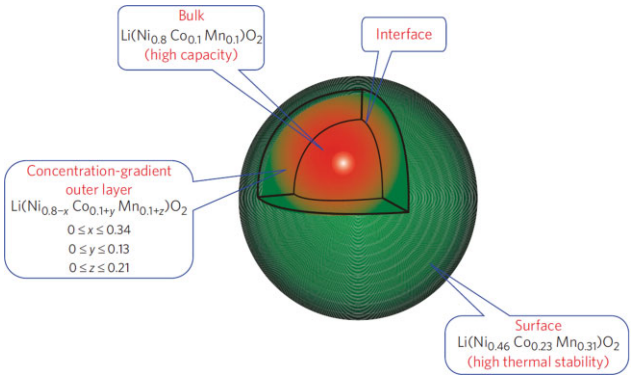

Figure 5. Schematic diagram of a positive-electrode particle with Ni-rich core surrounded by concentration-gradient outer layer. Reproduced with permission from Reference [161]. Copyright 2009, Macmillan Publishers Limited.

Li_2CO_3, $FeC_2O_4.2H_2O$, and $NH_4H_2PO_4$ so that the coating constituents phase-separate from $LiFePO_4$ when it forms during heat treatment, thereby creating the active material and coating in a single process. The particle size of the obtained material was about 50 nm, and a poorly crystallized thin layer was coated on the particle surface. This active material possessed extremely high discharge rates: at 200C (corresponding to a 18 s discharge time) and 400C, more than 100 and 60 mAh g^{-1} were obtained, respectively. While the nanometer-sized particles definitely contribute to the high discharge rate capability by reducing the ion and electron transport path, the coating is considered to play a crucial role. The amorphous nature of the coating removes the anisotropy of the surface properties and enhances the delivery of Li ions to the (010) facet of $LiFePO_4$ where it can be inserted. It is also plausible that the disordered nature of the coating material modifies the surface potential of $LiFePO_4$ to facilitate the adsorption of Li ions from the electrolyte by providing different sites with a wide range of energies that can be matched to the energy of Li in the electrolyte.[162] However, Zaghib et al. commented on this work very recently and pointed out that the limiting rate at which a LIB can be charged/discharged does not come from the cathode but from the anode, and the statement that the $LiFePO_4$-based LIB for EVs can be charged in seconds or even minutes is not justified.[163]

Wang et al. reported SnO_2/C coaxial nanotubes that deliver a capacity of 542 mAh g^{-1} over 200 charge/discharge cycles at 0.5C,[164] where "i) the tubular organization of SnO_2 nanoparticles limits the mobility of particles during cycling; ii) the flexible CNT skin further improves the stability of SnO_2 particles against agglomeration; iii) the large internal void in the core/shell construction buffers well against the local volume change in Li−Sn alloying and de-alloying reactions; iv) the good electrical conductivity of CNTs is useful in keeping the SnO_2 nanoparticles electrically connected during charging and discharging stages; and v) the porosity of the SnO_2 nanotubes and the large surface area available from both the interior and exterior of the core/shell nanotubes also contribute positively to Li-ion diffusion."[164] In addition, core/shell structured MnO_2/CNT,[165] crystalline-amorphous core/shell Si nanowires,[166] $Sn_{78}Ge_{22}$@C nanowires,[167] mesoporous Si@C nanowires,[168] Sn nanocluster/SnO_2 nanowires,[169] and SnO_2/In_2O_3 nanowires[170] were also reported.

3.3.2. Designing Unique Configurations

Commercially used electrode materials are usually solid particles with sphere-like or irregular configurations. It was recently found that specific design and optimization on the configuration of electrode materials is an effective manner for enhancing electrochemical performance.

Hollow Structures: As pointed out by Lou et al., the advantages brought by hollow structured electrode materials are mainly that the cavities in hollow structure may provide extra space for the storage of Li ions, beneficial for enhancing specific capacity, that a hollow structure is often associated with a larger surface area and a reduced effective diffusion distance for Li ions, leading to better rate capability, and that the void space in hollow structures buffers against the local volume change during Li insertion/desertion and is able to alleviate pulverization and aggregation of the electrode material, hence improving cycling performance.[171] The composition of hollow structures can be simple elements, oxides, or hydrates with high Li storage capacity, such as Si,[172] Sb,[173] TiO_2,[174] SnO_2,[175] Fe_2O_3,[176] V_2O_5,[177] and VOOH.[177]

Chen et al. synthesized a hollow nest-like Si nanosphere composed of fine and flexible nanowires with diameters of 5–10 nm. Unlike solid Si particles, the nest-like Si nanospheres exhibit good cycling performance and high rate capability. Moreover, a hollow structure can increase the Coulombic efficiency of the electrode due to the increase of active sites for reversible electrochemical Li storage.[172,178] Cao et al. reported a hollow microspherical structure composed of V_2O_5 nanorods. The hollow microspheres in combination with the porous and rugged nanorod structure are favorable in reducing the diffusion length of Li ions. Thus, the intercalation and extraction processes of Li ions are of much higher efficiency, which leads to a high charge/discharge efficiency of 97.2%.[179]

Yu et al. prepared a thin-film anode material composed of hollow porous spheres with a mean diameter of 5 μm. Each of the porous spheres consists of a multideck-cage structure, where the thickness of the "grids" ranges from around 60 to 100 nm (Fig. 6a). The ternary $Li_2O-CuO-SnO_2$ composite (molar ratio Li/Cu/Sn = 1:1:1) thin-film electrode shows a high reversible capacity of 1185.5 mAh g^{-1}, a low initial irreversible capacity loss of 17.6%, and nearly 100% capacity retention after 100 cycles at 0.5C (Fig. 6b). Excellent rate capability is also demonstrated with an 8C rate capacity of 525mAh g^{-1}. The outstanding electrochemical performance of the $Li_2O-CuO-SnO_2$ electrode is attributed to its special multideck-cage morphology and the ternary composition, where Li_2O can suppress the aggregation of Li−Sn alloy, while the function of CuO is to combine more Li in Sn and to improve the discharge capacity by enlarging the voltage range. In addition, the nanostructured particles shorten the transport lengths of Li ions, while the unique porous structure ensures a large electrode–electrolyte contact area and confers the ability to accommodate the volume change during charge/discharge processes.[180]

Urchin-like Structures: The so-called urchin-like structure usually contains a microscale spherical inner core, from which numerous nanowires or nanofibers protrude out. Compared with

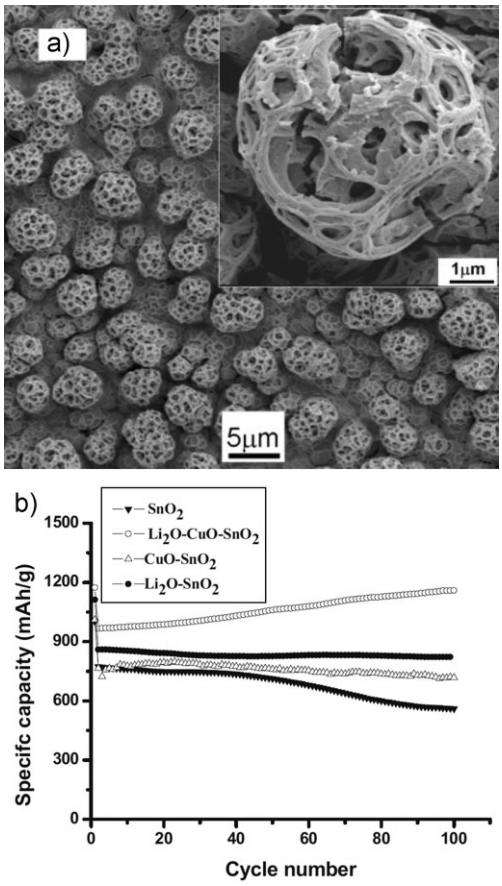

Figure 6. a) SEM image of the as-deposited thin film composed of a multideck-cage structured $Li_2O-CuO-SnO_2$. b) Capacity retention of the thin-film electrodes cycled between 0.01 and 3 V versus Li^+/Li at 0.5 C. Reproduced from Reference [180].

the normal spherical electrode materials, the protruding spines of urchin-like structures may connect with one another to form a 3D network and hence improve the conductivity of the electrode. In addition, the voids formed between the spines and the inner core may facilitate the contact of active material with electrolyte and enhance Li-ion transport. Urchin-like electrode materials composed of carbon,[181,182] α-MnO_2,[183] and CuO[184] were recently reported.

Zhang et al. designed and fabricated an urchin-like anode material for LIBs, where microscale graphite materials act as the core and CNFs as the surrounding spines (Fig. 7a). CNFs with an outer diameter of ≈100 nm and length of several micrometers were homogeneously grown on the surface of the natural graphite spheres by catalytic chemical vapor deposition (CVD). Detailed characterizations of interface structure indicated a sound combination between the CNFs and the graphite spheres (Fig. 7b). The CNF-coated graphite spheres display a significantly improved cycling performance and better rate capability compared to the original graphite spheres and the mechanical mixture of graphite spheres and CNFs (Fig. 7c). Moreover, the designing concept of an urchin-like nano-/microstructure for the LIB electrode is applicable to other materials, such as Cr_2O_3. The functions of CNFs homogeneously grown on the surface of the microscale active materials were analyzed: i) forming a continuous conductive network in the bulk of electrodes to decrease electrode polarization, beneficial to the improvement of cyclic performance; ii) improving the adsorption and immersion of electrolyte on the surface of electroactive materials to facilitate the electrode reaction kinetics; iii) as a buffer among electroactive materials due to their superior resiliency, thus restraining cracking and crumbling, and keeping the integrity of the electrode; and iv) being an electroactive material itself without notably lowering the whole capacity of anode materials.[181]

Other Special Configurations: Except for the above hollow and urchin-like structures, electrode materials with other special configurations, such as desert-rose structured $LiCoO_2$[185] and teardrop-shaped $SnP_{0.94}$,[186] have also been reported. Chen et al. synthesized the desert-rose structured $LiCoO_2$ by a molten hydroxide flux method. The desert-rose $LiCoO_2$ shows desirable high rate performance, ascribed to its special morphology where the surfaces of the balls are covered by Li-insertion active surfaces. This morphology also appears to have an advantage over $LiCoO_2$ particle cathode materials, since the individual particles within the ball are well electrically connected.[185]

3.3.3. Control of Pore Structures

The diffusion of Li ions in electrolyte, electrodes, and at the electrolyte/electrode interface influences directly the electrochemical performance of LIBs, especially for rate capability. Therefore, the pore structure of electrode materials is an important factor that largely determines the transport behavior of Li ions. The typical porous materials for the electrode of LIBs are categorized into 3D and 1D porous materials.

3D Porous Structure: 3D macroporous materials are composed of well-interconnected cores and walls with a thickness of tens of nanometers, and these materials can be readily used for enhancing the rate performance of LIBs since the solid-state diffusion length is much shorter and their relatively large surface area can also benefit the charge-transfer rate. In particular, 3D macroporous carbons provide several advantages for applications in LIBs: they can be prepared in a monolithic form and used as an active electrode without adding binders or conducting agents; their well-interconnected wall structure can provide a continuous electron pathway, yielding a good electrical conductivity as Li ions in electrolytes can be easily accessible to the 3D macroporous pore surfaces.

Lee et al. synthesized a 3D macroporous monolith of carbon via a resorcinol-formaldehyde sol–gel process. The porous monolith shows a superior rate capability compared to spherical carbon and bulk carbon monoliths, but displays low first Coulombic efficiency and limited volumetric density due to a large surface area and highly porous feature. SnO_2 nanoparticles were then coated on the surface of the 3D macroporous carbon to enhance the energy density. As a result, the first discharge capacity of 278 mAh g^{-1} was obtained, which is about 25% higher than that of pure 3D macroporous carbon.[187] Wang et al. prepared monolithic carbon/carbon nanocomposites with a hierarchical macroporous structure by filling a 3D ordered macro-/mesoporous carbon monolith with *N*-doped graphitic carbon via a CVD process. The coating on the macro-/mesoporous surface with chemical vapor deposited soft carbon significantly reduces the

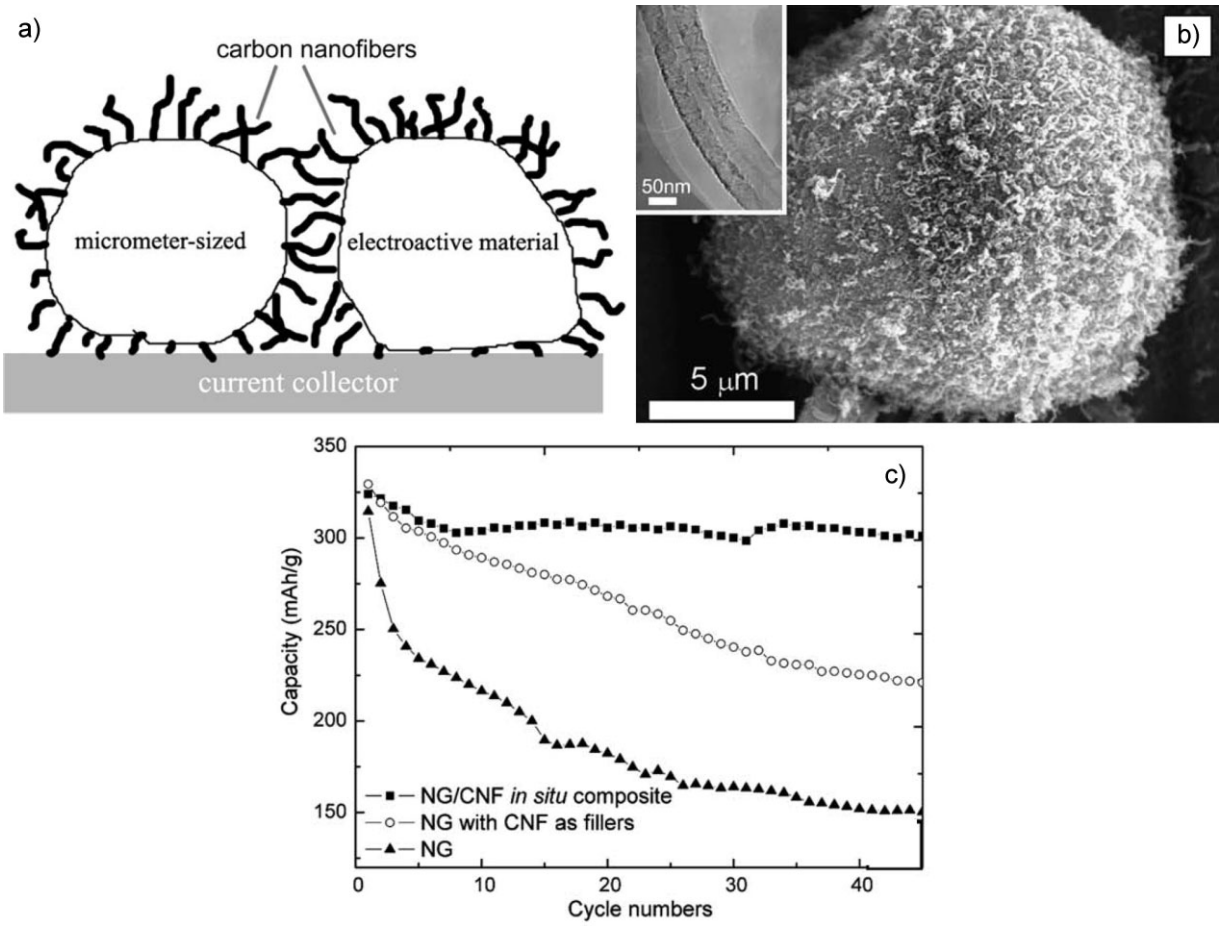

Figure 7. a) Schematic diagram, b) morphology, and c) electrochemical cycling performance of the urchin-like natural graphite/CNF hybrid material. Reproduced with permission from Reference [181]. Copyright 2006, Elsevier Ltd.

surface area and is beneficial to reduce undesirable solid electrolyte interface (SEI) layer formation, which contributes to an increased rate capability.[188] Although these 3D macroporous materials possess a large specific energy and specific power, an inherent disadvantage is their low volumetric energy density because of the high porosity of the structure.

Guo et al. proposed an optimized nanostructure design of electrode materials for LIBs with high power and high energy density (Fig. 8). The nanoscopic network structure is composed of a dense net of metalized mesopores that allow both Li^+ and e^- to migrate. This network, with a mesh size of about 10 nm, is superimposed by a similar net on the microscale, formed by the composite of mesoporous particles and conductive admixture. A mesoporous TiO_2:RuO_2 nanocomposite was prepared following the above design strategy. A charge capacity of ≈214 mAh g^{-1} was obtained at 0.2C after 20 cycles, and it was lowered to 190, 147, 125, and 91 mAh g^{-1} at 1, 5, 10, and 30C, respectively. These performances at such high rates are much better than that of commercial TiO_2, TiO_2-B nanowires, or nanosized anatase and rutile TiO_2. The nanosized network is the key to the extremely good power performance because it provides negligible diffusion time, enhanced local conductivity, and possibly faster phase

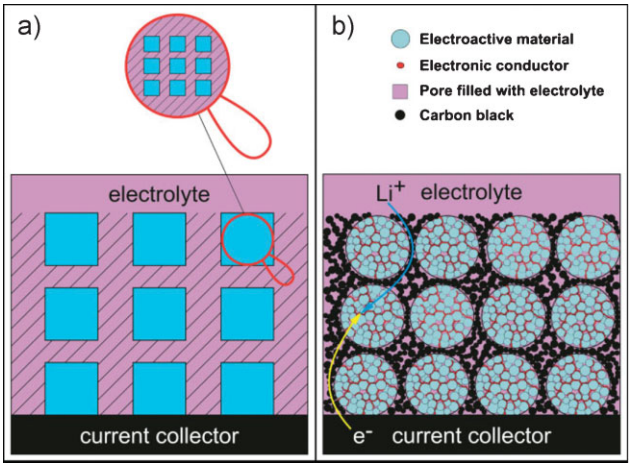

Figure 8. a) Conceptual representation of the desired design comprising a self-similar structure concerning the transportation from micro- to nanoscale. Shaded areas represent the efficient mixed conducting parts. b) Sketch of the realistic composite meeting this concept. Reproduced from Reference [189].

transfer reactions, and the microscopic network guarantees high absolute capacity, ease of fabrication, and quick infiltration.[189]

In addition to carbon,[187–190] porous Si,[191] β-MnO_2,[192] $Li_{1+x}Mn_{2-x}O_4$,[193] and $LiCoO_2$[194] electrode materials were also reported. In these cases, the pores may contribute both to alleviate volume changes during Li insertion/deinsertion and to shorten ion-diffusion length. As an example, Jiao et al. reported an ordered mesoporous $Li_{1+x}Mn_{2-x}O_4$ spinel material for the positive electrode of LIBs. This mesoporous material shows an improved capacity retention compared with bulk materials. At 30C, its capacity retention is 50% higher than that of the equivalent bulk phase. The improved cycling performance is due to the nanometer-sized walls better accommodating the strain of cubic/tetragonal phase transformation and the superior rate capability is mainly attributed to the higher surface area in contact with the electrolyte and the thin walls resulting in a short ion-diffusion length.[193]

1D Porous Structure: Another category of porous materials is a 1D material with modified pore structure. These materials show unique structural features such as numerous active sites for charge transfer reaction, a short diffusion pathway for both Li ions and electrons, and a reasonable electrical conductivity provided by the good contact between neighboring nanostructures.[195] Porous TiO_2 nanotubes,[196] CNFs,[195] and CNF@CNTs[197] are examples. Wang et al. prepared TiO_2 nanotubes with mesoporous walls using an anodic Al_2O_3 membrane as a template. It was found that well-defined mesopores in the nanotube walls are packed in a hexagonal manner. The mesoporous TiO_2 nanotubes show a good cycling performance up to 100 cycles, with capacities of 162, 120, and 105 mAh g^{-1} obtained at the 100th discharge for current densities of 1, 10, and 40 A g^{-1}, respectively. The 3D network structure of the mesoporous TiO_2 nanotubes provides both electron and Li-ion pathways that are essential for a high rate rechargeable LIB.[196]

Selective incorporation of foreign carbons into CNTs could improve the spatial occupancy inside CNT channels in a controlled manner, thereby providing a potential way to optimize their porosity for various applications.[197] Zhang et al. synthesized CNT-encapsulated CNFs (CNFs@CNTs) via selective deposition of Co nanoparticles on the inner surface of CNTs followed by growth of CNFs by means of CVD. The specific surface area and the pore volume increased from 82 m^2 g^{-1} and 0.17 cm^3 g^{-1} to 347 m^2 g^{-1} and 0.61 cm^3 g^{-1} after the growth of CNFs inside the CNTs. The CNFs@CNTs electrode shows a superior rate capability and cycling performance compared to the pristine CNTs, which is ascribed to the steric hindrance effect of the resulting compact structure that suppresses the diffusion of big electrolyte molecules through wall defects.[197]

3.3.4. Combination of Micro-/Nanostructures

The rapidly developing nanomaterials show enhanced charge/discharge kinetics and high Li storage capacity when serving as electrodes of LIBs. However, these nanomaterials suffer from low thermodynamic stability, surface side-reactions, and high cost.[198] Therefore, designing and fabricating micro-/nanoscale hybrid materials to take advantage and restrain shortcomings of micro-/nanocomponents are an important trend for developing high performance LIBs. According to how nanomaterials and micromaterials are combined, the micro-/nanoscale hybrid materials can be sorted into nanoscale materials encapsulated by a microscale shell, microscale active materials with a nanostructured coating layer, nanoscale active materials uniformly dispersed and confined in a microscale matrix, and random mixtures of 1D nanostructures in microscale active materials, as shown in Figure 9.

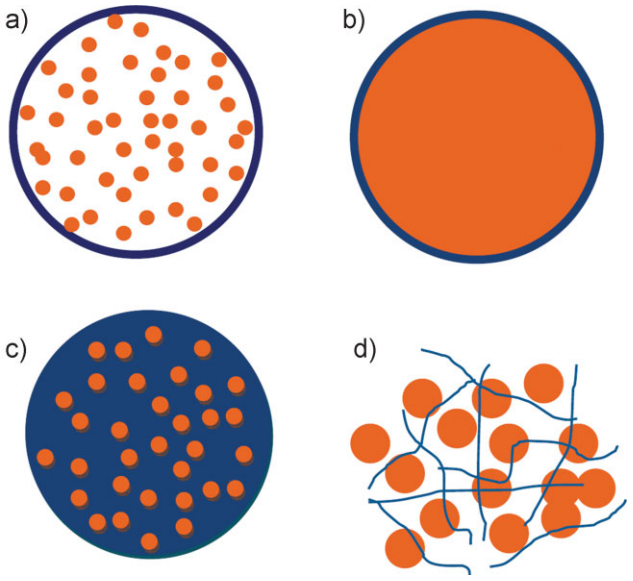

Figure 9. A schematic illustration of four types of micro-/nanoscale hybrid electrode materials. a) Nanoscale materials encapsulated in a microscale hollow structure. b) A microscale active material with a nanostructured coating layer. c) Nanoscale active materials uniformly dispersed and confined in a microscale matrix. d) Mixture of microscale active material and 1D nanostructures that form a conductive network.

Nanoscale Materials Encapsulated into a Microscale Shell: For this category, the encapsulated materials are usually nanoscale particles with a high Li storage capacity and the outer shell is a thin conductive layer (such as carbon). The conductive shell can stabilize the nanoparticles against agglomeration and keep electrically connected to other grains. The existence of a large internal surface and a large cavity to encapsulate nanoparticles is essential. Even in the event of nanoparticle detachment from the internal surface of the shell, the encapsulated particles can be captured by other parts of the same surface and immobilized again. As a result, this kind of materials shows a superior rate capability and cycling performance.[199]

Wang et al. prepared SnO_2 nanoparticles encapsulated in crystalline carbon hollow spheres by microwave-assisted hydrolysis.[200] The SnO_2 nanoparticles were 1–3 nm in diameter, while the diameter of the carbon sphere was about 650 nm and the thickness of the carbon layer was about 50 nm. For the hybrid material containing 25.6 wt% SnO_2, the initial specific capacity is 468 mAh g^{-1} and 91.4% of this capacity could be retained after 60 cycles, showing a notable improvement over the reported results for Sn-encapsulated amorphous carbon hollow spheres[199] and SnO_2-decorated 3D macroporous carbon.[187] Deng et al. prepared a hollow core/shell structure where both the core and the shell were aggregates of crystalline SnO_2

nanoparticles with a mean diameter of 11 nm.[201] The spheres were 1–3 μm in overall dimension, the thickness of the shell was about 200 nm, and there were well-discerned hollow interiors between the core and the shell. These hollow spheres show a high first discharge capacity of 1303 mAh g^{-1}. After 30 cycles at a rate of 100 mA g^{-1}, the retained capacity is still comparable to the theoretical capacity of SnO_2. Fan et al. prepared an ordered, nanostructured tin-based oxide/carbon composite, where SnO_2 nanoparticles were loaded into the channels of CMK-3 ordered mesoporous carbon. This material shows a first charge capacity of 1347 mAh g^{-1} and a capacity retention of 42.8%, much higher than those of nanosized SnO_2.[202]

Microscale Active Material with a Nanostructured Coating Layer: In this case, the functions of the nanoscale coating layer are summarized as preventing the exfoliation of the inner active material, enhancing the conductivity of the electrode material, and decreasing the irreversible capacity. The composition of a coating layer can be carbon, a conductive polymer, amorphous silicon, and so on. Zhang et al. coated natural graphite spheres with pyrolytic carbon by thermal decomposition of acetylene at 900 °C and the thickness of the pyrolytic carbon layer was about 250 nm. The first Coulombic efficiency and the reversible capacity after 15 cycles of the coated natural graphite were 88% and 320 mAh g^{-1}, compared to 80% and 200 mAh g^{-1} for those of the original natural graphite spheres. The remarkably improved electrochemical performance of the coated natural graphite spheres are attributed to the uniformly coated carbon layer and its subsequent functions of lowering the specific surface area of the material, inhibiting the formation of internal SEI film along the cracks, and forming a thin and compact SEI film on the outer surface of the coated natural graphite spheres.[203] Zhang et al. further studied the influence of the carbonization procedure on the structure and electrochemical properties of poly(vinyl carbonate) (PVC)-coated natural graphite spheres. The morphology, specific surface area, pore size distribution, and electrochemical performance of the materials are closely related to the carbonization procedures. Under an optimized carbonization condition, the carbon coating layer is uniform and the resulted material shows desirable electrochemical properties superior to commercial MCMBs. The improved performance is mainly ascribed to the proper coating effect and the lowered impedance of SEI film and charge transfer.[204] Hu et al. prepared a RuO_2–C–$LiFePO_4$ composite where RuO_2 nanoparticles with a size of about 5 nm were directly deposited on the surface of $LiFePO_4$. As a result, incomplete carbon network parts are repaired by the nanometer-sized RuO_2. Specific reversible capacities of 124 and 93 mAh g^{-1} were obtained at 2C and 10C, respectively, whereas the corresponding values for the sample without RuO_2 coating were 105 mAh g^{-1} (2C) and only 2 mAh g^{-1} (10C). The improved kinetics and rate capability of the composite are attributed to the interconnection effect of the nanometer-sized RuO_2.[205] Xie et al. reported a core/shell composite that consists of a spherical $LiFePO_4$ structure coated by a p-bond character conductive planar polymer (polyacene, PAS). The composite can deliver a specific capacity of 126 mAh g^{-1} after 250 cycles at 1C. Even at a high rate of 5C, the capacity still maintains 92 mAh g^{-1} after 500 cycles. Since individual $LiFePO_4$ particles are connected with the PAS network that has a high electrical conductivity, the active $LiFePO_4$ material can be fully utilized for Li extraction and insertion reactions.[206] Obrovac et al. proposed a cycling method in which crystalline Si can be used as a practical anode material. The principle of the cycling method is that the crystalline Si is partially converted to amorphous Si in situ under conditioned cycling so that an amorphous Si shell surrounding the crystalline Si core is formed. This core/shell structured Si shows good Coulombic efficiency and little over-lithiation during the followed normal cycling.[207]

Nanoscale Active Materials Uniformly Dispersed and Confined in a Microscale Matrix: Much attention has been focused on novel anode materials that may provide high capacity and hence a high energy storage density. Li-alloying elements such as Si, Sn, Al, and Sb are able to store Li^+ in a high capacity, but large volume changes accompanied with the insertion and extraction of Li^+ lead to severe internal stress, exfoliation of the active material, and rapid fading of the capacity. An approach to solving this problem is to prepare composites, where Si or other metals are finely dispersed in a conductive matrix. Carbon is an ideal matrix for this application because of its small volume expansion, good electrical conductivity, and desirable ionic conductivity. The embedded and confined materials in a carbon matrix include Si,[208,209] Si@SiO_x,[210] Sn,[211,212] Co_3O_4,[213] SnO_2,[142] P,[214] and so on.

Saint et al. prepared a Si–C composite by the pyrolysis of an intimate mixture of PVC and Si powder. A capacity of ≈1000 mAh g^{-1} was retained after 20 cycles, significantly higher than that of bare Si particles. It is proposed that the carbon matrix induced pressure and the accompanying improved electrical connectivity are the key parameters accounting for the improved cycling performance of Si particles.[208] Derrien[211] et al. and Hassoun[212] et al. reported Sn–C composites, where sphere-like tin particles with sizes ranging from 10 to 50 nm were highly dispersed and confined within a carbon matrix (Fig. 10a). The Sn–C electrode delivered a reversible and stable capacity of 500 mAh g^{-1}, which remains stable over more than 200 cycles at 0.8C. An excellent rate capability of the composite is demonstrated: at 5C, the electrode can deliver 40% of its total capacity (Fig. 10b). The unique structure of the Sn–C composite, where Sn nanoparticles are confined within a protective carbon matrix, is responsible for the enhanced electrochemical property and desirable structural stability, and the carbon matrix not only acts as a buffer to relieve the strain associated with the volume variation but also prevents the aggregation of the tin particles upon cycling.

Zhi et al. reported a Co_3O_4–C composite containing ≈10 wt% carbon and ≈90 wt% nanosized Co_3O_4. The nanosized Co_3O_4 nanoparticles were homogeneously dispersed in the carbon matrix, which acts as a structural buffer for the large volume expansion during Li insertion, enabling good electrical contact among the nanoparticles upon cycling. In addition, the SEI formation on carbon is much more stable than on Co_3O_4, which also ensures the structural stability upon cycling.[213] Kim et al. reported a nanosized $Ca_3Co_4O_9$ anode material for LIBs. Li insertion reaction results in the formation of an active/inactive nanocomposite composed of highly dispersed Co nanoclusters embedded in a pseudoamorphous Li_2O–CaO matrix. This nanocomposite electrode, which contains an inactive CaO matrix, shows an improved cycling performance and rate capability.[215]

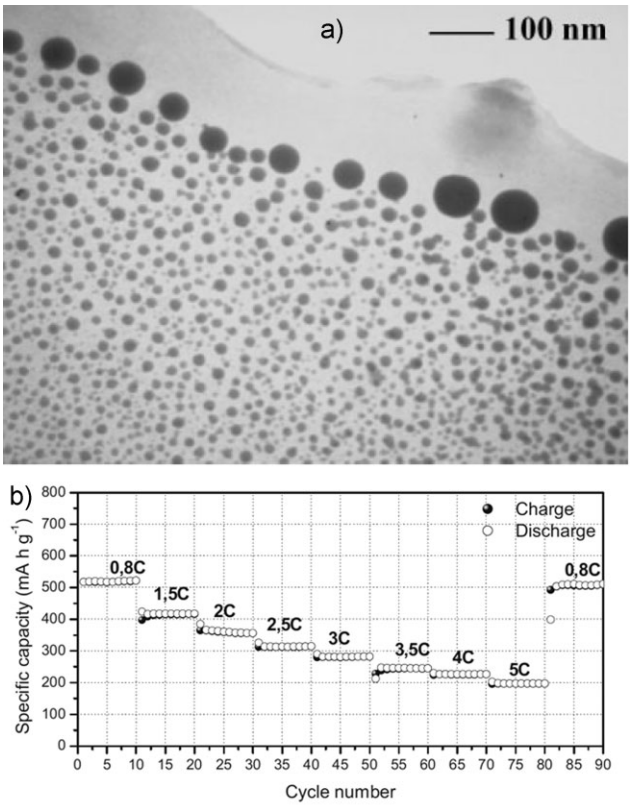

Figure 10. a) TEM image of the Sn–C composite material. b) Cycling response at various rates of the Sn–C composite electrode in an electrochemical cell having Li metal as a counter electrode and a $LiPF_6$ EC:DMC electrolyte. Reproduced from Reference [211].

Microscale Active Materials within a 1D Nanostructured Conductive Network: The conductivity of an electrode is closely related to the high rate and cycling performances of LIBs. In commercial LIBs, carbon black powders are employed as an electric conductive additive. 1D nanowires, nanotubes, or nanofibers have obvious advantages over the spherical carbon black particles in forming conductive networks in electrodes. With the improvement of synthesis techniques for making 1D nanostructures, their application as an additive in LIB electrodes has become practical. Among them, CNTs and CNFs are most widely used for this purpose.

Endo et al. first reported that by adding graphitized CNFs into graphite anode as conductive filler the cycling performance of the carbon anode could be improved significantly. It is considered that the addition of CNFs improves the conductivity of the anode and imparts other desirable properties that enhance the performance of LIBs, such as the ability to absorb and retain significant electrolyte and to provide resiliency and compressibility to the electrode structure.[216]

Zhang et al. prepared a composite anode material of Si/graphite/MWCNTs for LIBs by ball-milling. The Si particles are embedded into the lamellar structures of flaked graphite particles and further tightly wrapped by a MWCNT network. After 20 charge/discharge cycles, a discharge capacity of 584 mAh g^{-1} was obtained, much higher than that of a Si/graphite composite and pure Si. The improved overall discharge capacity and cyclability of the Si/graphite/MWCNT composite anode material is mainly attributed to the excellent resiliency and good electrical conductivity of the MWCNT network.[217]

Lee et al. reported an amorphous $LiFePO_4$ (α-$LiFePO_4$)/SWCNT hybrid material as the cathode of LIBs. Two genes with peptide groups having affinity for SWCNTs on one end and peptides capable of nucleating α-$LiFePO_4$ were used to make a connection between α-$LiFePO_4$ nanoparticles and SWCNTs to form a percolating network. The two-gene-system hybrid material shows electrochemical properties comparable to that of crystalline $LiFePO_4$ and an excellent capacity retention upon cycling at 1C.[218]

Chen et al. reported a free-standing integrated CNT/carbon layer (CL) paper, which is composed of a dense CL with a thickness of less than 1 μm and a highly porous 3D structured CNT network grown on the CL. This material shows a significant and fully reversible capacity of 572 mAh g^{-1} after 100 cycles, much higher than that of CNTs reported previously. The high capacity obtained can be attributed to its novel, highly porous 3D nanostructure, whilst the mechanical robustness of the integrated layer provides stability for cycling.[219]

3.3.5. Modification of Surface Structure and Composition

The surface of electrode materials is an important factor influencing the performance of LIBs[220] because the structure of the SEI film formed in the first charge is largely determined by the interaction between the surface of the electrode and the electrolyte. A desirable surface structure leads to a uniform and compact SEI film that may enhance the efficiency and cycling performance of LIBs. Thus, modification of the composition and surface structure of electrode materials provides opportunities in controlling SEI film formation, ameliorating Li motion, and the relative redox process, thus improving the rate capability and capacity of LIBs.

Pan et al. modified the surface structure of natural graphite by covalently attaching a nitrophenyl multilayer via diazonium chemistry. The modified graphite anode keeps at least 98% of its initial capacity after 30 cycles. The presence of the nitrophenyl multilayer reduces the exposed surface edges to the electrolyte due to the shielding effect and results in a more conductive and thinner SEI film. This compact and uniform SEI film formed on the modified graphite is favorable to the reversible intercalation and deintercalation of Li ions.[221]

Park et al. modified the electrochemical properties of $Li_4Ti_5O_{12}$ by annealing in a NH_3 atmosphere. The $Li_4Ti_5O_{12}$ after nitridation shows a much better rate capability and the capacity of the nitridated $Li_4Ti_5O_{12}$ is about 6 times that of the pristine sample at 10C. The ammonia gas decomposes on the surface of $Li_4Ti_5O_{12}$ to form conductive TiN and Li_2CO_3 without changing the bulk lattice parameters, and it may also modify the surface structure in a way to accommodate Li insertion and extraction.[222]

Sun et al. synthesized vanadium oxide nanorolls with different microstructures, and some are highly ordered near-perfect rolls, while others contain more surface defects and have a larger interlayer spacing. The defect-rich material shows a higher capacity and better cyclability. It is proposed that the increased capacity is related to the additional redox sites resulting from the

atomic-scale disorder and that the better cycling life is associated with the enhanced accessibility of Li ions to the nanorolls due to the defects. The results suggest that perfectly ordered materials may not be the ideal structure for electrochemical applications due to the limited ion diffusion rate. These defect-rich vanadium oxide nanorolls represent a combination of highly accessible nanoscale architecture and atomic scale disorder that lead to desirable electrochemical properties.[223]

Kang et al. performed ab initio computational modeling and identified that low-valent transition-metal cations and low strain in the activated state are effective for increasing the rate capability of layered cathode materials. Following this principle, they experimentally prepared a well-layered $Li(Ni_{0.5}Mn_{0.5})O_2$ material by ion exchange (IE) of Li for Na in $Na(Ni_{0.5}Mn_{0.5})O_2$. Compared with the $Li(Ni_{0.5}Mn_{0.5})O_2$ material obtained by the conventional solid-state (SS) reaction method, the IE $Li(Ni_{0.5}Mn_{0.5})O_2$ shows a much lower Li–Ni exchange ratio and thus a larger slab space and lower activation energy for Li motion, and retains a much higher capacity at high rates than the SS $Li(Ni_{0.5}Mn_{0.5})O_2$. Even at 6C (one charge of 280 mAh g^{-1} in 10 min), the IE $Li(Ni_{0.5}Mn_{0.5})O_2$ delivers a discharge capacity of 183 mAh g^{-1}, much higher than that of SS $Li(Ni_{0.5}Mn_{0.5})O_2$.[224] In addition, some other cathode materials with modified compositions, such as $LiNi_{0.5+\delta}Mn_{0.5-\delta}O_2$[225] and A_2FePO_4F (A = Na, Li)[226] also show improved performance.

3.3.6. Enhanced Contact Between Active Electrode Materials and Current Collectors

Normally, active electrode materials are coated on current collectors. Upon long period cycling, loosening and desquamation of the active materials may occur, leading to degradation in capacity and rate capability of the battery. Enhancing the connection and contact between electrode materials and current collectors is important and has been realized by in situ growth of 1D nanostructured electrode materials on current collectors. The advantages of this strategy are as follows: each 1D active material is connected directly to the current collector so that all of them contribute to the capacity; the 1D nanostructure provides a direct pass for efficient charge transport; since every 1D active material is well-connected to the current-carrying electrode, the need for binders or conducting additives, which add extra weight, is eliminated.[227]

Taberna et al. prepared a Fe_3O_4-based Cu nanoarchitectured electrode for LIBs by a two-step electrode fabrication process. Firstly, a 3D array of copper nanorods with a uniform diameter of 200 nm and length of 1.8 μm was grown onto a copper foil by electrodeposition through a porous anodic alumina membrane, after which the anodic alumina template was eliminated and a layer of magnetite was electrodeposited onto the surface of each Cu nanorod by cathodic reduction of a Fe(III) chelate precursor. The nanoarchitectured electrode can recover 80% of their total capacity at 8C. Furthermore, the cells retain the full capacity after many cycles at high rates, indicative of the chemical/mechanical robustness of the electrode.[228] The same group also reported an electrode based on Ni_3Sn_4 nanoparticles deposited on Cu nanorod arrays that displays excellent cyclability and rate capability.[229]

Chan et al. prepared Si nanowires grown directly on a metallic current collector (Fig. 11). Both charge and discharge capacities keep nearly constant during the 2nd to the 10th cycles. These Si nanowires display a high capacity at higher currents: at C/5, the capacity of the Si nanowires is stable at 3500 mAh g^{-1} for 20 cycles.[227] Similarly, Ge nanowires[230] and a Co_3O_4 nanowire array[231] connecting directly to current collectors were also demonstrated.

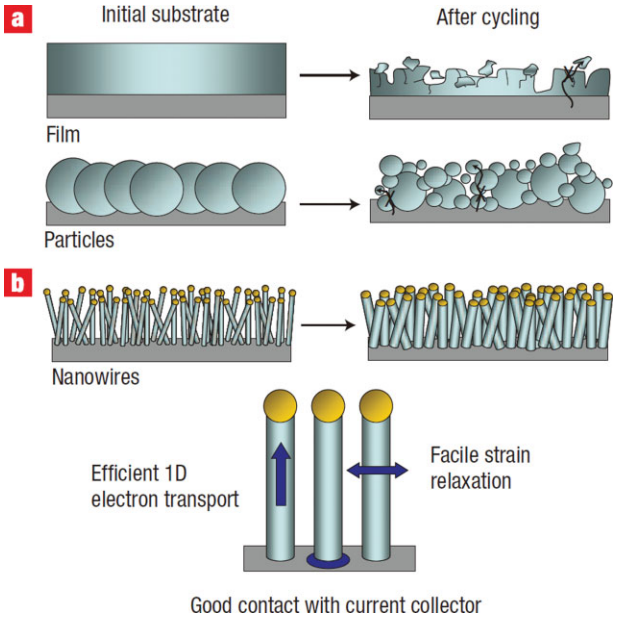

Figure 11. Schematic of morphological changes that occur in Si during electrochemical cycling. a) Si films and particles tend to pulverize during cycling due to the volume change. b) Si nanowires grown directly on the current collector do not pulverize or break into smaller particles after cycling. Reproduced with permission from Reference [227]. Copyright 2008, Nature Publishing Group.

Hu et al. proposed a nanoarchitectured electrode composed of an efficient mixed-conducting network, in which a carbon tube-in-tube (CTIT) serves as an "electronic wire" that provides electrons to the active material and the specifically designed tube diameter allows for easy electrolyte access (Fig. 12). This concept

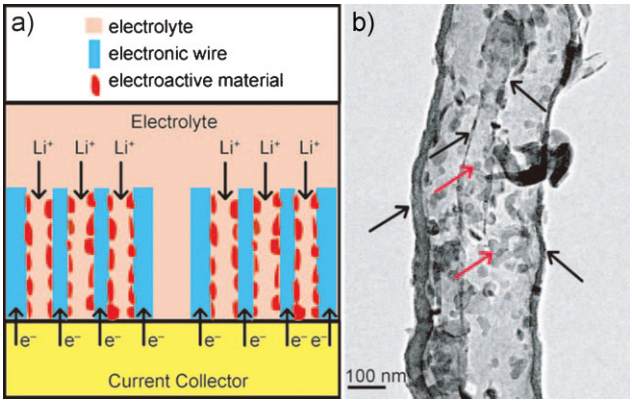

Figure 12. a) Schematic representation of the desired design based on an efficient mixed-conducting network. b) Typical TEM image of the V_2O_5/CTIT nanocomposites showing that most of the V_2O_5 nanoparticles are encapsulated within CTIT. The V_2O_5 nanoparticles are indicated by red arrows and CTIT by black arrows. Reproduced from Reference [232].

was realized by the synthesis of V_2O_5/CTIT nanocomposites, where a total reversible capacity of 280 mAh g^{-1} in the voltage range of 2.0–4.0 V was obtained at C/2.5 and a specific charge capacity of 265 mAh g^{-1} with a Coulombic efficiency of nearly 100% was achieved after 20 cycles.[232]

Except for the above strategies for obtaining advanced electrode materials, other novel electrode materials with promising electrochemical properties are also emerging. For example, Armand et al. reported organic salts of $Li_2C_8H_4O_4$ and $Li_2C_6H_4O_4$ with carboxylate groups conjugated within the molecular core, showing reversible capacities of 300 and 150 mAh g^{-1}. These materials show an enhanced thermal stability over carbon electrodes in 1 M $LiPF_6$ ethylene carbonate (EC)–dimethyl carbonate (DMC) electrolytes and hence may result in safer LIBs. The authors pointed out that the conjugated carboxylate family offers numerous chemical options to further adjust the redox potential and the capacity, and that the field of organics provides many opportunities to design negative electrodes with a suitable redox potential versus Li^+/Li^0, presenting limited reactivity with electrolyte in their discharged state and further enabling the use of Al current collectors.[233] Oumellal et al. reported that metal hydrides, such as MgH_2, can be promising candidates for negative electrodes in LIBs with the advantages of a high capacity in a safe potential window of 0.1–0.5 V versus Li^+/Li^0 and showing the lowest polarization ever reported for conversion reaction electrodes.[234] Yoo et al. reported the electrochemical properties of graphene nanosheets and those incorporated with CNTs and C_{60}.[235] We can see that Li-containing organic salts and novel nanostructured materials provide new opportunities in designing and developing advanced electrodes of LIBs.

3.4. Summary

As reviewed above, many electrode materials with desirable electrochemical properties have been designed and prepared. These materials are characterized by larger Li storage capacity, better cycling performance, and higher rate capability. The strategies for obtaining these materials and their characteristics are summarized in Table 1. We can understand that by using nanostructured materials, the Li-ion diffusion length is reduced and the inner stress can be alleviated and thus better rate capability and cyclability can be expected. Through configuration design, electrode materials with hollow structures can accommodate large volume changes during the charge/discharge process, and the hollow structures may provide extra space for Li-ion storage. For urchin-like materials, a conductive network is formed by connecting their extruding spines and therefore their cycling performance and rate capability are improved. The materials with optimized pore structures provide enhanced electrode/electrolyte contact and shorter Li-ion diffusion length, and hence show high power performance. By combining microscale and nanoscale materials, it is possible to capitalize on advantages and restrain shortcomings of the two components. The functions that are difficult to achieve by a single-phase material can be realized via the structural design and optimization of a composite material. Study of the effect of composition and microstructure of an electrode material on their electrochemical performance both theoretically and experimentally is important for searching for practical advanced electrodes of LIBs. Modification of the surface structure of electrode materials can improve compatibility with electrolytes, enrich redox sites, and enhance the surface conductivity, which lead to good electrochemical performance. Growth of active materials directly on a current collector remarkably enhances the electrical conductivity and the bonding of the components, and thus leads to improved rate capability and cycling performance. Along with the notable advantages, these subtly designed electrode materials also show shortcomings, such as a large irreversible capacity in the first cycle, complex synthesis processes, and a relatively high cost. Few of these materials have practical applications until now. Further investigations on improving overall performance and accelerating practical use are needed. Moreover, although rarely mentioned in this Review, the compatibility of anode materials, cathode materials, electrolytes, and separators is also greatly important.

4. Advanced Materials for Supercapacitors

4.1. Introduction to Supercapacitors

A supercapacitor, also known as an ultracapacitor, is an electrochemical energy storage device with a much larger capacity than conventional physical capacitors, and its charging/discharging rate capability is much higher than primary/secondary batteries. Supercapacitors are environmentally friendly, of high safety, and can be operated in a wide temperature range with a near-infinite long cycling life. Thus, supercapacitors show potential applications in communication, transportation, electronics, and aviation. For example, they can be used as uninterruptible power supplies (back-up supplies used to protect against power disruption) and load-levelers (backup power for memories, microcomputers, clocks, system boards, etc.). In combination with fuel cells or batteries, supercapacitors are anticipated to be used for powering HEVs and EVs, in particular, if the energy density of supercapacitors can be further improved while keeping their high power density unchanged.

A supercapacitor has two electrodes immersed in an electrolyte with a separator between the electrodes. The energy stored in supercapacitors is expressed by $E = 1/2\ CV^2$, where C is the capacitance and V the potential across the electrodes. A supercapacitor that consists of two electrodes with a capacitance C has a net capacitance of $C/2$. In aqueous electrolytes (KOH, H_2SO_4, salt, etc.), supercapacitors have an operating voltage of about 1 V limited by the electrochemical decomposition of water, whereas organic-electrolyte-based supercapacitors can be operated in a voltage range of 2.5 to 3.5 V. An even higher voltage of up to 4.0 V can be achieved for recent ionic-liquid-based supercapacitors. Although organic-electrolyte-based supercapacitors can store a high overall energy, since the electronic conductivity of organic electrolytes is very low (about 100 times lower than aqueous electrolytes), their power density is usually lower than that of aqueous electrolyte-based supercapacitors.

The working principles of a supercapacitor include an electric double layer (EDL) charge storage mode and a pseudo-capacitive

Table 1. A summary of the strategies for obtaining advanced LIB electrode materials and their characteristics (note: NP = nanoparticle, NT = nanotube, NW = nanowire, NR = nanorod).

Strategies		Advantages	Working principle	Typical examples	Remarks
Nanostructuring	LD materials	High capacity and high rate capability	Small dimension and high surface area enhance Li-ion diffusion; the stress caused by volume change can be alleviated.	TiO_2 NP,[135] $LiMn_2O_4$ NW[148] and NR,[150] porous Co_3O_4 NT,[152] needle-like Co_3O_4 NT,[153] nickel silicide nanosheet and nanobelt,[155] α-Fe_2O_3 nanoflake[157]	The large surface area of nanomaterials usually leads to a high irreversible discharge capacity in the first cycle; agglomeration of nanomaterials may lead to a performance fading.
	Core/shell nanostructures	Good cycling performance, high rate capability	The core part is usually an active material, while the shell layer functions by enhancing the electrical conductivity, preventing active material from aggregation, and buffering the inner stress.	C-coated Fe_3O_4 nanospindle,[158] amorphous C-coated Sn NP,[159] C-coated $LiFePO_4$ NP[160] SnO_2/C coaxial NT,[164] crystalline/amorphous core/shell Si NW,[166] $Sn_{78}Ge_{22}$@C NW,[167] mesoporous Si@C core/shell NW[168]	
Design of unique configurations	Hollow structures	High rate capability, good cycling performance	The void space buffers against the local volume change; the diffusion length for Li ions is shortened.	Nest-like Si nanosphere,[172] TiO_2 hollow particle,[174] VOOH hollow dandelion sphere,[177] Li_2O-CuO-SnO_2 hollow porous sphere,[180] SnO_2 hollow spheres[236,237]	The volumetric energy density may be lowered due to the hollow structured electrode materials.
	Urchin-like structures	Good cycling performance	The spines of the urchins form a conductive network, and hence improve the conductivity and structural stability of the electrode.	Graphite sphere/CNF urchins,[181] hard carbon sphere/CNT urchin,[182] α-MnO_2 hollow urchins,[183] CuO urchins[184]	More efficient synthesis techniques are needed.
Pore structure optimization		Good cycling performance and high rate capability	The optimized pore structure leads to short ion diffusion length, enhanced conductivity, and buffering effect to the stress.	SnO_2/3D ordered macroporous C monolith,[187] 3D porous C/C composite,[188] mesoporous TiO_2:RuO_2,[189] 3D porous Si,[191] mesoporous β-MnO_2 [192], porous CNF,[195] TiO_2 NT,[196] CNFs@CNT[197]	The volumetric energy density and first coulombic efficiency need to be improved.
Combination of micro-/nanostructures	Nanoparticles encapsulated with a microscale shell	Good cycling performance	The shell enhances the electrical connection of the materials and prevents the aggregation of the nanoparticles.	SnO_2@C shell,[200] SnO_2 NP@SnO_2 shell,[201] SnO_2 NP@mesoporous C[202]	The size and thickness of the shell is closely related to the performance of the electrode.
	Micromaterial with a nanostructured coating layer	Desirable cycling performance and rate capability	The covering layer can enhance the conductivity and prevent the active material from exfoliation.	Natural graphite/pyrolytic C,[204] RuO_2/C/$LiFePO_4$Li,[205] crystalline Si/amorphous Si[207]	The formation of a uniform and proper coating layer is important.
	Nanoparticles confined in a microscale matrix	Desirable cycling performance and rate capability	Carbon matrix acts as a buffer to relieve the strain, prevents aggregation of the nanoparticles, and enhances the conductivity.	Si/C composite,[208,209] Sn/C composite,[211,212] Co_3O_4/C composite[213], black P/C composite[214]	The capacity is tunable by changing the content ratio of active material to matrix.

Table 1. Continued

Strategies	Advantages	Working principle	Typical examples	Remarks
Microscale material mixed with 1D nanostructure	High rate capability, better cycling performance	The 1D nanostructure provides a conductive network and mechanical robustness.	Si/graphite/CNT,[217] α-$LiFePO_4$/SWCNT,[218] Sn/C/CNT[238]	A uniform dispersion and desirable content of the 1D nanostructure is crucial.
Composition optimization	Desirable rate capability and capacity	Optimized composition and microstructure lead to low-strain volume change and enhanced Li-ion diffusion capability.	$Li(Ni_{0.5}Mn_{0.5})O_2$ by ion exchanging,[224] $LiNi_{0.5+\delta}Mn_{0.5-\delta}O_2$,[225] A_2FePO_4F (A = Na, Li)[226]	Exploring novel electrode materials under the guidance of theoretical calculations will be attractive.
Surface modification	High capacity, good rate capability and improved coulombic efficiency	A compact and uniform SEI film and a conductive surface layer can be formed.	Chemically surface-modified graphite,[221] nitridated $Li_4Ti_5O_{12}$[222]	Control and stability of the modified surface structure is important.
Enhancing contact between electrode materials and current collectors	High rate capability, desirable cycling performance	Direct growth of nanostructures on current collectors enables efficient charge transport, and the exfoliation of the active material can be avoided.	Si/Ge NW on stainless steel,[227,230] Fe_3O_4/Ni_3Sn_4 based Cu nano-architecture,[228,229] Co_3O_4 NW on Ti foil[231]	The synthesis process is relatively complex; techniques for large-scale preparation are needed.
Exploration of novel electrode materials	Good thermal stability, high capacity, low polarization	—	Organic salts of $Li_2C_8H_4O_4$ and $Li_2C_6H_4O_4$,[233] MgH_2,[234] graphene[235]	The overall performance needs further investigation

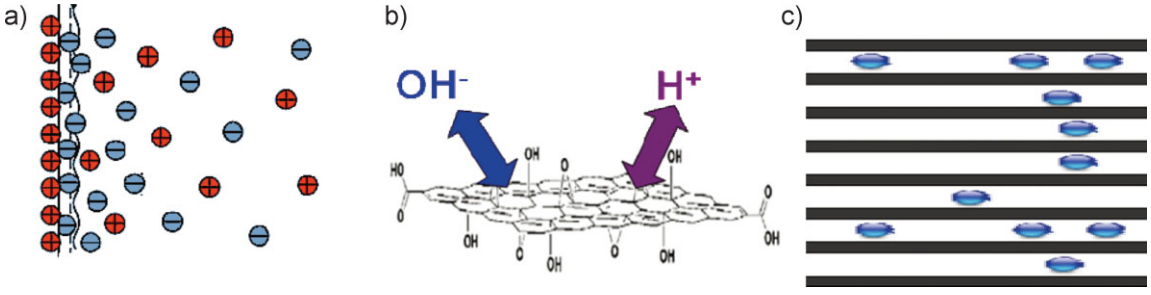

Figure 13. The working principle of supercapacitors. a) Electric double layer, b) redox reaction on surface, and c) redox reaction in bulk.

charge storage mode (Fig. 13). The former, similar to a physical dielectric capacitor, is an electrostatic process (Fig. 13a), and the latter, consisting of two kinds of mechanisms (surface process (Fig. 13b) and bulk process (Fig. 13c)), is a pure electrochemical process.[239] An EDL supercapacitor shares a similar principle with a dielectric capacitor, where polarization/depolarization takes place at the electrode surface. The major difference is that the insulating barrier in a dielectric capacitor is replaced by electrolytes in a supercapacitor.[239] The compartment of an EDL (with a thickness around 1 nm) involves a space charge layer in an electrode (usually highly porous carbon), a compact Helmholtz layer, and a diffusive layer in an electrolyte. Since the electric energy in an EDL is stored in aggregated charges at the surface of electrode materials, which is proportional to the electrode surface area, electrode materials essentially have a large pore volume and high surface area. Pseudocapacitive charge storage fundamentally relies on redox reactions between electrode materials and electrolyte ions. The electric energy is generated by fast Faradaic redox reaction, which produces pseudocapacitance. Depending on the location of these redox reactions, the pseudocapacitive charge storage can be catalogued into surface charge storage and bulk charge storage. The specific capacitance per unit surface area (C_s) of EDL in porous carbon is in the order of 0.1 to 0.2 F m^{-2}, while the C_s of pseudocapacitance is in the order of 1 to 5 F m^{-2}.

The performance of supercapacitors is mainly determined by the electrochemical activity and kinetic feature of the electrodes. To improve the power density of supercapacitors, it is crucial to enhance the kinetics of ion and electron transport in electrodes and at the electrode/electrolyte interface. Therefore, electrodes with proper pore structure and good electrical conductivity are highly desirable. On the other hand, by optimizing the structure

of electrode materials and designing energy storage devices according to energy storage mechanisms, the energy density of supercapacitors can be increased.

4.2. Electrode Materials for Supercapacitors

Electrode materials for supercapacitors mainly include carbon, metal oxides, and conducting polymers, which generate three categories of capacitors: EDL capacitors (EDLCs) based on carbon materials, pseudocapacitors (PCs) based on either transition metal oxides or conducting polymers, and hybrid capacitors (HCs) based on carbon and oxides or polymers. EDLCs are non-Faradaic, PCs are Faradaic, and HCs are a combination of both Faradaic and non-Faradaic reactions. HCs combine two different types of electrodes, operating on the same or different electrochemical mechanisms, which include composite and asymmetric HCs. Composite HCs employ a double-layer-type electrode against a pseudocapacitance electrode, such as carbon–MnO_2[240] and $LiCoO_2$–$Li_4Ti_5O_{12}$.[241] Asymmetric HCs combine a battery-type electrode (Faradaic in nature) with an EDL electrode (Faradaic/non-Faradaic), for example, $Li_4Ti_5O_{12}$–ACs.[242]

Carbon materials are widely utilized for electrode materials in supercapacitors due to their easy accessibility, good processing ability, large surface area/porosity, low electrical resistivity, robust surface chemical environment, physicochemical stability, and low cost. The energy storage in carbon materials is mainly due to the electric charges stored across the electrode/electrolyte interface. The typical capacitance of carbon materials is 50–200 F g^{-1} in aqueous electrolytes, 30–100 F g^{-1} in organic electrolytes and 20–70 F g^{-1} in ionic liquids. The carbon materials used include activated carbons (ACs), CNTs, graphene, CNFs, carbon aerogels, ordered mesoporous carbons (OMCs), hierarchical porous carbons (HPCs), and so on.

The most commonly used electro-active materials in PC electrodes are metal oxides and conductive polymers, and their capacitance originates from chemisorption processes or redox reactions at the electrode/electrolyte interface. Metal oxides can be divided into two groups: noble metal oxides and cheap metal oxides. One typical candidate for the former is RuO_2, while NiO and MnO_2 are well-known for the latter. The most attractive superiority of metal oxides to carbon materials is their much larger capacitance, due to multielectron transfer during fast Faradaic reactions. RuO_2 shows excellent supercapacitive properties, such as high specific capacitance and very long cycling life, but unfortunately, the high cost of RuO_2 limits its commercial application. The cheaper metal oxides suffer from poor electrical conductivity and poor cycling stability, which precludes the highly desirable performance of these materials. In addition to the above metal compounds, Ir, Co, Mo, Ti, V, Sn, Fe, and other metal oxides can also be used as electrode materials for supercapacitors. Nitrides (tungsten nitride, titanium nitride, etc.) have very good pseudocapacitance as well.

Conducting polymers are another kind of electrode materials capable of delivering Faradaic charge. The applicable conducting polymers for PCs mainly include polyaniline (PANi), poly(3,4-ethylenedioxythiophene) (PEDOT), and polypyrrole (PPy). Similar to oxide materials, the problem of conducting polymers is their relatively low electrical conductivity and high cost in comparison with carbon materials.

4.3. Advanced Materials for Supercapacitors

4.3.1. Control and Tailoring of Pore Structure

The pore structure of electrode materials is closely related to ion and electron transport processes, and therefore is most important for improving the performance of a supercapacitor. Porous electrodes for high-performance supercapacitors should meet the following requirements: sufficient pore volume to store electrolytes; suitable ion channel for electrolyte ions to access effectively and to transport quickly to or from the whole surface of electrode material; and plentiful chemically active sites to improve the capacitance. The exact mechanism of ion transport in pores is very complex, correlating with the tortuosity, connectivity, size distribution and shape of pores, surface oxygen functional group, nature of the electrolyte, and solid–liquid interface. Among these factors, three criteria including pore aspect ratio, pore regularity, and surface functional group population should be mainly considered.

Pore aspect ratio is defined as the ratio between the pore length and the pore size of a porous material.[243] In classical electrochemistry theory, the ion transport time (τ) can be expressed by the formula $\tau = L^2/D$, where L is ion transport length and D the ion transport coefficient. It is obvious that the shorter and the larger the mesopores, the smaller the ion transport time, and hence the better the ion transport behavior. Pore regularity reflects the content of pore defects, and the more the defects the lower the regularity. Since the pore defects significantly scatter ions, the higher the pore regularity the better the electrode kinetics.[244] For the OMC with defective pore channels, the gravimetric capacitance is greatly decayed when the voltage scan rate is increased.[244] A defect-free ordered mesoporous system enables electrolyte ions to transport more efficiently and ultimately enhances its supercapacitor performance. In summary, the pore aspect ratio is a geometrical criterion, combining the synergistic effects of pore length and pore diameter, which enables the comparison of different porous electrode materials and guides the design of high-performance electrode materials. The pore regularity reflects the content of pore defects. Surface functional groups can enhance the polarity of pore surfaces and then reduce ion transport resistance. The above understanding is rationalized by using OMCs with tailored pore structures and surface chemical properties (boron modification and nitric acid oxidation).[245,246] Therefore, it is highly important to reduce the pore aspect ratio, to keep regular pore channels, and to improve the hydrophilicity of pore surface, so that enhanced ion transport performance can be well achieved for porous electrodes.

Numerous efforts have been devoted to producing tailored porous carbon materials and ACs, carbon aerogels, OMCs, and HPCs are the most intensely investigated. ACs are the most commonly used electrode material in EDLCs because it is economical and possesses a high surface area. ACs have a complex porous structure composed of micropores (<2 nm), mesopores (2–50 nm), and macropores (>50 nm). Although ACs

have a very high specific surface area, not all of their high surface area contributes to the capacitance dependence on current-draining rates. For AC-based devices, it is found that larger pore sizes correlate with higher power density and smaller pore sizes correlate with higher energy density.[239] As a result, controlling the pore size distribution of AC electrodes is essential. ACs with different porous structures can be prepared by either physical or chemical activation methods.[247–249] Shi et al. studied the effect of specific surface area, pore volume, average pore size, and pore size distribution of ACs on their capacitance.[250] The results show that the capacitance of ACs is not linearly related with their surface area and pores with different sizes have different capacitance per unit surface area, for example, the specific capacitance of micropores is larger than that of mesopores. Chmiola et al. prepared a carbide-derived microporous carbon with narrow and tunable pore size distribution and studied the effect of pore size on the capacitance of the supercapacitors constructed from these microporous carbons.[251,252] It was found that the normalized capacitance decreases with decreasing pore size until a critical value close to 1 nm is reached, and then sharply increases when the pore size approaches the size of the electrolyte ions. The capacitance increase for the sub-nanometer pores indicates that removing the solvent shell from the ions leads to a higher energy storage capacity.[253–255]

OMCs have mesoporous channels ($4 \approx 6$ nm) with lower ion transport resistance, smaller particle size ($1 \approx 2$ μm), and shorter diffusion length ($0.5 \approx 1$ μm). Therefore, OMCs display a superior high power performance compared with ACs. Mesoporous carbons with high porosity and specific surface area show good supercapacitor performance.[256,257] In order to control the pore structures precisely, mesoporous carbons are usually fabricated by a template method. Fuertes et al. synthesized mesoporous carbons with different pore size distribution and specific surface areas using silica as a template: the highest specific surface area reaches 1700 m^2 g^{-1} and the capacitance is 200 F g^{-1}.[258] Xing et al. compared the performance of a series of mesoporous carbons and ACs and found that the mesoporous carbon materials with a larger pore size display better capacity and rate performance.[259] Therefore, a mesoporous carbon material with larger pores and enhanced transport performance can be a promising candidate for high-rate supercapacitors.

Carbon aerogels have a monolithic 3D mesoporous network of carbon nanoparticles. The pore structure of carbon aerogels is formed by the accumulation of carbon particles with similar diameter. Carbon aerogels can be synthesized by pyrolysis of organic aerogels, and their structure and morphology can be easily controlled by tuning the precursor gel composition and pyrolysis temperature. Carbon aerogels obtained from the carbonization of phenolic resin aerogels[260] show a unique advantage of a controlled mesoporous structure when used as the electrode materials of supercapacitors.[261] The superior electrochemical properties of carbon aerogels can be attributed to their interconnected pores, homogeneous pore size, high pore volume, large surface area, and good electrical conductivity.

However, even the porous texture of OMCs cannot fulfill high rate (<2 s) applications, where larger mesopores (>10 nm) and nanometer-scale diffusion distance (<100 nm) are highly preferred. Song et al.[262] and Lee et al.[263] predicted theoretically that hierarchical pore structure may lead to a better rate performance of supercapacitors. The hierarchical porous structure design is based on the different behaviors of electrolyte in pores with different sizes. Electrolyte in macropores, which maintains its bulk phase behavior, can reduce the transport length of ions inside a porous particle. Electrolyte ions have a smaller probability to crash against pore walls of large mesopores and hence reduce ion transport resistance. Macropores and mesopores can synergistically minimize the pore aspect ratio, while the strong electric potential in micropores can effectively trap ions and enhance the charge storage density. Therefore, combination of macro-/meso-/micropores can result in high-performance electrode materials with short ion transport distance, low resistance, and large charge storage density. A 3D aperiodic HPC that combines macropores, mesoporous walls, and micropores with excellent performance was recently designed and synthesized.[264] The pore structures of AC, mesoporous carbon, and the HPC are schematically shown for comparison in Figure 14.

This HPC (Fig. 15) was prepared by using an inorganic multitemplate method, which is cheap, facile, and scalable. The macro-/meso-/micropore size distribution, presence of localized graphitic structure, surface chemical property, and macroscopic form of HPC can be controlled by adjusting template types, concentrations, carbonization temperatures, and atmospheres. The HPC with a conductive localized graphitic structure has fast electron and ion transport and small equivalent series resistance (80 mΩ). Its power density can reach 25 kW kg^{-1} and its energy density can be increased by using high-voltage electrolytes (10 Wh kg^{-1} for a 1 V electrolyte, 18 Wh kg^{-1} for a 2.3 V electrolyte, and 69 Wh kg^{-1} for a 4 V electrolyte at 150 kW kg^{-1}).[265]

4.3.2. Hybridization of Carbon-Based Electrode Materials

Carbon-based electrode materials have long been marked by their low energy density. The crucial restriction that limits the energy density of carbon electrodes is the low capacity of charge storage in EDL. Two general concepts are presently to improve the energy density of carbon electrodes: increasing the specific surface area

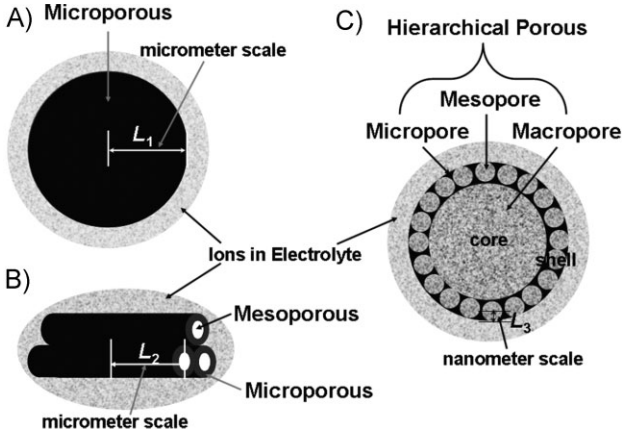

Figure 14. Illustration of the pore structures of AC (a), mesoporous carbon (b), and HPC (c). Reproduced from Reference [264].

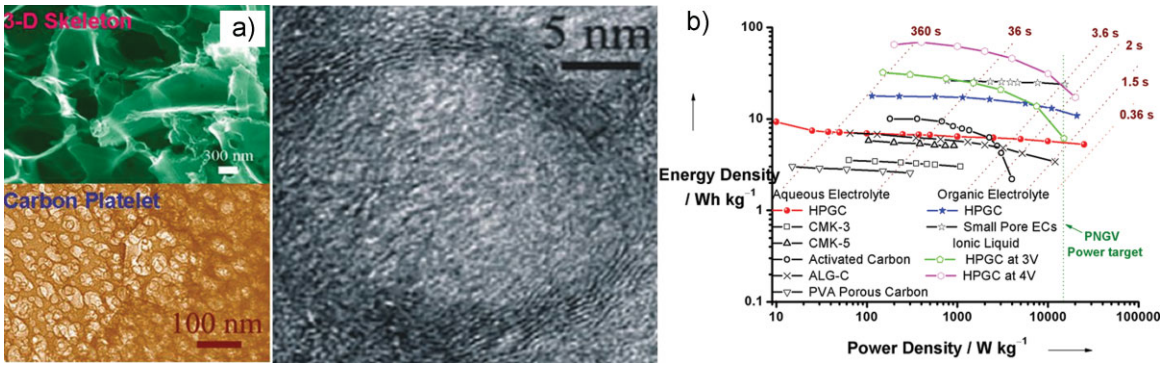

Figure 15. a) SEM and TEM images of the synthesized HPC. b) Ragone plot of the HPC in aqueous solution, organic electrolyte, and ionic liquid in comparison with other typical porous materials reported. Reproduced from Reference. [264,265].

and implanting pseudocapacitive species on carbon surfaces to exploit high energy density from these sites. Therefore, dual-functional hybrid electrodes can be more competitive. Three types of dual-functional electrodes are designed and prepared: carbon electrodes modified with surface functional groups containing oxygen, nitrogen, boron, and/or phosphorus; carbon electrodes decorated with electrically conducting polymers; and carbon electrodes loaded with metal oxides. The first type is a molecular-level hybrid electrode, while the latter two are actually composite materials. These carbon-based materials provide a capacitive double-layer of charge and also a high-surface-area backbone that increases the contact between the deposited pseudocapacitive material and electrolyte.

Among the surface functional groups, oxygen- and nitrogen-containing groups have been well-studied for years, and the electrochemical properties of oxygen functional groups and porous carbon can be modified by doping non-metal heteroatoms of phosphorus, boron, or nitrogen. Phosphorus can stabilize oxygen functional groups during electrochemical charging, improving cycling stability.[266] Boron in the carbon lattice at low concentrations is able to promote the chemisorption of oxygen, inducing a more reactive carbon surface.[245] Several functions and mechanisms of nitrogen-doping have been proposed, such as an electron donor to attract protons or enhance charge density of space charge layer,[267–269] strengthening oxidation/reduction of quinine,[270] and introducing redox reactions of amine groups.[271] It is also believed that quinine and hydroquinone groups are major active redox couples for charge conversion.[272]

Combination of metal oxides or conducting polymers with highly conductive carbon materials has been studied intensively. In these composite electrodes, the carbon substrate acts as a highly porous conducting network that enables a good access of ions and electrons to the active surfaces of polymers or metal oxides. Since the morphology and activity of composite electrodes depend on both the nature of polymers/oxides and preparation methods, our discussion will focus on the most commonly studied oxides and polymers, and shed special light on different fabrication methods. Fischer et al. obtained homogeneous, nanoscale MnO_2 within microporous carbon structures via self-limiting electroless deposition, which displays a high area-normalized capacitance of 1.5 F cm^{-2} as well as a high volumetric capacitance of 90 F cm^{-3}.[240] The chemical precipitation and sol–gel methods are the most general methods adopted for the preparation of a carbon/metal oxide composite electrode.[273–276] By using a chemical vapor impregnation method, Miller et al. prepared a well-dispersed nanostructured Ru/carbon aerogel composite with good cycling performance and high energy density.[277] Moreover, driven by the aim of developing well-defined porous networks, an incipient wetness method was developed for the formation of 3D porous composite of RuO_2/carbon black,[278] and the 3D porous channels facilitate the conductivity of the electrode.

Electrochemical and electroless deposition techniques are two most generally adopted approaches for fabricating conductive polymer/carbon materials. The electrochemical method aims to control the deposition quality by altering the solution concentration, electrode potential, and deposition rate.[279,280] The electroless deposition is more sensitively dependent on the pH value of the solution as well as the surface acidity/basicity of the carbon substrate.[240] As a representative conducting polymer for supercapacitors, PANi is generally obtained by oxidative polymerization of aniline. Although major available oxidative polymerization methods are chemical and electrochemical oxidation, researchers have developed different tricks to control the structure of PANi/C composite electrode. Ordered whisker-like growth of PANi on the surface of mesoporous carbon was subtly realized by Wang et al., and its specific capacitance reaches 1221 F g^{-1}.[281] The V-shaped nano-PANi structure is believed to facilitate ionic conduction and enable a full ionic access favoring both higher energy and power densities. By electrochemical deposition, PANi was deposited on various carbon matrix with different structures, such as carbon aerogels,[282] HPC monoliths,[283] OMCs,[281] macroporous carbon,[284] and graphite oxide.[285] The combination of a vertically aligned CNT array framework and electrodeposition technique leads to a tube-covering-tube nanostructured PANi with hierarchical porous structure, which shows a high specific capacitance of 1030 F g^{-1} due to its large surface area and superior conductivity.[286]

4.3.3. Exploration of Novel Carbon Materials

CNTs and graphene are typical 1D and 2D carbon materials, respectively, which have been attempted as applications for

electrode materials of energy conversion/storage systems, owing to their excellent integrated electronic, mechanical, and chemical properties.[287–290]

CNTs have excellent electrical properties and unique pore structure, which enhance ion transport and electronic conduction capabilities. Generally, CNTs have specific surface areas in the range of 120–500 m^2 g^{-1}. Owing to their moderate high surface area and large accessible mesopores, CNTs are considered to be an attractive electrode material of supercapacitors. CNT electrodes also have a lower equivalent series resistance (ESR) than ACs because electrolyte ions can more easily diffuse into the mesoporous network. The specific capacitance of CNTs can be 15 to 200 F g^{-1}, depending on their morphology, purity, and treatment process, and it can be well-improved by post-treatments, where defects and oxygen-containing functional groups can be introduced.

Niu et al. reported a supercapacitor with capacitance of 113 F g^{-1} and power density of 8 kW kg^{-1} using MWCNTs with a narrow diameter distribution centered at 8 nm and a specific surface area of 430 m^2 g^{-1} as electrodes and 38 wt% H_2SO_4 as electrolyte.[291] Since then, studies on the layer structure, post-treatment, and activation of CNTs for supercapacitors have been performed.[288,290,292–300] For example, Frackowiak et al. reported the electrochemical behavior of supercapacitors built from MWCNTs with outer and inner diameters ranging from 10 to 20 nm and 2 to 5 nm and specific surface areas of 128 to 411 m^2 g^{-1}, and the highest capacitance was 80 F g^{-1} in a 6 M KOH electrolyte.[288] An et al. found that SWCNTs have a maximum specific capacitance of 180 F g^{-1}, a power density of 20 kW kg^{-1}, and an energy density of 6.5 to 7 Wh kg^{-1} at 0.9 V in 7.5 N KOH solution.[289] An electrochemical oxidation method is used to enhance the specific capacitance of SWCNT-based supercapacitors, and a specific capacitance of 163 F g^{-1} is obtained for the electrochemically oxidized SWCNTs and the supercapacitors also display better cycling performance compared to the pristine sample.[299] Zhang et al. obtained a low capacitance of 18.2 F g^{-1} for a MWCNT electrode in an organic-electrolyte system, but a high energy density of 20 Wh kg^{-1} with a 10 mA discharge current density was reached as a result of high operation voltage.[292] Improvement in the specific capacitance of CNT electrodes can be achieved by increasing their mass density. Yoon et al. synthesized MWCNTs directly on a nickel foil, which subsequently serves as the current collector of the integrated electrode.[300] An NH_3-plasma treatment increases the capacitance of the integrated electrode remarkably from 38.7 to 207.3 F g^{-1} in a 6 M KOH solution, which can be attributed to the enhanced surface area and wettability of the MWCNTs subjected to ammonia treatment. Similarly, Chen et al. synthesized MWCNTs directly on Ni-deposited graphite foil, which was treated in diluted HNO_3 and then used as an electrode for electrochemical characterizations, presenting the advantages of binder-free and low contact resistance between the activated material and current collector.[293] Zhang et al. explored the effect of synthesis method, microstructure, pore structure, and electrical conductivity on the capacitance performance of CNT arrays.[294] The CNT array electrode displayed an excellent rate capability (50.8% capacity retention at 77 A g^{-1}), high capacitance (199 F g^{-1} and 305 F cm^{-3}), and long cycling life (3% capacity loss after 20 000 charge/discharge cycles). The membranous macrostructure of CNTs can be directly used as an electrode material without adding any binder or collector.[295]

CNTs are also widely used as an additive for improving electrochemical properties of supercapacitors because of their low electric resistance, low mass density, high stability, and network structure (entangling with one another). CNTs can grow directly on substrates with high surface area and good conductivity, such as ACs, glassy carbon, and metal foils.[219] CNT/porous carbon and CNT/conductive polymer composites show very high specific capacitances up to 2200 F g^{-1}.[296] Jurewicz et al. reported that a maximum value of 163 F g^{-1} in 1 M H_2SO_4 can be obtained for MWCNTs prepared at 600 °C and modified by a PPy layer with 5 nm thickness, whereas only 50 F g^{-1} is obtained for the pristine CNTs.[297] The entangled network of the nanocomposite favors the formation of 3D electric double layers, allowing a more effective contribution of the pseudofaradaic capacitance of PPy. Pushparaj et al. reported nanoporous cellulose paper embedded with an aligned CNT electrode and electrolyte for thin mechanically flexible energy storage devices.[298] An electrochemical codeposition technique was proposed by Wu et al. to prepare a CNT/MnO_2 composite.[301] The rate/nucleation mechanism of MnO_2 deposition was significantly influenced by the introduction of CNTs in the plating bath. Significant progress was recently achieved by the layer-by-layer assembly of CNTs/MnO_2 nanosheets.[302] In this work, a sandwiched film of a MnO_2 nanosheet and MWCNTs was assembled based on electrostatic interaction of positively charged poly(diallyl dirnethyl ammonium chloride) and negatively charged MnO_2 nanosheets and MWCNTs. Its electrochemical capacitance properties are highly dependent upon the deposition sequence and the order of structural components in the sandwiched film. This indicates that the electron transfer and ion conduction in this sandwich-type film is quite important for the electrochemical performance. A surface-decoration method finds its application for the synthesis of CNTs/RuO_2 composite.[303,304] Special attention should be paid to the achievement of an aligned CNTs/RuO_2 composite electrode.[305] RuO_2 layers were formed by physical magnetic sputtering Ru metal in the atmosphere of Ar/O_2 on a CNT array. A nearly 50-fold increase in capacitance is accomplished in this aligned composite electrode after RuO_2 decoration. The results should be reasonably related to the well-occupied 1D ion conduction channels and the fast delivery of electrons through the matrix of the CNT forest.

Graphene, a new class of carbon material, exhibits good electrical conductivity ranging from 200 to 3000 S cm^{-1}. Chemical exfoliation of graphite enables mass production of chemically modified graphene materials with a large quantity of exposed active sites anchored with oxygen functional groups.[306] According to the adsorption isotherms and other measurements of graphene materials, the adsorption occurs on the surface of graphene sheets, which are overlayered with each other to form an aggregated structure, and these aggregated large pores contribute to the hysteresis loops at adsorption isotherms. In an aggregated structure of graphenes, graphene layers interact with each other to form an open pore system, through which electrolyte ions have easy access to the surface of graphene to form electric double layers. This unique open-pore system avoids the dynamic resistance of electrolyte ions within smaller pores, suggesting that graphene-based electrode materials may show

good power capability. The robust surface chemical properties of graphene materials make them feasible as supercapacitor electrode materials showing capacitances of 117 to 135 F g^{-1}.[307] Ruoff et al. reported that supercapacitors based on multilayered graphene display a specific capacitance of 135 F g^{-1} in an aqueous electrolyte solution.[307] In contrast to the conventional high-surface-area materials, the effective surface area of graphene as capacitor electrode materials does not depend on the distribution of pores. The electrochemical performance of graphene is intimately related to its surface chemistry.[308] Because graphene has a layer structure, we recently fabricated a flexible and electrochemically robust graphene electrode. Graphene/PANi was assembled layer-by-layer into a macroscopic flexible electrode that exhibits an excellent electrochemical capacitance of 233 F g^{-1} and 158 F cm^{-3}.[309] These intriguing features make it quite promising as a soft electrode for flexible supercapacitors. These attempts represent substantial progress towards applications of graphene-based materials and the development of flexible energy devices.

CNTs and graphene and their composites have shown promising features of high specific capacitance, good stability, and sound electrodynamics for serving as the electrodes of supercapacitors in specific applications. There is a great need for further investigations focusing on the optimization of the surface and pore structure and on improvement of electrode fabrication techniques to enhance the integrated performance of these electrode materials.

4.3.4. Design of Asymmetric Capacitors

An obvious disadvantage of supercapacitors is their low energy density. To solve this problem, Amatucci et al. first proposed to integrate bulk Li-ion storage and double-layer storage to assemble an asymmetric capacitor (Li-ion supercapacitor) for achieving high power and high energy density simultaneously.[239] An asymmetric capacitor combines two different types of electrodes operating on different electrochemical mechanisms. One such asymmetric hybrid capacitor system was reported by Amatucci et al. by combining nanostructured $Li_4Ti_5O_{12}$ (Faradaic) with ACs.[242] Nanostructured $Li_4Ti_5O_{12}$ was specially chosen as it possesses a low reduction potential, high specific capacity (≈170 mAh g^{-1}), good cycling life, and rate capability.

A main Li-ion-embedded pseudocapacitance electrode material is titania. Titania demonstrates low strain, high potential, long cycling life, and good safety reliability in the bulk Li-ion storage process. Among the crystalline (anatase, rutile, and brookite) and amorphous titania structures, amorphous titania has a pseudocapacitance behavior and crystalline titania has obvious redox potential and charge/discharge platform.[310] Titania electrode materials with different morphologies and pore structures have been intensively studied.[196,311–319] Amorphous nanostructured titania can effectively improve the kinetics of the Li-ion storage process and the mesopore structure in titania electrode materials can improve the efficiency of Li-ion transport. Very recently, Brezesinski et al. reported a high-surface-area crystalline mesoporous TiO_2 film with high levels of capacitive charge storage and high insertion capacities, indicating that both a mesoporous morphology and the use of nanocrystals are very promising for the rational development of metal oxide pseudo-/supercapacitors.[318]

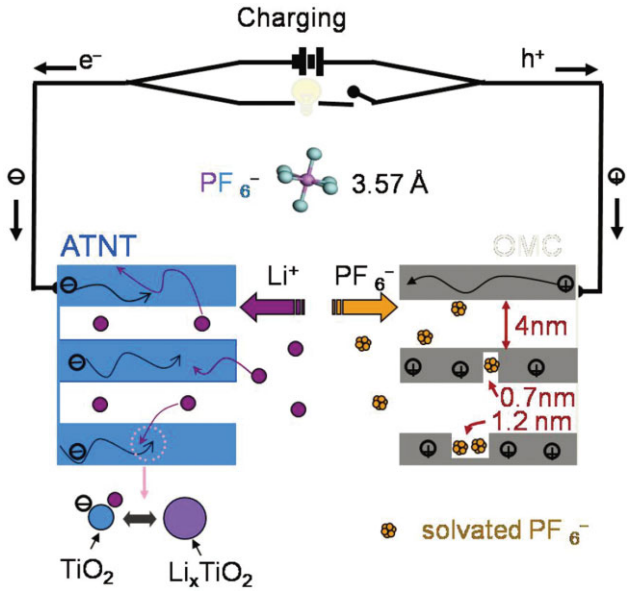

Figure 16. Schematic illustration of the Li-ion supercapacitor.

An asymmetric supercapacitor incorporating an aligned titania nanotube anode and an OMC cathode, also called a Li-ion supercapacitor, was proposed by Wang et al.[320] This work is characterized by the optimization of ionic transport in the anode and ionic uptake in the cathode (Fig. 16). The aligned titania nanotubes have a high surface-to-volume ratio, a meso-/macroporous structure, excellent activity towards electrochemical reactions (e.g., Li storage), and are highly promising for use as an anode to overcome the kinetic problems involved in many electrochemical systems. The ionic transport in the anode is enhanced by reducing the tube length and wall thickness of aligned titania nanotubes. OMCs are superior to either ACs or CNTs because of their high-rate charge-storage capability. The ionic transport and uptake at the OMC cathode is significantly improved by combining ordered mesopores and a high specific surface area of OMCs. Remarkably, the constructed Li-ion supercapacitor can deliver a high energy density of 25 Wh kg^{-1} and a high power density of 3000 W kg^{-1} at a short current draining time of 30 s. Another advantage of this Li-ion supercapacitor is its safety and stability for a long period of operation due to the absence of dendrite Li metal and a solid electrolyte interphase. In terms of the fundamental electrochemistry, the superior performance of such Li-ion supercapacitors is attributed to the shortened electrolyte penetration depth and Li-ion diffusion length in the aligned titania nanotube anode, facilitating an effective lithiation anode process and fast ion uptake at the OMC cathode.[320]

4.4. Summary

In summary, to obtain high performance electrode materials for supercapacitors, it is important to design and synthesize materials with desirable structures and compositions based on a thorough understanding of the interaction between electrodes

and electrolyte ions. Pore structure is closely related to ion transport and charge accommodation, and it is demonstrated that electrodes with hierarchical pores and moderately high surface areas display high electrochemical performance. Carbonaceous porous electrode materials show advantages of high electrical conductivity, good structural controllability, and low production cost, and thus are attractive for making high power-density supercapacitors. A drawback of carbon electrodes is their low capacity and the combination of carbon and metal oxides or conductive polymers has been shown to be effective in improving the energy density of supercapacitors. Asymmetric capacitors composed of a battery-type electrode and a supercapacitor electrode are receiving increasing interest because of their high energy density. Nanostructured materials are used as the Faradaic battery-type electrode because they show enhanced ionic transport ability due to their small size. Optimization of the structure and composition of nanomaterials may further improve the performance of the asymmetric capacitors.

5. Conclusive Remarks and Prospects

Energy storage materials are receiving tremendous attention and research interest due to the increasing concern on the sustainable development of energy, economy, and society, which is closely related to the high efficiency and versatile storage and consumption of energy. To fulfill the newly emerging applications, such as powering EVs/HEVs and portable electronics, advanced energy storage materials with superior integrated performance that enables high energy and power density and environmentally benign, convenient, and flexible storage of energy are highly demanded.

As described above, several general strategies for making advanced energy storage materials have been developed, such as nanostructuring, nano-/microcombination, hybridization, pore-structure control, configuration design, surface modification, composition optimization, and novel device design. Notable progress has been made in recent years: the capacity, rate capability, and cycling life of electrode materials for LIBs and supercapacitors have been evidently enhanced and the capacity, thermodynamics, and kinetics of hydrogen storage materials are being steadily improved. These energy storage materials with high capacity, long cycling life, good safety, and good reliability will undoubtedly boost the performance of energy storage devices constructed on them and facilitate their wide application.

While desirable properties are achieved for the subtly designed energy storage materials, drawbacks still exist. For example, nanostructured electrode materials for LIBs show enhanced Li diffusion and alleviated inner stress, which leads to an improved rate capability and cycling performance, but their first Coulombic efficiency is decreased due to the large surface area of the nanomaterials; when the nanoconfining technique offers a new possibility to addressing the dilemma between dehydrogenation temperature and reversibility encountered in hydrides, a significant capacity penalty resulting from ''inert'' nanoscaffolds needs to be minimized prior to any potential vehicular application. It is yet difficult to find an omnipotent energy storage material. A wise way is to design and fabricate energy storage materials according to specific application requirements, such as high power-density materials for power systems and high capacity materials for long-term and stable energy supplies. Except for the performance indexes, issues of safety, environment compatibility, cost, and ease of manipulation and fabrication should also be taken into account when developing an industrially applicable energy storage material.

Continuous efforts are undoubtedly required in developing high-performance energy storage materials, and a few new trends are noteworthy and may be very promising. Firstly, organic materials are playing increasingly important roles in energy storage. The currently explored energy storage media are basically inorganic materials, while from the viewpoint of sustainability and ecoefficiency, the development of renewable organic energy storage materials is very important. Organic and organic/inorganic hybrid electrode materials have been reported to show desirable electrochemical energy storage properties, and it is predicted that biomass could be used as electrodes of LIBs in the future.[233,321] Organic chemistry is also used in cation/anion substitution and exchange to explore AB-based compounds and metal borohydrides for hydrogen storage. Secondly, optimization of the matching capability and structure of energy storage devices is crucial. Except for active materials, each energy storage system contains ''inert'' parts, such as electrolytes, additives, current collectors, and separators in LIBs and supercapacitors. To make full use of active materials, perfect matching between cathode/anode materials and electrodes/electrolyte is most desirable. For example, it can be expected that, by using an ionic liquid as the electrolyte, the energy density of supercapacitors and the safety reliability of LIBs can be largely improved. The design and fabrication of asymmetric supercapacitors and 3D nanoarchitectured LIB cells will lead to an enhanced performance of energy storage units. Thirdly, the combination of theoretical calculations and experimental investigations will promote the exploration of novel high-performance energy storage materials. Theoretical and computational modeling and simulation are effective in predicting the properties and optimizing the composition of electrode materials and catalysts used in energy storage systems. Guided by theoretical predictions, the efficiency of developing novel energy storage materials will be significantly improved. For example, Kang et al. at first performed ab initio computational modeling and then experimentally prepared well-layered $Li(Ni_{0.5}Mn_{0.5})O_2$ with desirable rate capability and high energy density.[224] DFT calculations were employed to thermodynamically predict favorable hydrogen storage reactions coupled with optimized capacity.[322]

Based on an in-depth understanding on the principles of energy storage and combined with smart material-design strategies and ever-improved synthesis technologies, more and more advanced energy storage materials with excellent performances are being developed. Their practical applications will play important roles in solving the serious energy and environment problems. By powering EVs, HEVs, fuel-cell-driven vehicles, aeronautic/astronautic aircrafts, and various portable electronics, energy storage materials/systems are anticipated to contribute greatly to the advancement of modern civilization. However, to achieve such goals, great efforts are required to tackle a series of technological barriers. Since energy storage correlates to a wide range of subjects and fields, collaborations and joint research of scientists from a wide range of disciplines will be essential and crucial in future development.

Finally, we want to cite a phrase from "New Science for a Secure and Sustainable Energy Future" by Hemminger et al.[323] to conclude this review: "It becomes clear that the magnitude of the challenge is so immense that existing approaches—even with improvements from advanced engineering and improved technology based on known concepts—will not be enough to secure our energy future. Instead, meeting the challenge will require fundamental understanding and scientific breakthroughs in new materials and chemical processes to make possible new energy technologies and performance levels far beyond what is now possible."

Acknowledgements

This work was financially supported by the NSFC (No. 50921004, No. 90606008, 50702063, and 50672103), MOST (No. 2006CB932701, 2009AA03Z337, and 2008DFA51400), and CAS (No. KJCX2-YW-M01). The authors acknowledge Dr. Ping Wang for his contribution on hydrogen storage materials and Dr. Quanhong Yang, Dr. Haitao Fang, Dr. Hongli Zhang, Dr. Chengzhang Wu, Dr. Dawei Wang, and Dr. Lei Wen for the constructive discussion and comments on this article.

Received: September 28, 2009
Published online: January 14, 2010

[1] H. S. Chen, T. N. Cong, W. Yang, C. Q. Tan, Y. L. Li, Y. L. Ding, *Prog. Nat. Sci.* **2009**, *19*, 291.
[2] A. Saito, *Int. J. Refrig.* **2002**, *25*, 177.
[3] A. F. Regin, S. C. Solanki, J. S. Saini, *Renewable Sustainable Energy Rev.* **2008**, *12*, 2438.
[4] A. Sharma, V. V. Tyagi, C. R. Chen, D. Buddhi, *Renewable Sustainable Energy Rev.* **2009**, *13*, 318.
[5] M. M. Farid, A. M. Khudhair, S. A. K. Razack, S. Al-Hallaj, *Energy Convers. Manage.* **2004**, *45*, 1597.
[6] N. Gokon, D. Nakano, S. Inuta, T. Kodama, *Sol. Energy* **2008**, *82*, 1145.
[7] K. Lovegrove, H. Kreetz, A. Luzzi, *J. Phys. IV* **1999**, *9*, 581.
[8] D. Mori, K. Hirose, *Int. J. Hydrogen Energy* **2009**, *34*, 4569.
[9] L. Schlapbach, A. Zuttel, *Nature* **2001**, *414*, 353.
[10] S. Satyapal, J. Petrovic, C. Read, G. Thomas, G. Ordaz, *Catal. Today* **2007**, *120*, 246.
[11] W. Grochala, P. P. Edwards, *Chem. Rev.* **2004**, *104*, 1283.
[12] S. I. Orimo, Y. Nakamori, J. R. Eliseo, A. Zuttel, C. M. Jensen, *Chem. Rev.* **2007**, *107*, 4111.
[13] J. J. Vajo, G. L. Olson, *Scr. Mater.* **2007**, *56*, 829.
[14] P. Wang, X. D. Kang, *Dalton Trans.* **2008**, 5400.
[15] J. Yang, S. Hirano, *Adv. Mater.* **2009**, *21*, 3023.
[16] P. Benard, R. Chahine, *Scr. Mater.* **2007**, *56*, 803.
[17] M. Dinca, J. R. Long, *Angew. Chem. Int. Ed.* **2008**, *47*, 6766.
[18] L. F. Wang, R. T. Yang, *Energy Environ. Sci.* **2008**, *1*, 268.
[19] T. K. A. Hoang, D. M. Antonelli, *Adv. Mater.* **2009**, *21*, 1787.
[20] J. J. Reilly, R. H. Wiswall, *Inorg. Chem.* **1967**, *6*, 2220.
[21] J. J. Vajo, F. Mertens, C. C. Ahn, R. C. Bowman, B. Fultz, *J. Phys. Chem. B* **2004**, *108*, 13977.
[22] J. J. Vajo, S. L. Skeith, F. Mertens, *J. Phys. Chem. B* **2005**, *109*, 3719.
[23] J. Yang, A. Sudik, C. Wolverton, *J. Phys. Chem. C* **2007**, *111*, 19134.
[24] S. A. Jin, Y. S. Lee, J. H. Shim, Y. W. Cho, *J. Phys. Chem. C* **2008**, *112*, 9520.
[25] J. Wang, A. D. Ebner, J. A. Ritter, *J. Am. Chem. Soc.* **2006**, *128*, 5949.
[26] J. Graetz, J. Wegrzyn, J. J. Reilly, *J. Am. Chem. Soc.* **2008**, *130*, 17790.
[27] X. F. Liu, G. S. McGrady, H. W. Langmi, C. M. Jensen, *J. Am. Chem. Soc.* **2009**, *131*, 5032.
[28] J. Graetz, J. J. Reilly, *J. Alloys Compd.* **2006**, *424*, 262.
[29] B. Baranowski, M. Tkacz, *Z. Physik. Chem.* **1983**, *135*, 27.
[30] E. C. Ashby, *J. Am. Chem. Soc.* **1964**, *86*, 1882.
[31] R. Zidan, B. L. Garcia-Diaz, C. S. Fewox, A. C. Stowe, J. R. Gray, A. G. Harter, *Chem. Commun.* **2009**, 3717.
[32] P. Chen, Z. T. Xiong, J. Z. Luo, J. Y. Lin, K. L. Tan, *Nature* **2002**, *420*, 302.
[33] P. Chen, Z. T. Xiong, J. Z. Luo, J. Y. Lin, K. L. Tan, *J. Phys. Chem. B* **2003**, *107*, 10967.
[34] Y. H. Hu, E. Ruckenstein, *J. Phys. Chem. A* **2003**, *107*, 9737.
[35] T. Ichikawa, N. Hanada, S. Isobe, H. Y. Leng, H. Fujii, *J. Phys. Chem. B* **2004**, *108*, 7887.
[36] W. F. Luo, *J. Alloys Compd.* **2004**, *381*, 284.
[37] Z. T. Xiong, G. T. Wu, J. J. Hu, P. Chen, *Adv. Mater.* **2004**, *16*, 1522.
[38] Z. T. Xiong, J. J. Hu, G. T. Wu, P. Chen, W. F. Luo, K. Gross, J. Wang, *J. Alloys Compd.* **2005**, *398*, 235.
[39] F. E. Pinkerton, G. P. Meisner, M. S. Meyer, M. P. Balogh, M. D. Kundrat, *J. Phys. Chem. B* **2005**, *109*, 6.
[40] W. T. Klooster, T. F. Koetzle, P. E. M. Siegbahn, T. B. Richardson, R. H. Crabtree, *J. Am. Chem. Soc.* **1999**, *121*, 6337.
[41] F. Baitalow, J. Baumann, G. Wolf, K. Jaenicke-Rossler, G. Leitner, *Thermochim. Acta* **2002**, *391*, 159.
[42] G. Soloveichik, J. H. Her, P. W. Stephens, Y. Gao, J. Rijssenbeek, M. Andrus, J. C. Zhao, *Inorg. Chem.* **2008**, *47*, 4290.
[43] T. Ichikawa, H. Fujii, S. Isobe, K. Nabeta, *Appl. Phys. Lett.* **2005**, *86*, 241914.
[44] K. Miwa, N. Ohba, S. Towata, Y. Nakamori, S. Orimo, *J. Alloys Compd.* **2005**, *404*, 140.
[45] J. H. Wang, T. Liu, G. T. Wu, W. Li, Y. F. Liu, C. M. Araujo, R. H. Scheicher, A. Blomqvist, R. Ahuja, Z. T. Xiong, P. Yang, M. X. Gao, H. G. Pan, P. Chen, *Angew. Chem. Int. Ed.* **2009**, *48*, 5828.
[46] Z. T. Xiong, C. K. Yong, G. T. Wu, P. Chen, W. Shaw, A. Karkamkar, T. Autrey, M. O. Jones, S. R. Johnson, P. P. Edwards, W. I. F. David, *Nat. Mater.* **2008**, *7*, 138.
[47] X. D. Kang, Z. Z. Fang, L. Y. Kong, H. M. Cheng, X. D. Yao, G. Q. Lu, P. Wang, *Adv. Mater.* **2008**, *20*, 2756.
[48] X. D. Kang, P. Wang, H. M. Cheng, *Scr. Mater.* **2007**, *56*, 361.
[49] L. C. Yin, P. Wang, X. D. Kang, C. H. Sun, H. M. Cheng, *Phys. Chem. Chem. Phys.* **2007**, *9*, 1499.
[50] L. C. Yin, P. Wang, Z. Z. Fang, H. M. Cheng, *Chem. Phys. Lett.* **2008**, *450*, 318.
[51] M. Fichtner, O. Fuhr, O. Kircher, *J. Alloys Compd.* **2003**, *356*, 418.
[52] K. Chlopek, C. Frommen, A. Leon, O. Zabara, M. Fichtner, *J. Mater. Chem.* **2007**, *17*, 3496.
[53] Z. Z. Fang, L. P. Ma, X. D. Kang, P. J. Wang, P. Wang, H. M. Cheng, *Appl. Phys. Lett.* **2009**, *94*, 044104.
[54] S. Srinivasan, D. Escobar, Y. Goswami, E. Stefanakos, *Int. J. Hydrogen Energy* **2008**, *33*, 2268.
[55] T. Hugle, M. F. Kuhnel, D. Lentz, *J. Am. Chem. Soc.* **2009**, *131*, 7444.
[56] J. J. Mack, S. Tari, R. B. Kaner, *Inorg. Chem.* **2006**, *45*, 4243.
[57] C. M. Jensen, G. Severa, S. Zhang, L. Culnane, W. Langley, R. Ayabe, T. Humphries, U. Setthanan, G. S. McGrady, *DOE Hydrogen Program: FY 2008 Annual Progress Report*, US DOE, Washington DC **2008**.
[58] G. Barkhordarian, T. Klassen, R. Bormann, *Scr. Mater.* **2003**, *49*, 213.
[59] G. Barkhordarian, T. Klassen, R. Bormann, *J. Phys. Chem. B* **2006**, *110*, 11020.
[60] L. P. Ma, X. D. Kang, H. B. Dai, Y. Liang, Z. Z. Fang, P. J. Wang, P. Wang, H. M. Cheng, *Acta Mater.* **2009**, *57*, 2250.
[61] N. Hanada, T. Ichikawa, S. Hino, H. Fujii, *J. Alloys Compd.* **2006**, *420*, 46.
[62] B. Bogdanovic, M. Schwickardi, *J. Alloys Compd.* **1997**, *253*, 1.
[63] H. Gunaydin, K. N. Houk, V. Ozolins, *Proc. Natl. Acad. Sci. USA* **2008**, *105*, 3673.
[64] P. Chen, Z. T. Xiong, L. F. Yang, G. T. Wu, W. F. Luo, *J. Phys. Chem. B* **2006**, *110*, 14221.

[65] L. P. Ma, H. B. Dai, Y. Liang, X. D. Kang, Z. Z. Fang, P. J. Wang, P. Wang, H. M. Cheng, *J. Phys. Chem. C* **2008**, *112*, 18280.
[66] J. Yang, A. Sudik, D. J. Siegel, D. Halliday, A. Drews, R. O. Carter, C. Wolverton, G. J. Lewis, J. W. A. Sachtler, J. J. Low, S. A. Faheem, D. A. Lesch, V. Ozolins, *Angew. Chem. Int. Ed.* **2008**, *47*, 882.
[67] J. J. Hu, Y. F. Liu, G. T. Wu, Z. T. Xiong, Y. S. Chua, P. Chen, *Chem. Mater.* **2008**, *20*, 4398.
[68] L. P. Ma, H. B. Dai, Z. Z. Fang, X. D. Kang, Y. Liang, P. J. Wang, P. Wang, H. M. Cheng, *J. Phys. Chem. C* **2009**, *113*, 9944.
[69] D. Chen, L. Chen, S. Liu, C. X. Ma, D. M. Chen, L. B. Wang, *J. Alloys Compd.* **2004**, *372*, 231.
[70] C. Z. Wu, P. Wang, X. Yao, C. Liu, D. M. Chen, G. Q. Lu, H. M. Cheng, *J. Alloys Compd.* **2006**, *414*, 259.
[71] J. Wang, A. D. Ebner, J. A. Ritter, *J. Phys. Chem. B* **2006**, *110*, 17353.
[72] Y. Chen, P. Wang, C. Liu, H. M. Cheng, *Int. J. Hydrogen Energy* **2007**, *32*, 1262.
[73] Z. Z. Fang, X. D. Kang, P. Wang, H. M. Cheng, *J. Phys. Chem. C* **2008**, *112*, 17023.
[74] P. J. Wang, Z. Z. Fang, L. P. Ma, X. D. Kang, P. Wang, *Int. J. Hydrogen Energy* **2008**, *33*, 5611.
[75] P. A. Berseth, A. G. Harter, R. Zidan, A. Blomqvist, C. M. Araujo, R. H. Scheicher, R. Ahuja, P. Jena, *Nano Lett.* **2009**, *9*, 1501.
[76] X. D. Yao, C. Z. Wu, A. J. Du, J. Zou, Z. H. Zhu, P. Wang, H. M. Cheng, S. Smith, G. Q. Lu, *J. Am. Chem. Soc.* **2007**, *129*, 15650.
[77] C. Z. Wu, P. Wang, X. D. Yao, C. Liu, D. M. Chen, G. Q. Lu, H. M. Cheng, *J. Phys. Chem. B* **2005**, *109*, 22217.
[78] S. C. Amendola, S. L. Sharp-Goldman, M. S. Janjua, N. C. Spencer, M. T. Kelly, P. J. Petillo, M. Binder, *Int. J. Hydrogen Energy* **2000**, *25*, 969.
[79] U. B. Demirci, F. Garin, *J. Alloys Compd.* **2008**, *463*, 107.
[80] J. Lee, K. Y. Kong, C. R. Jung, E. Cho, S. P. Yoon, J. Han, T. G. Lee, S. W. Nam, *Catal. Today* **2007**, *120*, 305.
[81] H. B. Dai, Y. Liang, P. Wang, H. M. Cheng, *J. Power Sources* **2008**, *177*, 17.
[82] Independent Review Panel, *Go/No-Go Recommendation for Sodium Borohydride for On-Board Vehicular Hydrogen Storage*, National Renewable Energy Laboratory, Golden, CO **2007**.
[83] M. C. Denney, V. Pons, T. J. Hebden, D. M. Heinekey, K. I. Goldberg, *J. Am. Chem. Soc.* **2006**, *128*, 12048.
[84] M. E. Bluhm, M. G. Bradley, R. Butterick, U. Kusari, L. G. Sneddon, *J. Am. Chem. Soc.* **2006**, *128*, 7748.
[85] A. Zaluska, L. Zaluski, J. O. Strom-Olsen, *J. Alloys Compd.* **1999**, *288*, 217.
[86] C. P. Balde, B. P. C. Hereijgers, J. H. Bitter, K. P. de Jong, *J. Am. Chem. Soc.* **2008**, *130*, 6761.
[87] L. Xie, J. Zheng, Y. Liu, Y. Li, X. G. Li, *Chem. Mater.* **2008**, *20*, 282.
[88] R. W. P. Wagemans, J. H. van Lenthe, P. E. de Jongh, A. J. van Dillen, K. P. de Jong, *J. Am. Chem. Soc.* **2005**, *127*, 16675.
[89] W. Y. Li, C. S. Li, H. Ma, J. Chen, *J. Am. Chem. Soc.* **2007**, *129*, 6710.
[90] F. Schuth, B. Bogdanovic, A. Taguchi, Patent Application WO2005014469 (**2003**).
[91] A. Gutowska, L. Y. Li, Y. S. Shin, C. M. M. Wang, X. H. S. Li, J. C. Linehan, R. S. Smith, B. D. Kay, B. Schmid, W. Shaw, M. Gutowski, T. Autrey, *Angew. Chem. Int. Ed.* **2005**, *44*, 3578.
[92] H. Kim, A. Karkamkar, T. Autrey, P. Chupas, T. Proffen, *J. Am. Chem. Soc.* **2009**, *131*, 13749.
[93] A. F. Gross, J. J. Vajo, S. L. Van Atta, G. L. Olson, *J. Phys. Chem. C* **2008**, *112*, 5651.
[94] Z. Z. Fang, P. Wang, T. E. Rufford, X. D. Kang, G. Q. Lu, H. M. Cheng, *Acta Mater.* **2008**, *56*, 6257.
[95] M. J. Ingleson, J. P. Barrio, J. Bacsa, A. Steiner, G. R. Darling, J. T. A. Jones, Y. Z. Khimyak, M. J. Rosseinsky, *Angew. Chem. Int. Ed.* **2009**, *48*, 2012.
[96] G. Yushin, R. Dash, J. Jagiello, J. E. Fischer, Y. Gogotsi, *Adv. Funct. Mater.* **2006**, *16*, 2288.
[97] Z. X. Yang, Y. D. Xia, R. Mokaya, *J. Am. Chem. Soc.* **2007**, *129*, 1673.
[98] N. B. McKeown, B. Gahnem, K. J. Msayib, P. M. Budd, C. E. Tattershall, K. Mahmood, S. Tan, D. Book, H. W. Langmi, A. Walton, *Angew. Chem. Int. Ed.* **2006**, *45*, 1804.
[99] A. G. Wong-Foy, A. J. Matzger, O. M. Yaghi, *J. Am. Chem. Soc.* **2006**, *128*, 3494.
[100] A. C. Dillon, K. M. Jones, T. A. Bekkedahl, C. H. Kiang, D. S. Bethune, M. J. Heben, *Nature* **1997**, *386*, 377.
[101] G. G. Tibbetts, G. P. Meisner, C. H. Olk, *Carbon* **2001**, *39*, 2291.
[102] C. Liu, H. M. Cheng, *J. Phys. D: Appl. Phys.* **2005**, *38*, R231.
[103] A. Chambers, C. Park, R. T. K. Baker, N. M. Rodriguez, *J. Phys. Chem. B* **1998**, *102*, 4253.
[104] S. Iijima, M. Yudasaka, R. Yamada, S. Bandow, K. Suenaga, F. Kokai, K. Takahashi, *Chem. Phys. Lett.* **1999**, *309*, 165.
[105] A. D. Leonard, J. L. Hudson, H. Fan, R. Booker, L. J. Simpson, K. J. O'Neill, P. A. Parilla, M. J. Heben, M. Pasquali, C. Kittrell, J. M. Tour, *J. Am. Chem. Soc.* **2009**, *131*, 723.
[106] X. B. Zhao, B. Xiao, A. J. Fletcher, K. M. Thomas, D. Bradshaw, M. J. Rosseinsky, *Science* **2004**, *306*, 1012.
[107] A. J. Lachawiec, G. S. Qi, R. T. Yang, *Langmuir* **2005**, *21*, 11418.
[108] Y. W. Li, R. T. Yang, *J. Am. Chem. Soc.* **2006**, *128*, 726.
[109] C. S. Tsao, M. S. Yu, C. Y. Wang, P. Y. Liao, H. L. Chen, U. S. Jeng, Y. R. Tzeng, T. Y. Chung, H. C. Wu, *J. Am. Chem. Soc.* **2009**, *131*, 1404.
[110] Y. F. Zhao, Y. H. Kim, A. C. Dillon, M. J. Heben, S. B. Zhang, *Phys. Rev. Lett.* **2005**, *94*, 155504.
[111] T. Yildirim, S. Ciraci, *Phys. Rev. Lett.* **2005**, *94*, 175501.
[112] E. Durgun, S. Ciraci, W. Zhou, T. Yildirim, *Phys. Rev. Lett.* **2006**, *97*, 226102.
[113] H. Lee, W. I. Choi, J. Ihm, *Phys. Rev. Lett.* **2006**, *97*, 056104.
[114] X. Lin, J. H. Jia, X. B. Zhao, K. M. Thomas, A. J. Blake, G. S. Walker, N. R. Champness, P. Hubberstey, M. Schroder, *Angew. Chem. Int. Ed.* **2006**, *45*, 7358.
[115] M. Dinca, J. R. Long, *J. Am. Chem. Soc.* **2007**, *129*, 11172.
[116] M. Dinca, A. Dailly, Y. Liu, C. M. Brown, D. A. Neumann, J. R. Long, *J. Am. Chem. Soc.* **2006**, *128*, 16876.
[117] M. Dinca, W. S. Han, Y. Liu, A. Dailly, C. M. Brown, J. R. Long, *Angew. Chem. Int. Ed.* **2007**, *46*, 1419.
[118] A. G. Wong-Foy, O. Lebel, A. J. Matzger, *J. Am. Chem. Soc.* **2007**, *129*, 15740.
[119] J. G. Vitillo, L. Regli, S. Chavan, G. Ricchiardi, G. Spoto, P. D. C. Dietzel, S. Bordiga, A. Zecchina, *J. Am. Chem. Soc.* **2008**, *130*, 8386.
[120] A. Hamaed, M. Trudeau, D. M. Antonelli, *J. Am. Chem. Soc.* **2008**, *130*, 6992.
[121] S. B. W. A. Schalkwijk, *Advances in Lithium-Ion Batteries*, Kluwer Academic Publications, New York **2002**.
[122] J. L. Tirado, *Mater. Sci. Eng, R* **2003**, *40*, 103.
[123] N. A. Kaskhedikar, J. Maier, *Adv. Mater.* **2009**, *21*, 2664.
[124] M. S. Whittingham, *Chem. Rev.* **2004**, *104*, 4271.
[125] K. Mizushima, P. C. Jones, P. J. Wiseman, J. B. Goodenough, *Mater. Res. Bull.* **1980**, *15*, 783.
[126] G. G. Amatucci, J. M. Tarascon, L. C. Klein, *J. Electrochem. Soc.* **1996**, *143*, 1114.
[127] M. M. Thackeray, *Prog. Solid State Chem.* **1997**, *25*, 1.
[128] P. G. Bruce, B. Scrosati, J. M. Tarascon, *Angew. Chem. Int. Ed.* **2008**, *47*, 2930.
[129] F. F. C. Bazito, R. M. Torresi, *J. Braz. Chem. Soc.* **2006**, *17*, 627.
[130] A. K. Padhi, K. S. Nanjundaswamy, J. B. Goodenough, *J. Electrochem. Soc.* **1997**, *144*, 1188.
[131] J. B. Goodenough, *J. Power Sources* **2007**, *174*, 996.
[132] C. S. Sun, Z. Zhou, Z. G. Xu, D. G. Wang, J. P. Wei, X. K. Bian, J. Yan, *J. Power Sources* **2009**, *193*, 841.
[133] N. Meethong, Y. H. Kao, S. A. Speakman, Y. M. Chiang, *Adv. Funct. Mater.* **2009**, *19*, 1060.

[134] S. H. Lee, Y. H. Kim, R. Deshpande, P. A. Parilla, E. Whitney, D. T. Gillaspie, K. M. Jones, A. H. Mahan, S. B. Zhang, A. C. Dillon, *Adv. Mater.* **2008**, *20*, 3627.
[135] Y. S. Hu, L. Kienle, Y. G. Guo, J. Maier, *Adv. Mater.* **2006**, *18*, 1421.
[136] Z. P. Guo, G. D. Du, Y. Nuli, M. F. Hassan, H. K. Liu, *J. Mater. Chem.* **2009**, *19*, 3253.
[137] M. G. Kim, S. Lee, J. Cho, *J. Electrochem. Soc.* **2009**, *156*, A89.
[138] Y. Sharma, N. Sharma, G. V. S. Rao, B. V. R. Chowdari, *Adv. Funct. Mater.* **2007**, *17*, 2855.
[139] D. Son, E. Kim, T. G. Kim, M. G. Kim, J. H. Cho, B. Park, *Appl. Phys. Lett.* **2004**, *85*, 5875.
[140] S. C. Zhang, X. P. Qiu, Z. Q. He, D. S. Weng, W. T. Zhu, *J. Power Sources* **2006**, *153*, 350.
[141] M. Jo, Y. S. Hong, J. Choo, J. Cho, *J. Electrochem. Soc.* **2009**, *156*, A430.
[142] S. M. Paek, E. Yoo, I. Honma, *Nano Lett.* **2009**, *9*, 72.
[143] J. Kim, M. Noh, J. Cho, H. Kim, K. B. Kim, *J. Electrochem. Soc.* **2005**, *152*, A1142.
[144] T. Fang, J. G. Duh, S. R. Sheen, *J. Electrochem. Soc.* **2005**, *152*, A1701.
[145] Y. Wang, G. Z. Cao, *Adv. Mater.* **2008**, *20*, 2251.
[146] M. S. Park, G. X. Wang, Y. M. Kang, D. Wexler, S. X. Dou, H. K. Liu, *Angew. Chem. Int. Ed.* **2007**, *46*, 750.
[147] M. S. Park, Y. M. Kang, G. X. Wang, S. X. Dou, H. K. Liu, *Adv. Funct. Mater.* **2008**, *18*, 455.
[148] E. Hosono, T. Kudo, I. Honma, H. Matsuda, H. S. Zhou, *Nano Lett.* **2009**, *9*, 1045.
[149] Y. J. Lee, M. G. Kim, J. Cho, *Nano Lett.* **2008**, *8*, 957.
[150] D. K. Kim, P. Muralidharan, H. W. Lee, R. Ruffo, Y. Yang, C. K. Chan, H. Peng, R. A. Huggins, Y. Cui, *Nano Lett.* **2008**, *8*, 3948.
[151] C. Kim, K. S. Yang, M. Kojima, K. Yoshida, Y. J. Kim, Y. A. Kim, M. Endo, *Adv. Funct. Mater.* **2006**, *16*, 2393.
[152] N. Du, H. Zhang, B. Chen, J. B. Wu, X. Y. Ma, Z. H. Liu, Y. Q. Zhang, D. Yang, X. H. Huang, J. P. Tu, *Adv. Mater.* **2007**, *19*, 4505.
[153] X. W. Lou, D. Deng, J. Y. Lee, J. Feng, L. A. Archer, *Adv. Mater.* **2008**, *20*, 258.
[154] K. T. Nam, D. W. Kim, P. J. Yoo, C. Y. Chiang, N. Meethong, P. T. Hammond, Y. M. Chiang, A. M. Belcher, *Science* **2006**, *312*, 885.
[155] H. L. Zhang, F. Li, C. Liu, H. M. Cheng, *Nanotechnology* **2008**, *19*, 165606.
[156] J. W. Seo, J. T. Jang, S. W. Park, C. J. Kim, B. W. Park, J. W. Cheon, *Adv. Mater.* **2008**, *20*, 4269.
[157] M. V. Reddy, T. Yu, C. H. Sow, Z. X. Shen, C. T. Lim, G. V. S. Rao, B. V. R. Chowdari, *Adv. Funct. Mater.* **2007**, *17*, 2792.
[158] W. M. Zhang, X. L. Wu, J. S. Hu, Y. G. Guo, L. J. Wan, *Adv. Funct. Mater.* **2008**, *18*, 3941.
[159] G. L. Cui, Y. S. Hu, L. J. Zhi, D. Q. Wu, I. Lieberwirth, J. Maier, K. Mullen, *Small* **2007**, *3*, 2066.
[160] Y. G. Wang, Y. R. Wang, E. J. Hosono, K. X. Wang, H. S. Zhou, *Angew. Chem. Int. Ed.* **2008**, *47*, 7461.
[161] Y. K. Sun, S. T. Myung, B. C. Park, J. Prakash, I. Belharouak, K. Amine, *Nat. Mater.* **2009**, *8*, 320.
[162] B. Kang, G. Ceder, *Nature* **2009**, *458*, 190.
[163] K. Zaghib, J. B. Goodenough, A. Mauger, C. Julien, *J. Power Sources* **2009**, *194*, 1021.
[164] Y. Wang, H. C. Zeng, J. Y. Lee, *Adv. Mater.* **2006**, *18*, 645.
[165] A. L. M. Reddy, M. M. Shaijumon, S. R. Gowda, P. M. Ajayan, *Nano Lett.* **2009**, *9*, 1002.
[166] L. F. Cui, R. Ruffo, C. K. Chan, H. L. Peng, Y. Cui, *Nano Lett.* **2009**, *9*, 491.
[167] H. Lee, J. Cho, *Nano Lett.* **2007**, *7*, 2638.
[168] H. Kim, J. Cho, *Nano Lett.* **2008**, *8*, 3688.
[169] P. Meduri, C. Pendyala, V. Kumar, G. U. Sumanasekera, M. K. Sunkara, *Nano Lett.* **2009**, *9*, 612.
[170] D. W. Kim, I. S. Hwang, S. J. Kwon, H. Y. Kang, K. S. Park, Y. J. Choi, K. J. Choi, J. G. Park, *Nano Lett.* **2007**, *7*, 3041.
[171] X. W. Lou, L. A. Archer, Z. C. Yang, *Adv. Mater.* **2008**, *20*, 3987.
[172] H. Ma, F. Y. Cheng, J. Chen, J. Z. Zhao, C. S. Li, Z. L. Tao, J. Liang, *Adv. Mater.* **2007**, *19*, 4067.
[173] H. Kim, J. Cho, *Chem. Mater.* **2008**, *20*, 1679.
[174] X. W. Lou, L. A. Archer, *Adv. Mater.* **2008**, *20*, 1853.
[175] X. W. Lou, Y. Wang, C. L. Yuan, J. Y. Lee, L. A. Archer, *Adv. Mater.* **2006**, *18*, 2325.
[176] S. Y. Zeng, K. B. Tang, T. W. Li, Z. H. Liang, D. Wang, Y. K. Wang, W. W. Zhou, *J. Phys. Chem. C* **2007**, *111*, 10217.
[177] C. Z. Wu, Y. Xie, L. Y. Lei, S. Q. Hu, C. Z. OuYang, *Adv. Mater.* **2006**, *18*, 1727.
[178] J. Chen, F. Y. Cheng, *Acc. Chem. Res.* **2009**, *42*, 713.
[179] A. M. Cao, J. S. Hu, H. P. Liang, L. J. Wan, *Angew. Chem. Int. Ed.* **2005**, *44*, 4391.
[180] Y. Yu, C. H. Chen, Y. Shi, *Adv. Mater.* **2007**, *19*, 993.
[181] H. L. Zhang, Y. Zhang, X. G. Zhang, F. Li, C. Liu, J. Tan, H. M. Cheng, *Carbon* **2006**, *44*, 2778.
[182] J. Shu, *Electrochem. Solid State Lett.* **2008**, *11*, A219.
[183] B. X. Li, G. X. Rong, Y. Xie, L. F. Huang, C. Q. Feng, *Inorg. Chem.* **2006**, *45*, 6404.
[184] J. C. Park, J. Kim, H. Kwon, H. Song, *Adv. Mater.* **2009**, *21*, 803.
[185] H. L. Chen, C. P. Grey, *Adv. Mater.* **2008**, *20*, 2206.
[186] Y. Kim, H. Hwang, C. S. Yoon, M. G. Kim, J. Cho, *Adv. Mater.* **2007**, *19*, 92.
[187] K. T. Lee, J. C. Lytle, N. S. Ergang, S. M. Oh, A. Stein, *Adv. Funct. Mater.* **2005**, *15*, 547.
[188] Z. Y. Wang, F. Li, N. S. Ergang, A. Stein, *Chem. Mater.* **2006**, *18*, 5543.
[189] Y. G. Guo, Y. S. Hu, W. Sigle, J. Maier, *Adv. Mater.* **2007**, *19*, 2087.
[190] H. S. Zhou, S. M. Zhu, M. Hibino, I. Honma, M. Ichihara, *Adv. Mater.* **2003**, *15*, 2107.
[191] H. Kim, B. Han, J. Choo, J. Cho, *Angew. Chem. Int. Ed.* **2008**, *47*, 10151.
[192] F. Jiao, P. G. Bruce, *Adv. Mater.* **2007**, *19*, 657.
[193] F. Jiao, J. L. Bao, A. H. Hill, P. G. Bruce, *Angew. Chem. Int. Ed.* **2008**, *47*, 9711.
[194] F. Jiao, K. M. Shaju, P. G. Bruce, *Angew. Chem. Int. Ed.* **2005**, *44*, 6550.
[195] L. W. Ji, X. W. Zhang, *Nanotechnology* **2009**, *20*, 155705.
[196] K. X. Wang, M. D. Wei, M. A. Morris, H. S. Zhou, J. D. Holmes, *Adv. Mater.* **2007**, *19*, 3016.
[197] J. Zhang, Y. S. Hu, J. P. Tessonnier, G. Weinberg, J. Maier, R. Schlogl, D. S. Su, *Adv. Mater.* **2008**, *20*, 1450.
[198] Y. G. Guo, J. S. Hu, L. J. Wan, *Adv. Mater.* **2008**, *20*, 2878.
[199] K. T. Lee, Y. S. Jung, S. M. Oh, *J. Am. Chem. Soc.* **2003**, *125*, 5652.
[200] Y. Wang, F. B. Su, J. Y. Lee, X. S. Zhao, *Chem. Mater.* **2006**, *18*, 1347.
[201] D. Deng, J. Y. Lee, *Chem. Mater.* **2008**, *20*, 1841.
[202] J. Fan, T. Wang, C. Z. Yu, B. Tu, Z. Y. Jiang, D. Y. Zhao, *Adv. Mater.* **2004**, *16*, 1432.
[203] H. L. Zhang, S. H. Liu, F. Li, S. Bai, C. Liu, J. Tan, H. M. Cheng, *Carbon* **2006**, *44*, 2212.
[204] H. L. Zhang, F. Li, C. Liu, H. M. Cheng, *J. Phys. Chem. C* **2008**, *112*, 7767.
[205] Y. S. Hu, Y. G. Guo, R. Dominko, M. Gaberscek, J. Jamnik, J. Maier, *Adv. Mater.* **2007**, *19*, 1963.
[206] H. M. Xie, R. S. Wang, J. R. Ying, L. Y. Zhang, A. F. Jalbout, H. Y. Yu, G. L. Yang, X. M. Pan, Z. M. Su, *Adv. Mater.* **2006**, *18*, 2609.
[207] M. N. Obrovac, L. J. Krause, *J. Electrochem. Soc* **2007**, *154*, A103.
[208] J. Saint, M. Morcrette, D. Larcher, L. Laffont, S. Beattie, J. P. Peres, D. Talaga, M. Couzi, J. M. Tarascon, *Adv. Funct. Mater.* **2007**, *17*, 1765.
[209] M. Holzapfel, H. Buqa, W. Scheifele, P. Novak, F. M. Petrat, *Chem. Commun.* **2005**, 1566.
[210] Y. S. Hu, R. Demir-Cakan, M. M. Titirici, J. O. Muller, R. Schlogl, M. Antonietti, J. Maier, *Angew. Chem. Int. Ed.* **2008**, *47*, 1645.
[211] G. Derrien, J. Hassoun, S. Panero, B. Scrosati, *Adv. Mater.* **2007**, *19*, 2336.
[212] J. Hassoun, G. Derrien, S. Panero, B. Scrosati, *Adv. Mater.* **2008**, *20*, 3169.
[213] L. J. Zhi, Y. S. Hu, B. El Hamaoui, X. Wang, I. Lieberwirth, U. Kolb, J. Maier, K. Mullen, *Adv. Mater.* **2008**, *20*, 1727.
[214] C. M. Park, H. J. Sohn, *Adv. Mater.* **2007**, *19*, 2465.

[215] D. W. Kim, Y. D. Ko, J. G. Park, B. K. Kim, *Angew. Chem. Int. Ed.* **2007**, *46*, 6654.
[216] M. Endo, Y. A. Kim, T. Hayashi, K. Nishimura, T. Matusita, K. Miyashita, M. S. Dresselhaus, *Carbon* **2001**, *39*, 1287.
[217] Y. Zhang, X. G. Zhang, H. L. Zhang, Z. G. Zhao, F. Li, C. Liu, H. M. Cheng, *Electrochim. Acta* **2006**, *51*, 4994.
[218] Y. J. Lee, H. Yi, W. J. Kim, K. Kang, D. S. Yun, M. S. Strano, G. Ceder, A. M. Belcher, *Science* **2009**, *324*, 1051.
[219] J. Chen, A. I. Minett, Y. Liu, C. Lynam, P. Sherrell, C. Wang, G. G. Wallace, *Adv. Mater.* **2008**, *20*, 566.
[220] L. J. Fu, H. Liu, C. Li, Y. P. Wu, E. Rahm, R. Holze, H. Q. Wu, *Solid State Sci.* **2006**, *8*, 113.
[221] Q. M. Pan, H. B. Wang, Y. H. Jiang, *J. Mater. Chem.* **2007**, *17*, 329.
[222] K. S. Park, A. Benayad, D. J. Kang, S. G. Doo, *J. Am. Chem. Soc.* **2008**, *130*, 14930.
[223] D. Sun, C. W. Kwon, G. Baure, E. Richman, J. MacLean, B. Dunn, S. H. Tolbert, *Adv. Funct. Mater.* **2004**, *14*, 1197.
[224] K. S. Kang, Y. S. Meng, J. Breger, C. P. Grey, G. Ceder, *Science* **2006**, *311*, 977.
[225] S. B. Schougaard, J. Breger, M. Jiang, C. P. Grey, J. B. Goodenough, *Adv. Mater.* **2006**, *18*, 905.
[226] B. L. Ellis, W. R. M. Makahnouk, Y. Makimura, K. Toghill, L. F. Nazar, *Nat. Mater.* **2007**, *6*, 749.
[227] C. K. Chan, H. L. Peng, G. Liu, K. McIlwrath, X. F. Zhang, R. A. Huggins, Y. Cui, *Nat. Nanotechnol.* **2008**, *3*, 31.
[228] L. Taberna, S. Mitra, P. Poizot, P. Simon, J. M. Tarascon, *Nat. Mater.* **2006**, *5*, 567.
[229] J. Hassoun, S. Panero, P. Simon, P. L. Taberna, B. Scrosati, *Adv. Mater.* **2007**, *19*, 1632.
[230] C. K. Chan, X. F. Zhang, Y. Cui, *Nano Lett.* **2008**, *8*, 307.
[231] Y. G. Li, B. Tan, Y. Y. Wu, *Nano Lett.* **2008**, *8*, 265.
[232] Y. S. Hu, X. Liu, J. O. Muller, R. Schlogl, J. Maier, D. S. Su, *Angew. Chem. Int. Ed.* **2009**, *48*, 210.
[233] M. Armand, S. Grugeon, H. Vezin, S. Laruelle, P. Ribiere, P. Poizot, J. M. Tarascon, *Nat. Mater.* **2009**, *8*, 120.
[234] Y. Oumellal, A. Rougier, G. A. Nazri, J. M. Tarascon, L. Aymard, *Nat. Mater.* **2008**, *7*, 916.
[235] E. Yoo, J. Kim, E. Hosono, H. Zhou, T. Kudo, I. Honma, *Nano Lett.* **2008**, *8*, 2277.
[236] S. J. Han, B. C. Jang, T. Kim, S. M. Oh, T. Hyeon, *Adv. Funct. Mater.* **2005**, *15*, 1845.
[237] Q. R. Zhao, Y. Xie, T. Dong, Z. G. Zhang, *J. Phys. Chem. C* **2007**, *111*, 11598.
[238] D. Deng, J. Y. Lee, *Angew. Chem. Int. Ed.* **2009**, *48*, 1660.
[239] B. E. Conway, *Electrochemical Supercapacitors: Scientific Fundamentals and Technological Applications*, Plenum Publishers, New York **1999**.
[240] A. E. Fischer, K. A. Pettigrew, D. R. Rolison, R. M. Stroud, J. W. Long, *Nano Lett.* **2007**, *7*, 281.
[241] K. Dokko, J. Sugaya, H. Munakata, K. Kanamura, *Electrochim. Acta* **2005**, *51*, 966.
[242] G. G. Amatucci, F. Badway, A. Du Pasquier, T. Zheng, *J. Electrochem. Soc.* **2001**, *148*, A930.
[243] D. W. Wang, F. Li, M. Liu, G. Q. Lu, H. M. Cheng, *J. Phys. Chem. C* **2008**, *112*, 9950.
[244] D. W. Wang, F. Li, H. T. Fang, M. Liu, G. Q. Lu, H. M. Cheng, *J. Phys. Chem. B* **2006**, *110*, 8570.
[245] D. W. Wang, F. Li, Z. G. Chen, G. Q. Lu, H. M. Cheng, *Chem. Mater.* **2008**, *20*, 7195.
[246] D. W. Wang, F. Li, M. Liu, H. M. Cheng, *New Carbon Mater.* **2007**, *22*, 307.
[247] A. Janes, H. Kurig, E. Lust, *Carbon* **2007**, *45*, 1226.
[248] F. C. Wu, R. L. Tseng, C. C. Hu, C. C. Wang, *J. Power Sources* **2005**, *144*, 302.
[249] H. S. Teng, Y. J. Chang, C. T. Hsieh, *Carbon* **2001**, *39*, 1981.
[250] H. Shi, *Electrochim. Acta* **1996**, *41*, 1633.
[251] J. Chmiola, G. Yushin, R. Dash, Y. Gogotsi, *J. Power Sources* **2006**, *158*, 765.
[252] J. Chmiola, G. Yushin, R. K. Dash, E. N. Hoffman, J. E. Fischer, M. W. Barsoum, Y. Gogotsi, *Electrochem. Solid State Lett.* **2005**, *8*, A357.
[253] J. Chmiola, C. Largeot, P. L. Taberna, P. Simon, Y. Gogotsi, *Angew. Chem. Int. Ed.* **2008**, *47*, 3392.
[254] J. Chmiola, G. Yushin, Y. Gogotsi, C. Portet, P. Simon, P. L. Taberna, *Science* **2006**, *313*, 1760.
[255] C. Largeot, C. Portet, J. Chmiola, P. L. Taberna, Y. Gogotsi, P. Simon, *J. Am. Chem. Soc.* **2008**, *130*, 2730.
[256] J. Lee, S. Han, T. Hyeon, *J. Mater. Chem.* **2004**, *14*, 478.
[257] C. Vix-Guterl, S. Saadallah, K. Jurewicz, E. Frackowiak, M. Reda, J. Parmentier, J. Patarin, F. Beguin, *Mat. Sci. Eng. B* **2004**, *108*, 148.
[258] A. B. Fuertes, F. Pico, J. M. Rojo, *J Power Sources.* **2004**, *133*, 329.
[259] W. Xing, S. Z. Qiao, R. G. Ding, F. Li, G. Q. Lu, Z. F. Yan, H. M. Cheng, *Carbon* **2006**, *44*, 216.
[260] T. Horikawa, J. Hayashi, K. Muroyama, *Carbon* **2004**, *42*, 1625.
[261] W. C. Li, G. Reichenauer, J. Fricke, *Carbon* **2002**, *40*, 2955.
[262] H. K. Song, Y. H. Jung, K. H. Lee, L. H. Dao, *Electrochim. Acta* **1999**, *44*, 3513.
[263] G. J. Lee, S. I. Pyun, *Langmuir* **2006**, *22*, 10659.
[264] D. W. Wang, F. Li, M. Liu, G. Q. Lu, H. M. Cheng, *Angew. Chem. Int. Ed.* **2008**, *47*, 373.
[265] D. W. Wang, F. Li, M. Liu, G. Q. Lu, H. M. Cheng, *Angew. Chem. Int. Ed.* **2009**, *48*, 1525.
[266] D. Hulicova, A. M. Puziy, O. I. Poddubnaya, F. Surez-García, J. M. D. Tascn, G. Q. Lu, *J. Am. Chem. Soc.* **2009**, *131*, 5026.
[267] D. Hulicova, M. Kodama, H. Hatori, *Chem. Mater.* **2006**, *18*, 2318.
[268] D. Hulicova, J. Yamashita, Y. Soneda, H. Hatori, M. Kodama, *Chem. Mater.* **2005**, *17*, 1241.
[269] G. Lota, K. Lota, E. Frackowiak, *Electrochem. Commun.* **2007**, *9*, 1828.
[270] C. O. Ania, V. Khomenko, E. Raymundo-Pinero, J. B. Parra, F. Beguin, *Adv. Funct. Mater.* **2007**, *17*, 1828.
[271] W. R. Li, D. H. Chen, Z. Li, Y. F. Shi, Y. Wan, J. J. Huang, J. J. Yang, D. Y. Zhao, Z. Y. Jiang, *Electrochem. Commun.* **2007**, *9*, 569.
[272] E. Raymundo-Pinero, F. Leroux, F. Beguin, *Adv. Mater.* **2006**, *18*, 1877.
[273] Y. Y. Liang, H. L. Li, X. G. Zhang, *J. Power Sources* **2007**, *173*, 599.
[274] C. C. Hu, C. C. Wang, *Electrochem. Commun.* **2002**, *4*, 554.
[275] X. F. Wang, Z. You, D. B. Ruan, *Chin. J. Chem. Phys.* **2006**, *19*, 341.
[276] V. Panic, A. Dekanski, S. Gojkovic, S. Milonjic, V. B. Miskovic-Stankovic, B. Nikolic, *Curr. Res. Adv. Mater. Process* **2005**, *494*, 235.
[277] J. M. Miller, B. Dunn, *Langmuir* **1999**, *15*, 799.
[278] M. Min, K. Machida, J. H. Jang, K. Naoi, *J. Electrochem. Soc.* **2006**, *153*, A334.
[279] M. Q. Wu, G. A. Snook, G. Z. Chen, D. J. Fray, *Electrochem. Commun.* **2004**, *6*, 499.
[280] H. Zhang, G. P. Cao, Z. Y. Wang, Y. S. Yang, Z. J. Shi, Z. N. Gu, *Nano Lett.* **2008**, *8*, 2664.
[281] Y. G. Wang, H. Q. Li, Y. Y. Xia, *Adv. Mater.* **2006**, *18*, 2619.
[282] H. Talbi, P. E. Just, L. H. Dao, *J. Appl. Electrochem.* **2003**, *33*, 465.
[283] L. Z. Fan, Y. S. Hu, J. Maier, P. Adelhelm, B. Smarsly, M. Antonietti, *Adv. Funct. Mater.* **2007**, *17*, 3083.
[284] S. W. Woo, K. Dokko, H. Nakano, K. Kanamura, *J. Power Sources* **2009**, *190*, 596.
[285] H. L. Wang, Q. L. Hao, X. J. Yang, L. D. Lu, X. Wang, *Electrochem. Commun.* **2009**, *11*, 1158.
[286] H. Zhang, G. P. Cao, Z. Y. Wang, Y. S. Yang, Z. J. Shi, Z. N. Gu, *Electrochem. Commun.* **2008**, *10*, 1056.
[287] E. Frackowiak, F. Beguin, *Carbon* **2002**, *40*, 1775.
[288] E. Frackowiak, K. Metenier, V. Bertagna, F. Beguin, *Appl. Phys. Lett.* **2000**, *77*, 2421.
[289] K. H. An, W. S. Kim, Y. S. Park, J. M. Moon, D. J. Bae, S. C. Lim, Y. S. Lee, Y. H. Lee, *Adv. Funct. Mater.* **2001**, *11*, 387.
[290] E. Frackowiak, F. Beguin, *Carbon* **2001**, *39*, 937.

[291] C. M. Niu, E. K. Sichel, R. Hoch, D. Moy, H. Tennent, *Appl. Phys. Lett.* **1997**, *70*, 1480.
[292] B. Zhang, J. Liang, C. L. Xu, B. Q. Wei, D. B. Ruan, D. H. Wu, *Mater. Lett.* **2001**, *51*, 539.
[293] J. H. Chen, W. Z. Li, D. Z. Wang, S. X. Yang, J. G. Wen, Z. F. Ren, *Carbon* **2002**, *40*, 1193.
[294] H. Zhang, G. P. Cao, Y. S. Yang, Z. N. Gu, *J. Electrochem. Soc.* **2008**, *155*, K19.
[295] Q. F. Liu, W. C. Ren, D. W. Wang, Z. G. Chen, S. F. Pei, B. L. Liu, F. Li, H. T. Cong, C. Liu, H. M. Cheng, *ACS Nano.* **2009**, *3*, 707.
[296] M. Hughes, M. S. P. Shaffer, A. C. Renouf, C. Singh, G. Z. Chen, J. Fray, A. H. Windle, *Adv. Mater.* **2002**, *14*, 382.
[297] K. Jurewicz, S. Delpeux, V. Bertagna, F. Beguin, E. Frackowiak, *Chem. Phys. Lett.* **2001**, *347*, 36.
[298] V. L. Pushparaj, M. M. Shaijumon, A. Kumar, S. Murugesan, L. Ci, R. Vajtai, R. J. Linhardt, O. Nalamasu, P. M. Ajayan, *Proc. Natl. Acad. Sci. USA* **2007**, *104*, 13574.
[299] C. G. Liu, H. T. Fang, F. Li, M. Liu, H. M. Cheng, *J. Power Sources* **2006**, *160*, 758.
[300] B. J. Yoon, S. H. Jeong, K. H. Lee, H. S. Kim, C. G. Park, J. H. Han, *Chem. Phys. Lett.* **2004**, *388*, 170.
[301] Y. T. Wu, C. C. Hu, *J. Electrochem. Soc.* **2004**, *151*, A2060.
[302] H. J. Zheng, F. Q. Tang, Y. Jia, L. Z. Wang, Y. C. Chen, M. Lim, L. Zhang, G. Q. Lu, *Carbon* **2009**, *47*, 1534.
[303] J. I. Sohn, Y. S. Kim, C. Nam, B. K. Cho, T. Y. Seong, S. Lee, *Appl. Phys. Lett.* **2005**, 87.
[304] C. Z. Yuan, L. Chen, B. Gao, L. H. Su, X. G. Zhang, *J. Mater. Chem.* **2009**, *19*, 246.
[305] J. S. Ye, H. F. Cui, X. Liu, T. M. Lim, W. D. Zhang, F. S. Sheu, *Small* **2005**, *1*, 560.
[306] D. A. Dikin, S. Stankovich, E. J. Zimney, R. D. Piner, G. H. B. Dommett, G. Evmenenko, S. T. Nguyen, R. S. Ruoff, *Nature* **2007**, *448*, 457.
[307] M. D. Stoller, S. J. Park, Y. W. Zhu, J. H. An, R. S. Ruoff, *Nano Lett.* **2008**, *8*, 3498.
[308] W. Lv, D. M. Tang, Y. B. He, C. H. You, Z. Q. Shi, X. C. Chen, C. M. Chen, P. X. Hou, C. Liu, Q. H. Yang, *ACS Nano*, DOI: 10.1021/nn900933u.
[309] D. W. Wang, F. Li, J. P. Zhao, W. C. Ren, Z. G. Chen, J. Tan, Z. S. Wu, I. Gentle, G. Q. Lu, H. M. Cheng, *ACS Nano.* **2009**, *3*, 1745.
[310] H. T. Fang, M. Liu, D. W. Wang, T. Sun, D. S. Guan, F. Li, J. G. Zhou, T. K. Sham, H. M. Cheng, *Nanotechnology* **2009**, *20*, 225701.
[311] E. Baudrin, S. Cassaignon, M. Koesch, J. P. Jolivet, L. Dupont, J. M. Tarascon, *Electrochem. Commun.* **2007**, *9*, 337.
[312] J. R. Li, Z. L. Tang, Z. T. Zhang, *Chem. Mater.* **2005**, *17*, 5848.
[313] F. Fabregat-Santiago, E. M. Barea, J. Bisquert, G. K. Mor, K. Shankar, C. A. Grimes, *J. Am. Chem. Soc.* **2008**, *130*, 11312.
[314] C. Y. Xu, Q. Zhang, H. Zhang, L. Zhen, J. Tang, L. C. Qin, *J. Am. Chem. Soc.* **2005**, *127*, 11584.
[315] A. R. Armstrong, G. Armstrong, J. Canales, R. Garcia, P. G. Bruce, *Adv. Mater.* **2005**, *17*, 862.
[316] L. Kavan, M. Kalbac, M. Zukalova, I. Exnar, V. Lorenzen, R. Nesper, M. Graetzel, *Chem. Mater.* **2004**, *16*, 477.
[317] D. H. Wang, D. W. Choi, Z. G. Yang, V. V. Viswanathan, Z. M. Nie, C. M. Wang, Y. J. Song, J. G. Zhang, J. Liu, *Chem. Mater.* **2008**, *20*, 3435.
[318] Z. Bing, Y. Yuan, Y. Wang, Z. W. Fu, *Electrochem. Solid State Lett.* **2006**, *9*, A101.
[319] T. Brezesinski, J. Wang, J. Polleux, B. Dunn, S. H. Tolbert, *J. Am. Chem. Soc.* **2009**, *131*, 1802.
[320] D. W. Wang, H. T. Fang, F. Li, Z. G. Chen, Q. S. Zhong, G. Q. Lu, H. M. Cheng, *Adv. Funct. Mater.* **2008**, *18*, 3787.
[321] M. Armand, J. M. Tarascon, *Nature* **2008**, *451*, 652.
[322] A. R. Akbarzadeh, V. Ozolins, C. Wolverton, *Adv. Mater.* **2007**, *19*, 3233.
[323] J. Hemminger, G. Crabtree, M. Kastner, *A Report from the Basic Energy Sciences Advisory Committee*, US Department of Energy, Washington DC **2008**.